ARISTOTLE UNIVERSITY OF THESSALONIKI
Interinstitutional Program of Postgraduate Studies in
PALAEONTOLOGY – GEOBIOLOGY

KRYSTALIA CHITOGLOU
Geologist

CONTRIBUTION TO THE STUDY OF PLIOCENE – EARLY PLEISTOCENE RHINOS FROM GREECE

MASTER THESIS

DIRECTION: Macropalaeontology
Directed by: Aristotle University of Thessaloniki

THESSALONIKI
2022

Interinstitutional
Program of
Postgraduate
Studies in
PALAEONTOLOGY – GEOBIOLOGY

supported by:

Τμήμα Γεωλογίας ΑΠΘ
School of Geology AUTh

Τμήμα Βιολογίας ΑΠΘ
School of Biology AUTh

National and
Kapodistrian

University of Athens
Faculty of
Geology and
Geoenvironment

Τμήμα Γεωλογίας &
Γεωπεριβάλλοντος ΕΚΠΑ

Faculty of Geology & Geoenvironment
NKUA

Department of GEOLOGY

Τμήμα Γεωλογίας Παν/μίου Πατρών
Department of Geology, Patras Univ.

UNIVERSITY OF THE AEGEAN

Τμήμα Γεωγραφίας Παν/μίου Αιγαίου
Department of Geography, Aegean Univ.

KRYSTALIA CHITOGLOY
ΚΡΥΣΤΑΛΙΑ ΧΙΤΟΓΛΟΥ
Πτυχιούχος Γεωλογίας

CONTRIBUTION TO THE STUDY OF PLIOCENE – EARLY PLEISTOCENE RHINOS FROM GREECE
ΣΥΜΒΟΛΗ ΣΤΗΝ ΜΕΛΕΤΗ ΤΩΝ ΠΛΕΙΟΚΑΙΝΙΚΩΝ-ΚΑΤΩ ΠΛΕΙΣΤΟΚΑΙΝΙΚΩΝ ΡΙΝΟΚΕΡΩΝ ΣΤΗΝ ΕΛΛΑΔΑ

Υποβλήθηκε στο ΔΠΜΣ Παλαιοντολογία-Γεωβιολογία

Ημερομηνία Προφορικής Εξέτασης: 17/03/2022
Oral Examination Date: 17/03/2022

Three-member Examining Board

Professor Dimitrios S. Kostopoulos, Supervisor
Professor Lorenzo Rook, Member
Professor Evangelia Tsoukala, Member

Τριμελής Εξεταστική Επιτροπή

Καθηγητής Δημήτριος Κωστόπουλος, Επιβλέπων
Καθηγητής Lorenzo Rook, Μέλος Τριμελούς Εξεταστικής Επιτροπής
Καθηγήτρια Ευαγγελία Τσουκαλά, Μέλος Τριμελούς Εξεταστικής Επιτροπής

External Assistant/Εξωτερικός Συνεργάτης (σύμφωνα με ΕΔΕ5/15-7-2019)
Dr. Luca Pandolfi

© Krystalia Chitoglou, Geologist, 2022
All rights reserved.
CONTRIBUTION TO THE STUDY OF THE EARLY PLEISTOCENE RHINOS FROM GREECE– *Master Thesis*

© Κρυσταλία Χίτογλου, Γεωλόγος, 2022
Με επιφύλαξη παντός δικαιώματος.
ΣΥΜΒΟΛΗ ΣΤΗΝ ΜΕΛΕΤΗ ΤΩΝ ΡΙΝΟΚΕΡΩΝ ΤΟΥ ΚΑΤΩ ΠΛΕΙΣΤΟΚΑΙΝΟΥ ΣΤΗΝ ΕΛΛΑΔΑ– *Μεταπτυχιακή Διπλωματική Εργασία*

Citation:
Chitoglou, K., 2022. – Contribution to the study of the Early Pleistocene rhinos from Greece. Master Thesis, Interinstitutional Program of Postgraduate Studies in Palaeontology-Geobiology. School of Geology, Aristotle University of Thessaloniki, 107 pp.

It is forbidden to copy, store and distribute this work, in whole or in part, for commercial purposes. Reproduction, storage and distribution are permitted for non-profit, educational or research purposes, provided the source of origin is indicated. Questions concerning the use of work for profit-making purposes should be addressed to the author.

The views and conclusions contained in this document express the author and should not be interpreted as expressing the official positions of the Aristotle University of Thessaloniki.

Cover Figure: Reconstruction of Leibnin's unicorn sketches, Kunsthistorisches Museum, modified.

CONTENTS

Acknowledgments

First of all, I would like to thank my supervisor, Professor Dimitris S. Kostopoulos, for his patience and for his active assistance through the writing process. I also want to thank the members of the examining board, Professor Lorenzo Rook, for accepting me to the University of Florence (UniFI), giving me the opportunity to study comparative rhinoceros material, and Professor Evangelia Tsoukala for allowing me to visit and study the rhinoceros material from Kalamotó. To Dr. Luca Pandolfi, I am grateful for his guidance and his repeated feedback on the manuscript, plus for sharing his knowledge and experience in rhinoceroses during and after my visit to the University of Florence. I thank Dr. George Konidaris, for his support and enlightening comments. Moreover, I want to thank Emer. Prof. George D. Koufos for his contribution in most of the studied localities. Thanks, are also due to all, the field members who participated in the excavations and unearthed the material concerning this study.

The excavations in Tsiotra Vryssi and Platanochori, were supported by the European Research Council STG no. 283503 (PaGE) and the European Research Council CoG 724703 (CROSSROADS), both awarded to Professor Aikaterini Harvati-Papatheodorou. The excavations in Dafnero is the result of a partnership fieldwork between the Laboratory of Geology and Paleontology of the Aristotle University of Thessaloniki, Greece and the Laboratoire Paleontologie Evolution Paleoecosystems Paleoprimatologie (PALEVOPRIM, CNRS-INEE and Universite de Poitiers, France). The rest of the studied material and collections is part of the Museum of Geology-Palaeontology-Palaeoanthropology which I would like to thank too. My research at the University of Florence was supported by the Erasmus+ student exchange program.

I am grateful to my family, team and friends, for supporting me throughout my studies. Without them, this thesis could have finished much earlier, nevertheless much more painfully. Finally, I thank my fellow birdfriends Anastasia x2, Georgia and Maria, and the paleo-friends Stelios, Saverio, Omar, Francesca and Andrea for the support all this time. Last but not least, my feline and avian friends of the university's campus, for bringing peace to my soul during stressful times.

Περίληψη

Η παρούσα μεταπτυχιακή διπλωματική εργασία ασχολείται με την συστηματική μελέτη των Ρινοκεροτίδων (Rhinocerotidae, Mammals, Perissodactyla), από διάφορες Πλειο-Πλειστοκαινικές απολιθωματοφόρες θέσεις της Βόρειας Ελλάδας.

Στην Ευρώπη, κατά την διάρκεια του Πλειοκαίνου, η οικογένεια των Ρινοκεροτίδων αντιπροσωπεύεται από δύο γένη (*Stephanorhinus* και *Pliorhinus)* και συνολικά από τέσσερα είδη: *P. miguelcrusafonti, P. megarhinus, S. etruscus* και *S. jeanvireti*. Τα δύο τελευταία συνεχίζουν να επιβιώνουν και μέχρι το Πλειστόκαινο, μαζί με τους *S. hundsheimensis, S. hemitoechus* και *S. kirchbergensis,* ενώ το γένος *Pliorhinus* εξαφανίζεται. Ένα άλλο Άνω Πλειστοκαινικό γένος είναι το *Coelodonta,* η εμφάνιση του οποίου δεν έχει καταγραφεί στις απολιθωματοφόρες θέσεις της εργασίας.

Μελετήθηκαν συνολικά δέκα απολιθωματοφόρες θέσεις από το Κάτω Πλειόκαινο μέχρι το άνω Κάτω Πλειστόκαινο (περίπου ~1.0 Ma). Οι περισσότερες βρίσκονται στην Λεκάνη της Μυγδονίας, και περιλαμβάνουν τις θέσεις: Απολλωνία, Ριζά, Πλατανοχώρι, Καλαμωτό, Κρήμνη και Τσιότρα Βρύση. Επίσης, μέρος του υλικού που μελετήθηκε προέρχεται από την Κάτω Πλειοκαινική θέση της Αλλατίνη, στην Θεσσαλονίκη και από τις Κάτω Πλειστοκαινικές θέσεις του Λίβακου, και του Δαφνερού στην Λεκάνη των Γρεβενών. Τέλος, από την λεκάνη της Δράμας, μελετήθηκε υλικό από την θέση Βώλακας.

Το υλικό, αποτελείται από 102 δείγματα τα οποία συγκρίθηκαν μορφολογικά και μορφομετρικά με υλικό από Πλειο-Πλειοστοκαινικές Ευρασιατικές θέσεις. Εκτός από τις θέσεις των Τσιότρα Βρύση (σύνολο 60 δειγμάτων) και του Καλαμωτό-2 (σύνολο 14 δειγμάτων), οι υπόλοιπες απολιθωματοφόρες θέσεις παρέχουν περιορισμένο αριθμό δειγμάτων προς μελέτη. Έτσι, από την απολιθωματοφόρα θέση της Αλλατίνη υπάρχει ένα δείγμα, από το Δαφνερό δύο, από τον Λίβακο τρία, από τον Βώλακα δύο, από την Απολλωνία επτά, από την Κρήμνη εννιά, από τα Ριζά τρία και ένα δείγμα από το Πλατανοχώρι.

Η παρούσα μελέτη καταγράφει την πρώτη εμφάνιση στην Ελλάδα των *Pliorhinus megarhinus* στην θέση Αλλατίνη, και του *Stephanorhinus* cf. *hundsheimensis* στις θέσεις Ριζά, Κρήμνη και Τσιότρα Βρύση· και την τελευταία γνωστή εμφάνιση του *S. jeanvireti* στην θέση Δαφνερό-3. Η παρουσία του *Stephanorhinus etruscus* επιβεβαιώνεται σε διάφορες θέσεις (Απολλωνία, Βώλακας, Λίβακος, Τσιότρα Βρύση και Καλαμωτό) με ένα χρονολογικό εύρος από ~2.3 Ma μέχρι ~1.0 Ma. Σύμφωνα με αυτό το εύρος, τα είδη *S. etruscus* και *S. jeanvireti* πιθανά συνυπήρξαν στον ελληνικό χώρο για ένα μικρό χρονικό διάστημα γύρω στα 2.3 Ma. Επίσης το υλικό της Τσιότρα Βρύσης υποδεικνύει την πρώτη συνύπαρξη των ειδών *S.* cf. *hundsheimensis* και *S. etruscus* στην Ελλάδα.

ABSTRACT

The present thesis is focused on the systematic study of Rhinocerotidae (Mammals, Perissodactyla), from several Plio-Pleistocene localities in Northern Greece, in comparison with Eurasian taxa.

During the Pliocene, European Rhinocerotidae are represented by two genera (*Stephanorhinus* and *Pliorhinus)* and in total by four species: *P. miguelcrusafonti, P. megarhinus, S. etruscus* and *S. jeanvireti*. The latter two survived within the Pleistocene, along with *S. hundsheimensis, S. hemitoechus* and *S. kirchbergensis,* while the genus *Pliorhinus* became extinct. Another Late Pleistocene European rhino genus is *Coelodonta,* which however is not recorded in any of the studied localities.

A total of ten rhino fossil-bearing localities were studied, ranging from Lower Pliocene to late Lower Pleistocene (about ~1.0 Ma). Most of them are in Mygdonia Basin, including the sites of Apollonia, Riza, Platanochori, Kalamotó, Krimni and Tsiotra Vryssi. Some more material from the Lower Pliocene locality of Allatini, near Thessaloniki, the Lower Pleistocene localities of Libakos and Dafnero in Grevena basin, as well as Volax, in Drama basin is also studied.

In summary, 102 rhinoceros specimens were studied and compared (biometrically and morphologically) with material from Plio-Pleistocene Eurasian localities. Apart from Tsiotra Vryssi locality (n= 60 specimens), and Kalamotó-2 (n= 14 specimens) the rest of the fossil sites provide a few rhino material (n<10 specimens), i.e., 1 specimen from Allatini, 2 from Dafnero, 3 from Libakos, 2 from Volax, 7 from Apollonia, 9 from Krimni, 3 from Riza and 1 from Platnochori.

The study records the first Greek occurrence of *Pliorhinus megarhinus* in Allatini and *Stephanorhinus* cf. *hundsheimensis* in the localities of Riza, Krimni and Tsiotra Vryssi. Additionally, the last occurrence of *S. jeanvireti* is recorded in Dafnero site. The species *Stephanorhinus etruscus* is confirmed from several localities such as Apollonia, Volax, Libakos, Tsiotra Vryssi, and Kalamotó with a chronological range from ~2.3 Ma to ~1.0 Ma. At the beginning of this time frame both *S. jeanvireti* and *S. etruscus* were present in Greece, whereas Tsiotra Vryssi material (from 1.78 to ~1.5Ma) indicates the first co-existence of *S. etrucsus* and *S.* cf. *hundhseimensis* in Greece.

1. INTRODUCTION

Rhinoceroses are odd-toed ungulates of the order Perissodactyla, along with tapirs, horses and the extinct chalicotheres. There are five extant rhino species which are either threatened or critically endangered (Milliken et al., 2009) occupying various habitats in Africa and Asia.

The two African extant species, both with two horns, are the black and white rhinoceros. The first one, *Diceros bicornis* (Linnaeus, 1758) lives in pocket populations in various type of sub-Saharan habitats with browsing diet. The white rhino, *Ceratotherium simun* (Burchell, 1817), an obligate grazer, lives in grassland and savanna habitats. There were two subspecies, the southern white rhino, *C. s. simun* (Burchell, 1817) living in southern Africa, and the virtually extinct northern white rhino *C. s. cottoni* (Lydekker 1908), in central Africa.

The other three species are hopefully still living in Asia. More specifically, the Indian-great one horned rhinoceros, *Rhinoceros unicornis* (Linnaeus, 1758) is a variable grazer from Northern India, southern Nepal, and Bhutan, habitant of flood plains, grasslands, and riverine forest. The Javan or lesser one horned rhinoceros, *Rhinoceros sondaicus* (Dermarest, 1822) lives only in Java and is considered a browser. Finally, the Sumatran (or Asiatic bi-horned rhinoceros), *Rhinoceros sumatrensis* (Fischer, 1814) is a folivore rhino surviving in Indonesia in tropical rain and mountain moss forest habitat (Milliken et al., 2009; Hullot et al., 2019; Giaourtsakis, 2022 and references herein).

In Greece, the rhino presence is only in the fossil record, which is abundant during Miocene, rare during Pliocene, and usually scarce during Pleistocene. The historical overview of the study of rhinoceros is reviewed by Giaourtsakis (2022) mentioning the first study of rhino recorded by Gaudry (1862) in Pikermi, followed by another Miocene locality of Samos which was recorded by Forsyth-Major (1894) and studied by Weber (1904). In Northern Greece, another Miocene locality in Axios valley near Thessaloniki, with rhinocerotids is studied by Arambourg and Piveteau (1929). After World War II there are no new records or revisions of rhino material published. However, Geraads (1988) published a revision of the localities of Pikermi and Samos. Later the description of new species of *Aceratherium kiliasi* from Pentalofos-1 by Geraads and Koufos (1990) revives the paleontological study of rhinoceroses in Greece. In the past two decades, the study of rhinoceroses has bloomed with the discovery of new Plio-Pleistocene localities and material (Giaourtsakis, 2022 and references herein).

Rhinocerotids are represented in Greece only by the family of Rhinocerotidae starting from Middle Miocene with the most known locality that of Upper Miocene Pikermi, near Athens with adequate material. The significant faunal turnover at the end of the Miocene, known as Messinian Salinity Crisis, resulted the extinction of Pikermian chronofaunal. Additionally, all the rhinocerotid tribes were completely disappeared from Europe or limited in Africa.

During Pliocene, the Miocene rhinocerotids are replaced by the genera of *Stephanorhinus* and *Pliorhinus,* with four species present in Europe, *P. megarhinus, S. jeanvrieti, P. miguelcrusafonti,* and *S. etruscus.* The first two are large sized, especially *P. megarhinus*, which preserves a massive skull and wide thick nasal bones without nasal septum (Pandolfi and Rook, 2017). Its first appearance in Kávás (Hungary), is recorded in MN12-MN13, and the species survived until the Late Pliocene in Europe (MN14-MN15) and until the latest Pliocene (MN15-MN16) in Russia. (Guérin, 1980; Fukuchi et al., 2009; Pandolfi, 2013; Pandolfi et al., 2016, 2015). There is no record of this species in Greece yet.

The species *P. miguelcrusafonti* is chronologically restricted, limited to a few Spanish French, and Georgian localities (Guérin, 1980; Pandolfi et al., 2021b; Pandolfi et al., 2022). This medium to small sized Pliocene species, larger than the larger specimens of *S. etruscus* but smaller than the rest of the Pliocene species, was found along with *P. megarhinus.* There weren't any new records since the 1900's, until the recent first records of this species in Georgia, in the locality of Kvabebi and in Spain (Guérin and Santafe-Llopis, 1978; Pandolfi et al., 2021b; Pandolfi et al., 2022).

S. etruscus and *S. jeanvireti* first found in MN16a throughout Europe (Cirilli et al., 2020). The first one is a slender, small sized rhino, more cursorial with head posture suggesting a primarily browsing diet, low crowned teeth, and shallow joints suggesting locomotion in open woodlands (Loose, 1975; Fortelius et al., 1993). It is one of the most abundant species in Europe, first appearing in the latest Pliocene and thriving until the Pleistocene. More precisely, in the late Early Pleistocene, *S. etruscus* got extinct from central Europe, however, it survived in Italy and the Iberian Peninsula until the Early-Middle Pleistocene Transition (Pandolfi et al., 2017). In Greece, it is known from several Villafranchian localities, but the material is usually limited (Giaourtsakis, 2022).

S. jeanvireti is a much larger sized, but still slender rhino, with browsing dominated diet. It lived in humid, forest-dominated environment with relatively open areas where gramineae and ferns grew (Guérin, 1980; Lacombat and Mörs, 2008; Szabó et al., 2017; Tsoukala, 2018). It is mainly present in MNQ 16, however it survived until the Early Pleistocene in Romania (Pandolfi et al., 2019). In Greece, this tandem horned rhino with a massive facial area with long and broad nasal bones is present in three localities, Milia, Angelochori and Saint George Priporos (Tsoukala, 2018; Giaourtsakis, 2022).

The last known occurrence of genus *Pliorhinus* is that of *P. miguelcrusafonti* in Kvabebi (Georgia) in MN16a (Pandolfi et al., 2021b), which did not survive Pleistocene. During the same time, the genus *Stephanorhinus* represented by *S. etruscus* and *S. jeanvireti* appear and continue to Pleistocene when more species of the same genus are reported, plus the genus *Coelodonta* which arrive from Asia (Fig. 1).

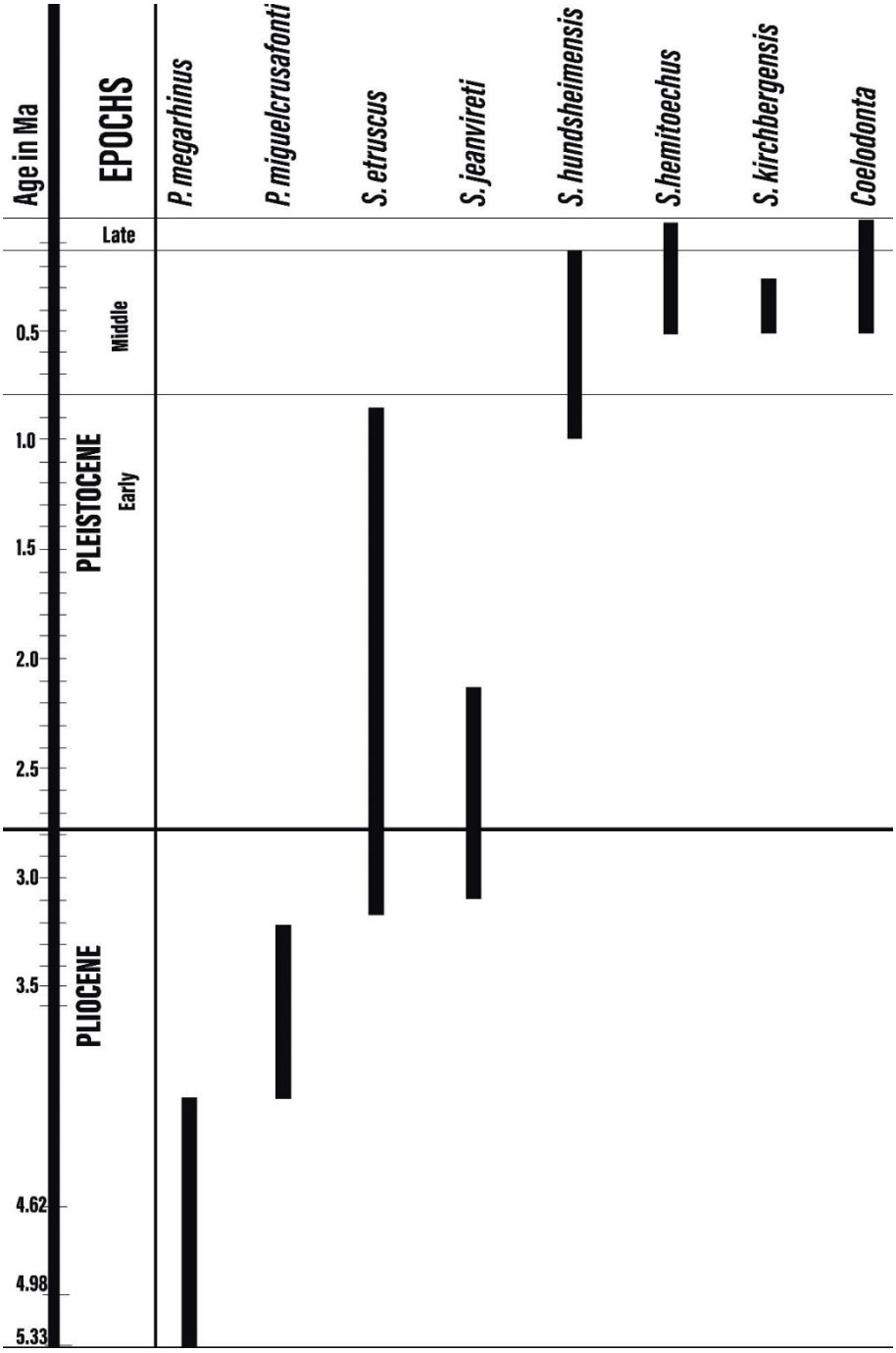

Figure 1 Chronological range of Plio-Pleiostocene rhinocerotids of Europe (Agustí et al., 2009; Deng et al., 2011; Masini and Sala, 2017; Pandolfi et al., 2018; Puzachenko et al., 2021)

The species *S. hundsheimensis* is commonly mistaken and re-ascribed as *S. etruscus.* Its certain presence in Europe is limited to a few localities in comparison with the most frequent *S. etruscus* (Kahlke, 2001; Madurell-Malapeira et al., 2010; Pandolfi

and Erten, 2017). Its earliest record is certified at ca. 1.1 Ma and continuous throughout the early Middle Pleistocene (Pandolfi and Erten, 2017; Radović et al., 2020; Pandolfi et al., 2021a). It is a long-legged rhino that lived in open woodland xeric grassland (Szabó et al., 2017) with a head posture suggesting a mixed diet of both grazing and browsing (intermediate heigh of vegetation). This dietary variability according to some authors, could be the reason for its extinction, as the arrival of more specialized grazers (*S. kirchbergensis)* and browsers (*S. hemitoechus)* were more successfully competitors for resources (Kahlke and Kaiser, 2011). In Greece, there are some localities with specimens assigned to *S. hundsheimensis* (e. g. Platanochori, Apollonia) however Giaourtsakis (2022) refers to them all as *Stephanorhinus* sp., due to inadequate material.

The species *S. hemitoechus,* also called the steppe-rhino, is a medium sized, narrow-nosed hypsodont rhinoceros, recorded from ca. 0.5 Ma until about 20 ka (Pandolfi and Tagliacozzo, 2015). It has graviportal locomotion in a temperate open habitat with rich and low grown vegetation. Its diet is flexible depending on the available environment (van Asperen and Kahlke, 2015). In Greece, it is present in Petralona Cave and Penios riverbank (Tsoukala and Guérin, 2016; Giaourtsakis, 2022).

There is one last species of the genus *Stephanorhinus* recorded in Europe, *S. kirchbergensis* or Merck's rhinoceros with its last occurrences dated shortly after the Eemian interglacial (van der Made, 2010). This tandem-horned, interglacial rhinoceros was earlier recorded in East Asia, since the Early Pleistocene, however, it is also present in Europe, Russia, and Korea (Billia and Petronio, 2009 and references therein). It is the largest sized *Stephanorhinus*, with long limbs, hypsodont premolars, sub-hypsodont molars and high head posture. Its diet is suggested as mixed, as it tended to browse on both foliage of trees or shrubs and also grasses and herbs (Kirillova et al., 2017). It is also called woodland or forest rhinoceros since its locomotion is graviportal (Tong and Wu, 2010). There are no confirmed known records of *S. kirchbergensis* in Greece, since its attribution in Asprochaliko, Megalopolis (old collection) and Petralona cave were reassigned to different species (Giaourtsakis, 2022).

Finally, the genus *Coelodonta* made its first appearance in Europe by a rhino close to *C. tologoijensis* Baliajeva, 1966, which migrated from the Tibetan plateau (Kahlke and Lacombat, 2008). However, the most widespread species is *C. antiquitatis*, the woolly rhino which was well-known in Eurasia during the Late Pleistocene and became extinct between 15,000 and 10,000 cal yr BP (Puzachenko et al., 2021). It is considered a true grazer with a relatively heavy mediportal stance. In Greece, there is a single certain presence of this species, in Aggitis Cave (Giaourtsakis, 2022).

2.1 Geological settings and fossiliferous localities

-Allatini (ALL)

The site of Allatini (Fig. 2) is the oldest of this study dated at the end of the Upper Miocene-Lower most Pliocene. It is located in East Thessaloniki and named after a private company that exploited clay pits (Syrides, 1990; Vlachos et al., 2015). The deposits belong to the Trilophos Formation (Fm) and nowadays are covered by domestic areas or have been fully exploited (Vlachos et al., 2015). The Trilophos Fm consists of sands, clays, sandstones, and limestones (Syrides, 1990; Vasileiadou et al., 2003). It overlies unconformably the Triglia Fm (red beds) and transits gradually the overlying Gonia Fm (fluvial-lacustrine sediments) (Syrides, 1990; Vlachos et al., 2015). The single rhino specimen from this site is a juvenile radius, which is labeled as "Rhinoceros" in the LGPUT collection and was previously ascribed as Rhinocerotidae indet. (Symeonidis et al., 2006; Giaourtsakis, 2022).

-Dafnero (DFN)

The locality of Dafnero (sites: DFN, DFN2, and DFN3) is located in the northern part of Greece, 128 km ESE of Thessaloniki and close to the homonymous village of Kozani (Fig. 2). The site of Dafnero-1 (DFN1) was discovered in 1990, while the other two sites were the result of partnership fieldwork between the Laboratory of Geology and Paleontology of the Aristotle University of Thessaloniki, Greece and the Laboratoire Paleontologie Evolution Paleoecosystems Paleoprimatologie (PALEVOPRIM, CNRS-INEE and Universite de Poitiers, France) (Kostopoulos et al., 2018). The sites are located within a 60m thick unit of fluvial deposits that represent the typical braided river sequence that is separated from the underlying molassic sediments of the Tsotylion Fm by an unconformity (Benammi et al., 2020). The sites DFN and DFN3 are at the basal part of fluvial deposits, into a layer of ochre silty sands which is below a dense conglomerate in the 20m high section (Kostopoulos et al., 2018). The rhino material found in DFN3 is poorly preserved and limited to a very worn out tooth and a McIII, previously referred to as "*Stephanorhinus ex. gr. etruscus"* (Koufos, 2001). The fauna has been recently dated at 2.3 Ma (MN17) (Benammi et al., 2020).

-Volax (VOL)

The locality of Volax (Fig. 2) was discovered by H. J. Martini (University of Hannover) in 1961 and since 1992 the fossils were stored at the Museum of Geology-Palaeontology-Palaeoanthropology of the Aristotle University of Thessaloniki (LGPUT). It is located about 11 km N-W of Drama, near the village of Volax. There is a small karstic-tectonic basin filled by clastic sediments of two alluvial fans consisting of alternating beds of conglomerates and calcareous sandstones within lenses of very hard calciticarenaceous clays that include the fossils. There are two fossil horizons, both located in Leptokaria ravine's wall, and the collection they provide is referred to as "Volax" or "Volakas" (VOL) as the material is mixed (Koufos and Vlachou, 1997). The fauna has been dated to MN17 and the rhino material is limited to a distal epiphysis of MtII and a distal epiphysis of a tibia which were previously referred to as "Rhinocerotidae

indet" (Kostopoulos, 1996; Koufos and Vlachou, 1997; Koufos, 2001; Symeonidis et al., 2006; Giaourtsakis, 2022).

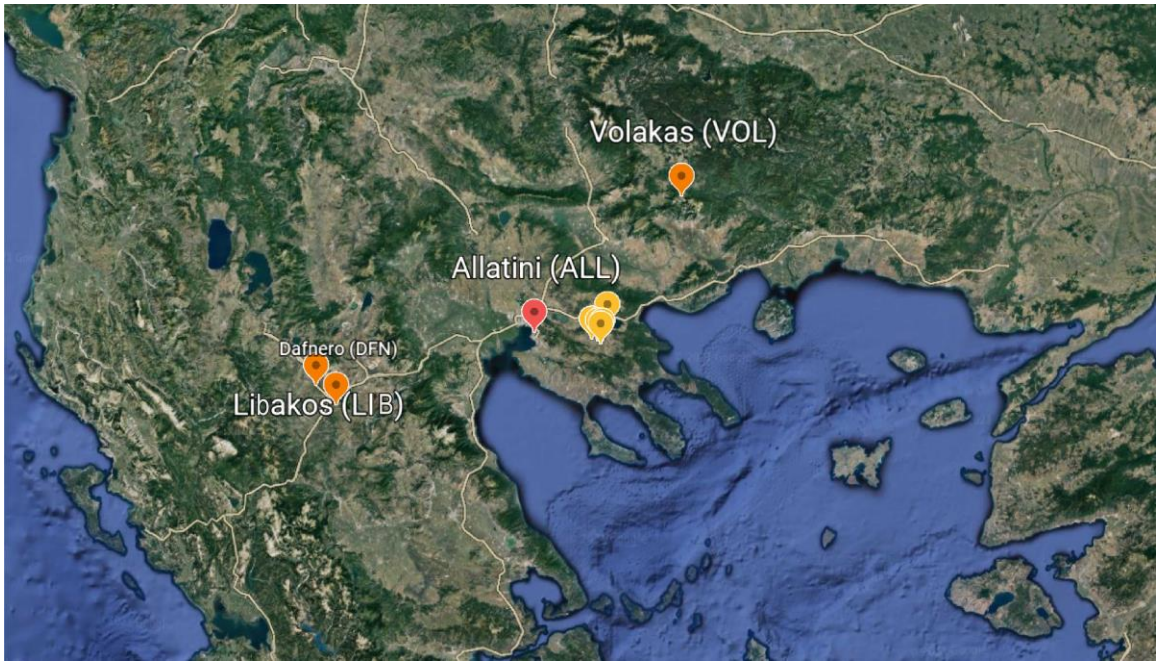

Figure 2 Some of the locations of fossiliferous localities studied: Volakas, Allatini, Dafnero and Libakos. With yellow arrows, are the localities from Mygdonia Basin, see below, (map from Google earth, modified).

-Libakos (LIB)

The fossiliferous locality of Libakos (LIB) was discovered by Prof. H. Eltgen (Clausthal University of Technology, Germany) in 1976 and the fossils were finally returned in LGPUT in 2014 (Fig. 2). There is no stratigraphic information on the locality, which however overlies stratigraphically the Dafnero fossil site, and located in the upper part of clay deposits of the same sedimentary succession. The fauna collected is referred to MN17 (Koufos, 2001). The rhino material of the locality of Libakos consists of a humerus (LIB-497), a calcaneus (LIB-180), and an atlas, previously described as *Stephanorhinus etruscus*, *Stephanorhinus* sp.,? *Stephanorhinus* sp., however the most recent attribution is *Stephanorhinus etruscus* (Koufos, 2001; Symeonidis et al., 2006; Giaourtsakis, 2022).

-Mygdonia Basin

The localities studied, Tsiotra Vryssi, Krimni, Platanochori, Riza, Apollonia, and Kalamotó are in Mygdonia Basin. The basement of the Mygdonia Basin is part of the metamorphic rocks of Serbomacedonian Massif consisted of schists gneisses and amphibolites at the central and eastern part. At the same time, the western section is part of the Circum-Rhodope Belt of slightly metamorphosed sediments like phyllites, limestones, and sandstones (Kockel et al., 1977). Mygdonia Basin's deposits are divided

into two lithostratigraphic units: The Pre-Mygdonian group and the Mygdonian group, with the former overlying the basement unconformably (Koufos et al., 1995). The initial Pre-Mygdonian group, including Miocene to Lower Pleistocene deposits, consists of fluvial-fluvioterrestial and lacustrine sediments. A new tectonic event, at the beginning of the Middle Pleistocene, caused the subdivision into smaller basins filled mainly with lacustrine sediments. During Pleistocene, Mygdonia basin was an elongated tectonic depression, with east-west orientation, forming a large lake (Psilovikos, 1977). The Pre-Mygdonian Group is subdivided into three Formations, the oldest of which is Chryssavgi Fm consists of “alternating grey-white loose conglomerates and sands with silty-clayey lenses or lenticular intercalations”. Gerakarou Fm follows with red-brown sands, gravels, sandy-silts and clays of fluvioterrestrial depositional environment. In this formation there are number rhino bearing fossiliferous localities studied in this thesis: Krimni-1, 3 (KRI, KMN), Kalamotó (KLT), and Tsiotra Vryssi (TSR) (Koufos et al., 1995; Tsoukala and Chatzopoulou, 2005; Konidaris et al., 2015). Platanochori Fm overlies Gerakarou Fm and it is considered as a transitional unit from Gerakarou Fm to the Mygdonian Group. It consists of sands, sandstones, conglomerates, silty sands, silts, clays, marls and marly limestones. Here, there are also number of localities studied: Apollonia-1 (APL), Riza-1 (RIZ), Kalamotó-1 (KAL) and Platanochori-1 (PLN) (Koufos et al., 1995; Tsoukala and Chatzopoulou, 2005; Konidaris et al., 2015).

The local stratigraphy ends by the Mygdonian Group consisted of lacustrine thin-bedded and fine sediments with the presence of sandstones, gravels, sands and travertines at the upper part.

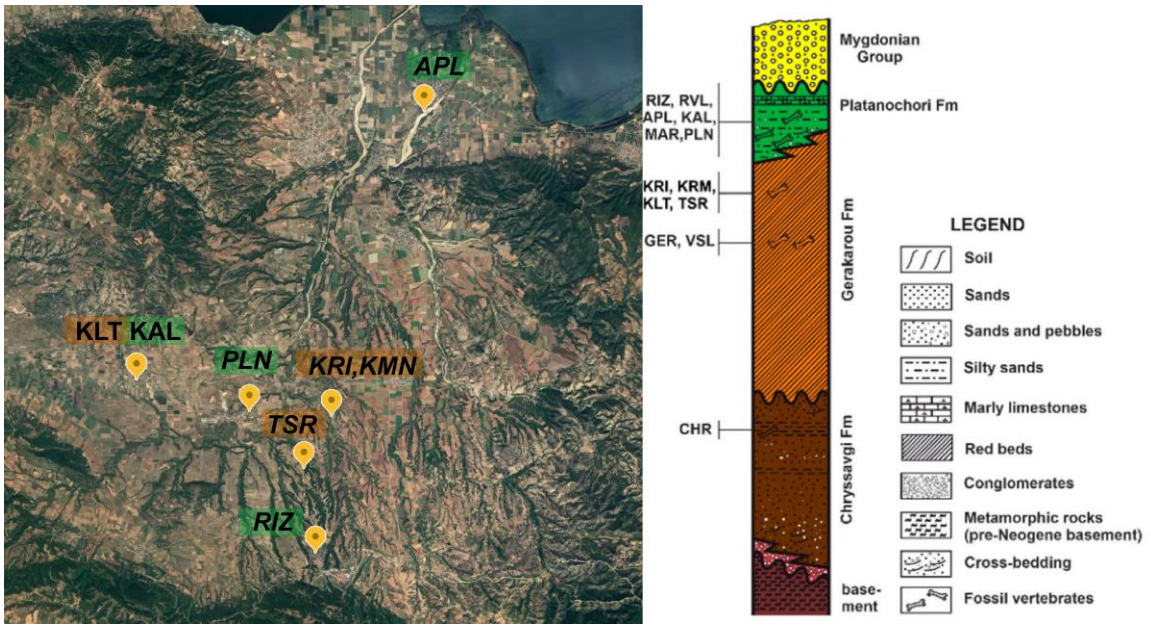

Figure 3 The fossiliferous localities from Mygdonia Basin, Apollonia (APL), Kalamotó (KLT, KAL), Platanochori (PLN), Krimni (KRI, KMN), Tsiotra Vryssi (TSR), Riza (RIZ) (map from Google earth; stratigraphy from Konidaris et al., 2015, updated from Koufos et al., 1995).

-Tsiotra Vryssi (TSR)

The site of Tsiotra Vryssi (TSR) was discovered in 2014 (Fig. 3) by researchers from Aristotle University of Thessaloniki and the Eberhard Karls University of Tübingen (Germany). It is located at northern Chalkidiki and it belongs to the upper parts of the Gerakarou Fm (Konidaris et al., 2015). Recent studies suggest an age for the mammal assemblage from this locality between 1.78 and ~1.5 Ma (Konidaris et al., 2021). The rhino remains unearthed from this site were previously referred to as *Stephanorhinus* sp. (Konidaris et al., 2015)

-Krimni (KRI, KMN)

The fossiliferous locality of Krimni-1 KRI (Fig. 3) is located SE to the homonymous village and close to the road Kimni-Paleochora. It was discovered in 1977 when locals found fossil bones and the excavations were led by the team of laboratory of Geology-Paleontology of Aristotle University of Thessaloniki. There are three fossiliferous spots, Krimni-1 (KRI) which is located closer to 194m altitude, Krimni-2 (KRM) which is located at a river terrace and do not preserve any rhinocerotids (Sakellariou et al., 1979) and the recently discovered Krimni-3 (KMN). They all belong to the upper parts of the Gerakarou Fm and their fauna is dated to the late Villafranchian, Early Pleistocene (Koufos et al., 1995; Konidaris et al., 2015). The rhino material from Krimni-1 (KRI) was previously described as "*Dicerorhinus etruscus*" (Sakellariou et al., 1979; Koufos, 1992) and later ascribed as "*Stephanorhinus etruscus*" (Koufos, 2001; Symeonidis et al., 2006). The rhino remains from Krimni-3 (KMN) are described here for the first time. The faunal age is estimated between Tsiotra Vryssi (between 1.78 and ~1.5 Ma) and Apollonia-1 (1.2- 1.0 Ma) (Kostopoulos et al. in press).

-Platanochori (PLN)

The site of Platanochori (Fig. 3) was discovered in 2013, 60km E-SE from Thessaloniki in northern Chalkidiki, and near the villages Platanochori and Krimni. No systematic excavation took place because the fossil spot is situated at the uppermost part of a vertical cliff and the material was collected from collapsed blocks of sediments. In the lower part of the section there are exposed sediments of the Gerakarou Fm, whereas in the upper part sediments of Platanochori Fm appear. The small fauna is assigned as Latest Villafranchian, similar to that of Apollonia-1 (Konidaris et al., 2015). The rhino material consists of a fragment of a maxilla with left DP3, DP4 and M1 previously referred to as "*Stephanorhinus hundsheimensis*" (Konidaris et al., 2015) or *Stephanorhinus* sp. (Giaourtsakis, 2022).

-Riza (RIZ)

The locality of "Riza-1" (Fig. 3) is situated near the homonymous village, in marly-sandy limestones of Platanochori Fm (Koufos, 1992). The rhino material is limited to a radius, an ulna and a tooth and it have not been previously described. The age of the locality is estimated to 1.0-1.2 Ma (MNQ 20) (Koufos, 2001).

-Apollonia (APL)

The site of Apollonia (APL) was discovered in 1991 from the team Laboratory of Geology and Paleontology of the Aristotle University of Thessaloniki (Fig. 3). It is located 65 km NW from Thessaloniki, near the homonymous village (Koufos et al., 1992). Stratigraphically it belongs to the Platanochori Fm (Koufos et al., 1992; Konidaris et al., 2015; Koufos, 2018). The age of Apollonia mammal fauna is indirectly estimated between 1.3–1.0 Ma and the paleoenvironment is considered patchy or mosaic landscape (Koufos, 2018). The rhino material from Apollonia consists of 6 specimens, which were previously referred to as "*Rhinocerotidae* indet" (Koufos et al., 1995; Koufos, 2001) or maybe "*Stephanorhinus hundsheimensis"* (Konidaris et al., 2015).

-Kalamotó (KAL, KLT)

The locality of Kalamotó (KAL, KLT) was discovered in 2000 and it is located 50 km NE from Thessaloniki. It consists of two sites (Fig. 3). The Kalamotó-1 (KAL) is placed into lacustrine deposits, gray marls, and silt sands and iis situated 1 km south of Kalamotó village, in the broader archaeological site of "Chiliodentra". From this site, there is only one rhinoceros specimen studied. The Kalamotó-2 (KLT) site is placed in the red-brown-yellowish terrestrial deposits of Gerakarou Fm and it is located 2 km SW of the same village, close to the archaeological site of "Toumbes" in Vasmouras Rema. This site has more abundant rhino material with 12 rhinocerotid specimens studied. The age of the fauna is estimated as Early Pleistocene / Latest Villafranchian (MNQ 20). The rhino material from both localities was previously assigned to "*Dicerorhinus etruscus*" (Tsoukala and Chatzopoulou, 2005).

2. MATERIALS AND METHODS

The studied material was morphologically compared with rhinoceros' material from several selected Eurasian localities of Lower Pliocene to Pleistocene age. The systematics of Rhinocerotidae is still troublesome and the revision of previously studied material results its assignment into different species. Due to this fact, the morphological conclusions provided by Guérin (1980) are referred here only for historical reasons. For the same reason, the size-range given by the same author, for several postcranial bones, are precluded. The dental nomenclature was based on Guérin (1980) and Lacombat (2006). For the cranial and postcranial specimens, we follow Mazza (1988); for the vertebra terminology we use Tong and Wang (2014); for the long bones, a combination of terminology proposed by Mazza (1988) and Mallet et al. (2019) is followed.

Measurements for biometrical comparison was based on the original study of material from Valdarno, Pirro Nord and Olivola (Natural History Museum of Florence, Geological and Paleontological Section), plus those derived from the existing literature (Guérin and Heintz, 1971; Guérin, 1972, 2004; Guérin and Santafe-Llopis, 1978; Apostol and Enache, 1979; Mazza, 1988; Fortelius et al., 1993; Kahlke, 2001; Lacombat, 2005; Lacombat and Moulle, 2005; Fukuchi et al., 2009; Pandolfi, 2011, 2013; Tsoukala and Guérin, 2013, 2016; Pandolfi and Tagliacozzo, 2015; Tsoukala, 2018; Pandolfi et al., 2017, 2021b).

Measurements were taken by digital caliper at 0.01mm precision. Photographs and illustrations were proceeded with GIMP Development Team. All data were analyzed with the software R (R Core Team, 2020). The revised Quaternary time scale (Gibbard et al., 2010) is used for chronological references in this text; Pliocene boundaries are placed at 5.4 Ma and 2.6 Ma. Measurements are given in the Appendix.

Abbreviations:

Capital letters for upper teeth, normal letters for lower teeth.

APD3tr: anteroposterior diameter of the third trochanter; APDanp: anteroposterior diameter of the anconeal process; APDb: antero-posterior diameter of the beak; APDm: antero-posterior diameter, taken on medial face; APDmax: maximal anteroposterior diameter; ApDov3tr: anteroposterior diameter over the third trochanter; APDS (in calcaneus): anteroposterior diameter of the tuber calcanei; APDS (in long bones): anteroposterior diameter of the shaft; D for deciduous teeth; DAPD: distal anteroposterior diameter; DAPDl: distal anteroposterior diameter, taken on lateral face; DAPDm: distal anteroposterior diameter, taken on medial face; DP1: depth of the proximal epiphysis, from the greater tubercle summit to the articular head; DP2: depth of the proximal epiphysis, from the lesser tubercle summit to the articular head; DTD: distal transversal diameter; DTDa: distal transversal diameter of the distal articular surface; Fm: Formation; Ha: height in anterior view; Hl: lateral height; Hltr: height of the

lateral lip of the distal trochlea; Hm: medial height; Hmax: maximal height; Hmtr: height of the medial lip of the distal trochlea; Hpa: heigh of the proximal articular surface, in medial view; Hs: height of the sigmoidal incisure; Htl: height of the lateral lip of the trochlea; Htm: height of the medial lip of the trochlea; Lf: psysiologic length; Ll: lateral length; LL: lingual length; Lmax: maximal length; Lmax: maximal width; Lml: Length of the medial lip of the trochlea; Lpa: length of the proximal articular surface; lpa: width of the proximal articular surface; M/m for molars; Mc: Metacarpals; McIII: third metacarpal; McIV: fourth metacarpal; Mt: metatarsal; MtII: second metatarsal; MtIII: theird metatarsal; MtIV: fourth metatarsal; MW: mesial width; PAPD: proximal anteroposterior diameter; PAPDa: anteroposterior diameter of the proximal articular surface; PAPDar: anteroposterior diameter of the proximal articular head; PAPDol: proximal antero-posterior diameter of the olecranon; P/p for premolars; PTD: proximal transversal diameter; PTDa: transversal diameter of the proximal articular surface; PTDar: transversal diameter of the articular head; TD3rd: transversal diameter at the level of the third trochanter; TDcp: transversal diameter of the distal posterior condyles; TDdelt: Transversal diameter at the level of the deltoid tuberosity; TDDmax: maximal distal transversal diameter; TDI: transversal diameter of the trochlea lips; Tdmax: maximal transversal diameter of the bone; TDmp: minimal posterior transversal diameter; TDo3tr: transversal diameter over the third trochanter; Tdof: Transversal diameter of the olecranic fossa; TDS: transversal diameter of the shaft; TDs: transversal diameter of the tuber calcanei; TDst: transversal diameter of the sustentaculum tali; TDtr: transversal diameter of the distal trochlea; Wmax: maximal width.

3. SYSTEMATIC PALEONTOLOGY

Order **Perissodactyla** Owen, 1848

Family **Rhinocerotidae** Gray, 1821

Subfamily **Rhinocerotinae** Gray, 1821

Tribe **Rhinocerotini** Gray, 1821

Subtribe **Rhinocerotina** Gray, 1821

Genus ***Pliorhinus***, Pandolfi et al., 2021

Type species: *Pliorhinus megarhinus (*de Christol, 1834)

Remarks: The species *Rhinoceros megarhinus* de Christol 1841 is one of the first extinct Plio-Pleistocene rhinoceros described by paleontologists. It is repeatedly included into the genus *Dicerorhinus* Glober 1841, represented by the extant species *Dicerorhinus sumatrensis* Fisher 1814; however, the two species differ in various diagnostic characteristics (Pandolfi et al., 2016). *R. megarhinus* is also referred to the genus *Dihoplus* based on Heissing's (1999) hypothesis of an evolutionary lineage from the Late Miocene *Dihoplus schleirmacheri* to the Late Pliocene *Dihoplus megarhinus*. Besides, Fortelius et al. (1993) and Cerdeno (1995) included the latter species into *Stephanorhinus*, though there are no important morphological characters in common (Pandolfi et al., 2016). The present study follows the most recent view by Pandolfi et al. (2021b) according to which the genus *Pliorhinus* includes the species *P. miguelcrusafonti* and *P. megarhinus*.

3.1 Site Allatini (ALL)

3.1.1. *Pliorhinus megarhinus*

Material:

A complete radius, LGPUT-ALL OP(7) 131-133

Description

The specimen from Allatini is a well-preserved right radius (Fig. 4), belonging to a sub-adult individual, since the suture between the distal epiphysis and the diaphysis is not completely fused. In anterior view (Fig. 4, A), the coronoid process is prominent forming an obtuse angle with the proximal border. In the same view, the radial and lateral tuberosities are evident, the posterior process is damaged, the proximo-medial border is convex, and the proximo-lateral border is straight and slightly shorter than the medial one; the medial border is longer and more downwards directed than the lateral one. In posterior view (Fig. 4, B), a triangular lateral articular surface for the ulna is

present, while the medial one is not preserved. In proximal view (Fig. 4, C), the medial articular surface is sub-squared, with a convex anterior border and roughly convex medial border. The anterior border of the proximal articulation is slightly concave at the level of the coronoid process. The posterior lateral border of the proximal epiphysis is roughly straight forming a ~45º angle with the posterior medial border.

Figure 4 P. megarhinus *radius from Allatini, in A. anterior, B. posterior, C. proximal and D. distal view. Scale bar 50 mm.*

On the distal epiphysis and in anterior view, the styloid process is prominent. The distal border of the articular surface for the semilunar is convex, with convex distal outline. In distal view (Fig. 4, D), the posterior portion of the articular surface for the scaphoid extends backwards. The anterior border of the epiphysis is concave at the level of the extensor carpi radialis. The articular surface for the semilunar is

mediolaterally concave; that for the scaphoid has rather concave anterior portion and convex posterior portion. The medial border of the articular surface for the scaphoid is straight, and the lateral border of the articular surface for the semilunar is slightly concave.

Comparison

The specimen from Allatini differs from *S. jeanvireti* which has, in anterior view a straight medial border and, in posterior view, a less protruding posterior process (Tsoukala, 2018). Additionally, the radius of *S. jeanvireti* from Angelochori, has in proximal view a more marked concavity in the anterior border in respect with the studied specimen. In distal view, the radius from Allatini differs from the radius of *S. jeanvireti* from Vialette, France, by a more convex posterior border of the articular surface for the scaphoid (Guérin, 1972; Tsoukala, 2018). The Allatini radius differs from *P. miguelcrusafonti*, since the latter displays, in anterior view, a less developed lateral tuberosity and a concave lateral and straight medial proximal borders (Guérin and Santafe-Llopis, 1978; Pandolfi et al., 2021b). The studied specimen differs from *S. etruscus* which has a less developed brachii biceps in anterior view and a weakly concave posterior border and a straight postero-medial border in proximal view.

The specimen from Allatini shares several common characters with *P. megarhinus*, such as an enlarged posteriorly articular surface for the scaphoid in distal view; a convex medial-proximal border and a straight lateral-proximal border in anterior view (Pandolfi et al., 2016, 2021b).

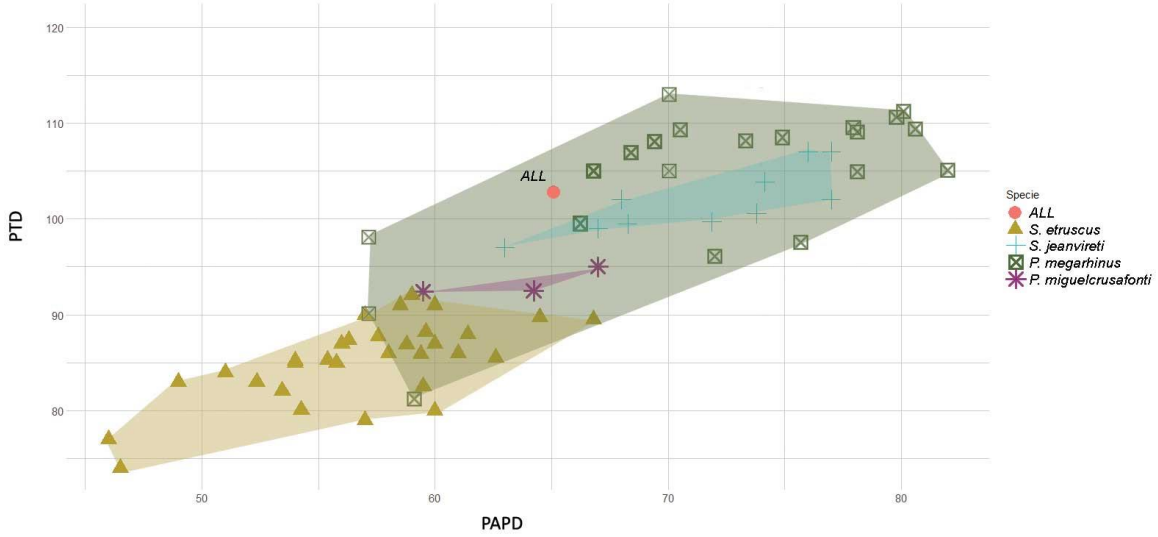

Figure 5 *Scatter plot of PTD and PAPD (in mm) of the radius from Allatini, data from: Guérin and Heintz (1971); Guérin (1972), (2004); Guérin and Santafe-Llopis (1978); Apostol and Enache (1979); Mazza (1988a); Fortelius et al. (1993); Mazo (1997); Kahlke (2001); Fukuchi et al. (2009);*

Guérin and Tsoukala (2013); Pandolfi (2013); Tsoukala and Guérin (2016); Pandolfi et al. (2017), (2021b).

The PTD and PAPD (Fig. 5) of the radii of S*. jeanvireti* and *P. megarhinus* are strongly overlapping. The specimen of Allatini is closer to the smaller known values for *P. megarhinus,* though it is a young individual. Considering only the biometrical comparison, it is not possible to discriminate between *P. megarhinus* and *S. jeanvireti* by the proportions of the proximal epiphysis.

The proportions of the distal epiphysis (Fig. 6) clearly distinguish the range of *S. etruscus* radius from that of the other species. The specimen of Allatini is close to the minimum values of *P. megarhinus* and *S. jeanvireti*, and larger than the specimens of *P. miguelcrusafonti*.

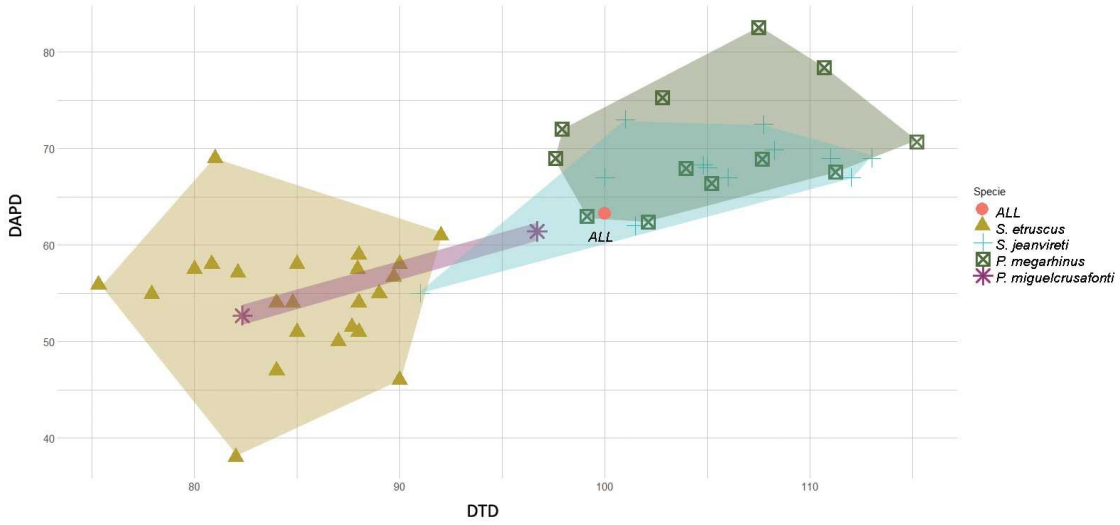

Figure 6 Scatter plot of DTD and DAPD (in mm) of the radius, data from: Guérin and Heintz (1971); Guérin (1972), (2004); Guérin and Santafe-Llopis (1978); Apostol and Enache (1979); Mazza (1988); Fortelius et al. (1993); Mazo (1997); Kahlke (2001); Fukuchi et al. (2009); Guérin and Tsoukala (2013); Pandolfi (2013);Tsoukala and Guérin (2016); Pandolfi et al. (2017), (2021b).

Order **Perissodactyla** Owen, 1848

Family **Rhinocerotidae** Gray, 1821

Tribe **Rhinocerotini** Gray, 1821

Genus ***Stephanorhinus*** Kretzoi, 1942

Type species*:* *Stephanorhinus etruscus* Falconer, 1868

3.2 Site of Dafnero (DFN)

3.2.1 *Stephanorhinus* sp.

Material:

DFN-341 premolar

Description:

The specimen DFN3-341 (Fig. 7, A) is an upper premolar of an individual aging between 10-21 years old, based on Louguet (2002) methodology, thus considering the shape, it could be a P2.

*Figure 7 The specimens from Dafnero-3 (DFN). The premolar (*Stephanorhinus *sp.) DFN-341 in A. occlusal view, and the McIII (*Stephanorhinus *cf.* jeanvireti*), DFN-340 in B. proximal, C. anterior and D. posterior view. Scale bar 50 mm.*

3.2.2 Stephanorhinus cf. *jeanvireti*

Material:

DFN-340 McIII

Description:

The specimen DFN3-340 (Fig. 7, B-D) is a complete left McIII quite well preserved however deformed (compressed antero-posteriorly). In proximal view, the anterior border of the proximal epiphysis is convex. The proximal articular surface is wider antero-posteriorly with extended postero-lateral border and a rather pentagonal shape, in proximal view (Fig. 7, B).

In anterior view (Fig. 7, C), the proximal border is concave and protrudes proximally. In lateral view, the anterior articular surface for the uncinate is damaged, although it looks wider than the posterior one for the McIV. It is located more proximally than the posterior one, in contact with the proximal articular surface. As a result, they create a saliency, which corresponds to the most proximal part of the bone. It is separated from the posterior articular surface with a strong wide and deep groove. The posterior articular surface is flat, quite triangular but elongated proximo-distally. In medial view, the medial articular surface is oval shaped with the posterior corner more obtuse and pointed. The medial articular surface is flat and in contact with the proximal articular surface, creating a crest. The diaphysis is transversally more developed, although it is crashed. The cross section is oval with flattened anterior and posterior borders. In anterior view, the distal epiphysis is symmetrical with a convex proximal border. The articulation is narrower than the epiphysis and the lateral trochlea slightly greater extended than the medial one.

Comparison

The specimen DFN-340 differs from *S. etruscus* as per the proximal articular surface which is more developed antero-posteriorly and the concave anterior border, in proximal view. It differs from *S. hundsheimensis*, at the more protruding medial crest and the more concave proximal border in anterior view. Likewise, it differs from *S. hemitoechus* because the latter taxon preserves a groove delimiting the proximal articular surface in anterior view, plus the distal articular surface has the same width with the distal epiphysis (Pandolfi and Tagliacozzo, 2015). It differs from *S. kirchbergensis*, in the proximal articular surface, as it is more elongated transversally than antero-posteriorly, in proximal view (Kahlke, 1975). It shares common characters with *S. jeanvireti,* such as the concave proximal border in anterior view and the protruding crest (Tsoukala, 2018). However, it differs from *S. jeanvireti* from Millia, at the more elongated transversally proximal articular surface (Guérin and Tsoukala, 2013).

The specimen DFN3-340 is deformed, compressed anteroposteriorly, however its maximal length falls into the range of *S. jeanvireti* (Fig. 8).

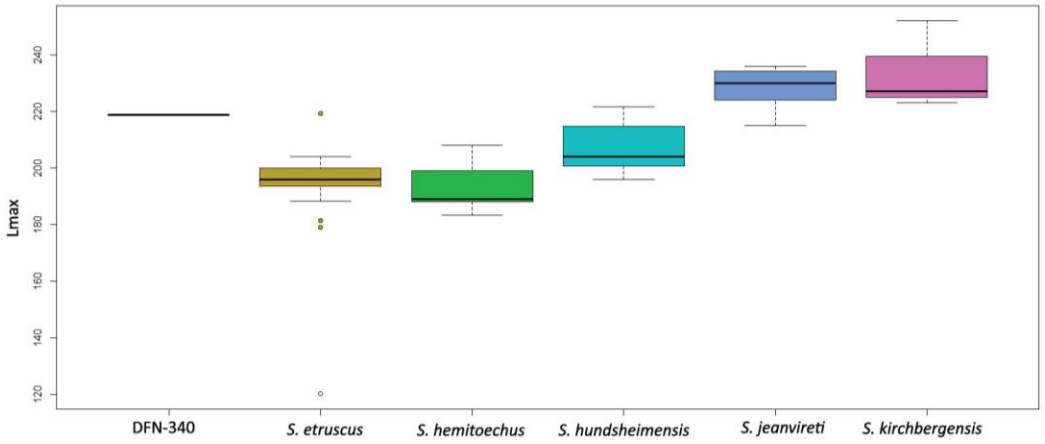

Figure 8 Boxplot of the maximal Length (Lmax) of S. cf. *jeanvireti, specimen DFN-340 (in mm). Data from: Guérin (1973), (1972); Mazza (1988); Cerdeño (1990); Fortelius et al. (1993); Kahlke (2001); Lacombat (2005); Tsoukala (2018).*

3.3 Site Volax (VOL)

3.3.1 Stephanorhinus sp.

Material:

VOL-216 distal epiphysis of MtII

Description:

The specimen VOL-216 is a distal epiphysis and part of the diaphysis of a quite damaged MtII with limited morphological characters preserved, such as the narrow and symmetrical distal trochlea (Fig. 9, A).

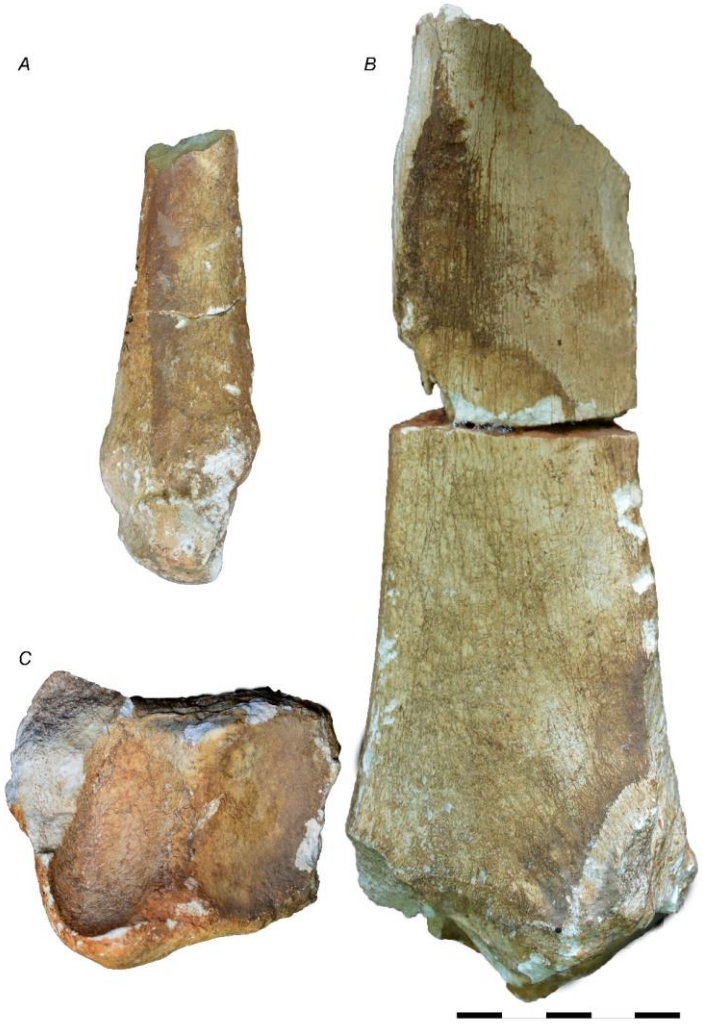

Figure 9 The specimens from Volax. The tibia VOL-215 of S. etruscus *(B, C) and MtII VOL-216 of* Stephanorhinus *sp. (A). In anterior (A, B) and distal view (C). Scale bar 50mm.*

3.3.2 Stephanorhinus etruscus

Material:

VOL-215, distal epiphysis of tibia

Description

The specimen VOL-215 is a left distal epiphysis of a tibia with part its diaphysis (Fig. 9, B, C). The distal epiphysis is weakly developed transversally with a trapezoid outline and the medial malleolus damaged. The lateral articular surface is wide transversally, and oval shaped. It is slightly concave and double the width of the medial one. The medial articular surface is more concave, narrow, oval shaped, and inclined to the lateral side. The epiphysis preserves strong caudal apophysis, the incisure of the fibula is triangular, high, and flat and the cross section of the diaphysis is triangular, forming a crest at the lateral side.

Comparison

The tibia VOL-215, differs from that of *S. kirchbergensis* which is more elongated transversally than antero-posteriorly with wider medial articular surface (Lobachev et al., 2021). It shares common characters with *S. etruscus* from Poggio Rosso and *S. hundsheimensis*, such as the more antero-posteriorly developed distal epiphysis and the elongated transversally medial articular surface. The development of the medial malleolus is different in *S. hundsheimensis* and *S. etruscus*, however it is damaged in VOL-215 (Kahlke, 2001).

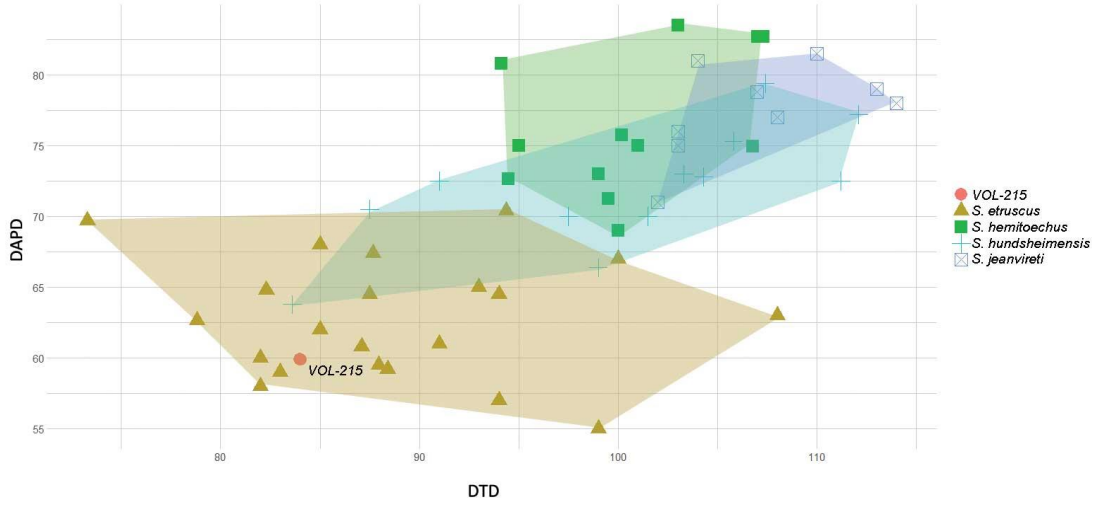

Figure 10 The scatter plot of the Distal Anteroposterior diameter (DAPD) and the Distal Transversal Diameter of tibia, VOL-214 (in mm). Comparative material from: Guérin (1972), (2004); Mazza (1988); Fortelius et al. (1993); Kahlke (2001); Lacombat and Moulle (2005); Guérin and Tsoukala (2013); Pandolfi and Tagliacozzo (2015); Pandolfi et al. (2017).

The metrical comparison of the distal tibia VOL-215 shows that it is dimensionally placed within the range of *S. etruscus* and smaller than other taxa in comparison (Fig. 10). The transversal diameter is approximate because it has been partially damaged. For this reason, there is an extra box plot of the anteroposterior diameter of the distal epiphysis of the Volakas specimen, showing that VOL-215 is within the size variability of *S. etruscus* and close to its mean value (Fig. 11).

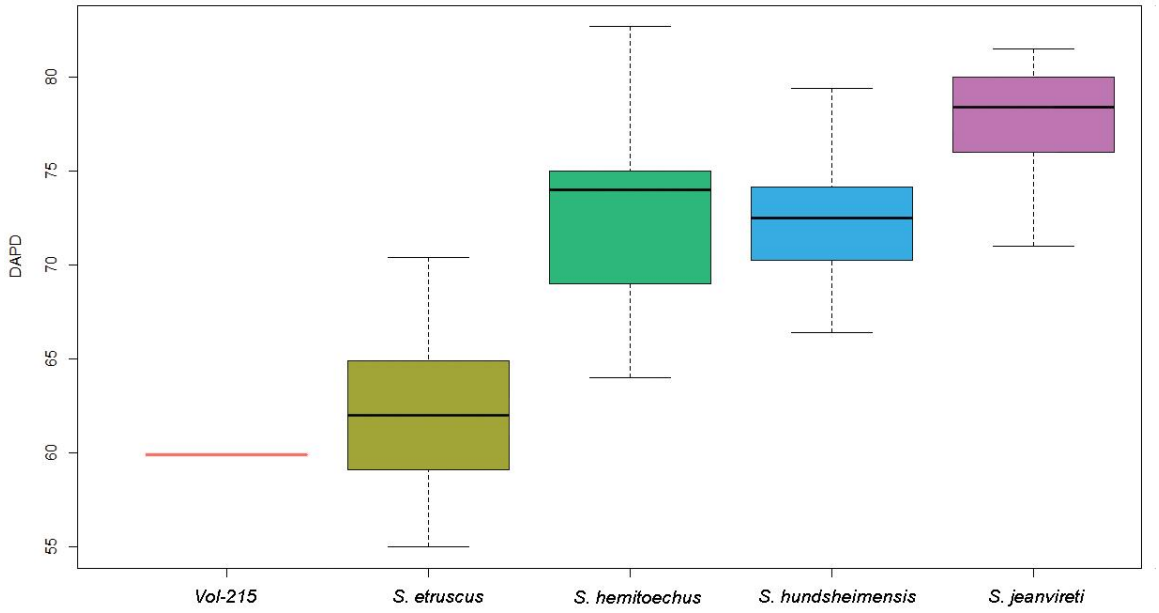

Figure 11 Boxplot of the Distal Anteroposterior diameter (DAPD) of the tibia VOL-215 (in mm). Data from: Guérin (1972), (2004); Mazza (1988); Fortelius et al. (1993); Kahlke (2001); Lacombat and Moulle (2005); Guérin and Tsoukala (2013); Pandolfi et al. (2017).

Site Libakos (LIB)

3.3.3 *Stephanorhinus* sp.

Material:

LIB-336 atlas

Description

The specimen LIB-336 is a well-preserved atlas (C1) (Fig. 12, A-D). In dorsal view, the dorsal tubercle is strongly marked; the left alar notch is well preserved, but the right one is damaged. The alar (suboccipital) foramina are both present, however, the left one is quite damaged. In ventral view, the ventral tubercle is not preserved, and the superior notch is shallow U-shaped. In anterior view, there are the two articular surfaces for the occipital condyles wide and rounded, and the inferior notch forms a slightly obtuse angle. In posterior view, the caudal articular surfaces for the axis are much narrower and elongated transversally.

Comparison

There is limited comparative material for atlas. However, the specimen LIB-336 looks similar to *S. etruscus*, apart from the narrower foramen magnum in cranial view, the wide V-shaped cranial incisure in dorsal arch and in dorsal view, the less proximo-distal diameter of the latter one (Mazza, 1988). The comparison with *S. hemitoechus* can be accomplished only biometrically because there are only sketches available (Tsoukala and Guérin, 2016). The atlas TSR-C15-11a from Tsiotra Vryssi is very deformed for comparison.

Dimensionally LIB-336 is slightly smaller than the atlas of Tsiotra Vryssi, and clearly smaller than *S. hemitoechus* from Petralona (Tsoukala and Guérin, 2016).

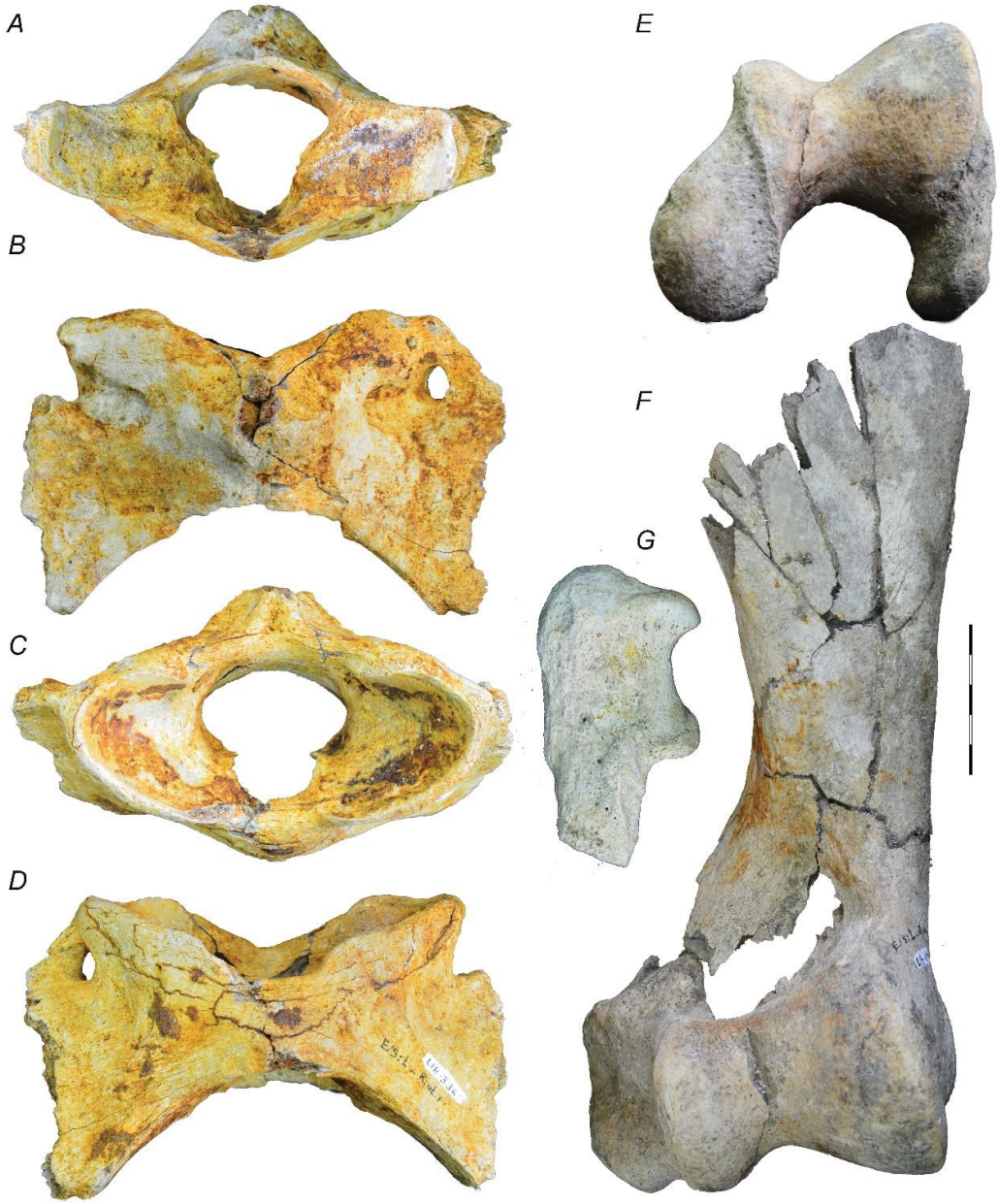

Figure 12 The material from Libakos, Stephanorhinus *sp. atlas LIB-336 (A-D) and* Stephanorhinus etruscus*: LIB-497 humerus (E, F) and LIB-180 calcaneum (F). In distal (A, E), anterior (B, F), proximal (C), posterior (D) and lateral views (G). Scale bar 50mm.*

3.4.2 *Stephanorhinus etruscus*

Material:

LIB-497, distal epiphysis of humerus and its humeral head; LIB-180, calcaneus

Description

The specimen LIB-497 is a distal epiphysis of a right humerus with part of the diaphysis quite well preserved (Fig. 12.E-F). They are in different pieces with the articular head which preserves damaged borders, making it impossible to characterize its shape. The trochlea is asymmetric, with the medial lip much greater and more robust than the lateral one. The medial lip is located higher and has convex medial border. The lateral lip is reduced, short, more rounded, and parallel to the medial lip. In anterior view, the axis of the trochlea is inclined, and the groove separates the two lips is wide and deep, even though the proximal border is shallow and curved. The lateral epicondyle is very robust and strongly protruding laterally, and posteriorly with an enlargement in its distal part. In medial view, the medial epicondyle is strongly developed posteriorly. In distal view, the lateral epicondyle is twice the size of the medial epicondyle and there is a strong groove separating the medial epicondyle from the trochlea. In the posterior view, the coronoid fossa is damaged. The posterior-lateral border of the preserved diaphysis is damaged, and the posterior part of the distal epiphysis is quite damaged with the lateral and medial epicondyles partially preserved. The coronoid and olecranon fossa are both damaged.

The specimen of LIB-180 is a right calcaneus (Fig. 12, G). In lateral view, the proximal tuberosity (summital tuberosity) is reduced. There is a small difference in height of the most proximal part of the bone and the most anterior part of tuber calcanei. The beak and the tuber calcanei have the same width. The posterior border is straight and parallel to the main axis of the bone, with a concavity (a “step”), above the location of the beak. In medial view, the anterior articular surface for the astragalus is at the proximal half convex proximal-distally and concave at the distal half, however it is quite polished. The other two articular surfaces for the astragalus, along with the sustentaculum tali are not preserved. In distal view, the distal articular surface is orthogonal shaped. In anterior view, the lateral border is concave.

Comparison

The humerus specimen LIB-497 shares common characters with *S. etruscus*, especially from Poggio Rosso, Italy, such as the deep trochlear groove and the curved proximal border in anterior view. Those characters make it different from *S. hundsheimensis* from Untermaßfeld which has slightly undulated anterior border and shallower groove of the trochlea (Kahlke, 2001). LIB-497 differs from *S. hemitoechus* as the latter one has, in anterior view, a sinuous medial border of the medial lip of the trochlea (Pandolfi and Tagliacozzo, 2015) and more distally concave groove of the

trochlea. In anterior view, the specimen LIB-497 differs from TSR-G19-13 and APL-408, at the shallow and curved anterior border of the trochlea groove. In distal view, though they are all very similar, LIB-497 preserves a stronger lateral condyle.

The calcaneus LIB-180 shares common characters with *S. etruscus* from Poggio Rosso and Olivola, such as the almost straight posterior border in lateral view and the slightly greater width of the beak in relation to the anterior part of tuber calcanei. It differs from *S. hundsheimensis* in the convex proximally posterior border in lateral view and at the same width of the tuber calcanei and the beak in anterior view (Toula, 1902; Kahlke, 2001). It differs from *S. hemitoechus* in the concave distally posterior border in lateral view (Pandolfi and Tagliacozzo, 2015). The characters distinguish *S. jeanvireti* are not preserved in this specimen. The specimen LIB-180 is very similar with APL-213, except that the latter shows in lateral view a greater difference in heigh between the most proximal part of the summital tuberosity and the anterior point of the more robust tuber calcanei.

The dimensions of the distal epiphysis of the humerus are falling into the variability of *S. etruscus* and *S. hundsheimenis* within the range given by Guérin (1980). *S. etruscus* and *S. hundsheimensis* are strongly overlapping, however the dimensions of the Libakos specimen are close to those from Apollonia and Tsiotra Vryssi.

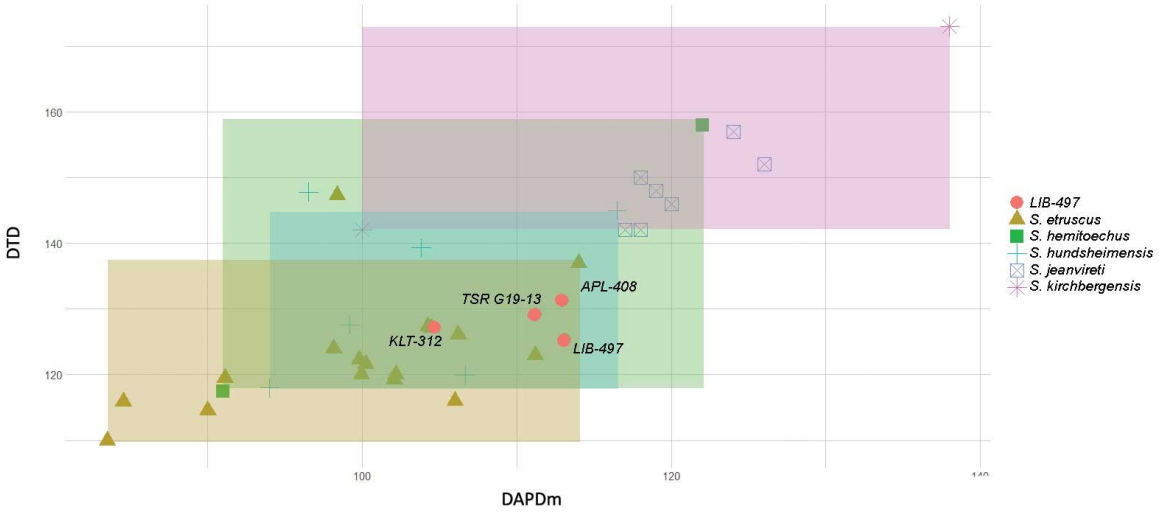

Figure 13 Scatter plot of the distal epiphysis of the humerus (in mm). Data from: Guérin and Heintz (1971); Guérin (1972), (1980), (2004); Mazza (1988); Fortelius et al. (1993); Mazza et al. (1993); Kahlke (2001); Lacombat (2003), (2005); Pandolfi et al. (2017). The square areas represent the range given from Guérin (1980).

The metrical comparison of the calcaneus LIB-180, shows that it is dimensionally placed within the *S. etruscus* range and close to the smaller values of the specimens from Pietrafitta and Valdarno (Fig. 14).

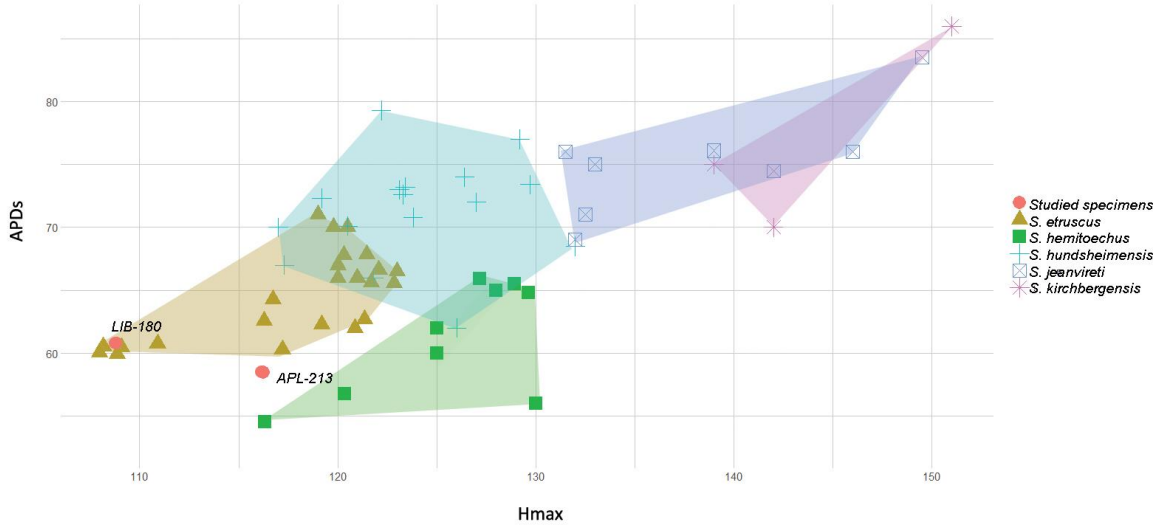

Figure 14 *Scatter plot of the APDS and Hmax (in mm) of the calcaneus of LIB-180 and APL-213 in comparison with European Pleistocene localities. Data from: Guérin (1972), (2004); Guérin and Santafe-Llopis (1978); Mazza (1988); Fortelius et al. (1993); Kahlke (2001); Lacombat and Moulle (2005); Guérin and Tsoukala (2013); Pandolfi and Tagliacozzo (2015); Tsoukala and Guérin (2016); Pandolfi et al. (2017)*.

3.4 Site Tsiotra Vryssi (TSR)

3.5.1 Stephanorhinus sp.

Material:

TSR-G17-6, TSR-F20-24 maxillar; TSR-D18-24, mandibular rami with right p2-p4 and left p4; TSR-G21-47, right D4; TSR-F14-19, right P4; TSR-E19-9, left M2; TSR-D19-8, left M3; TSR-165, right M3; TSR-E19-10, right M3, TSR-F14-4, TSR-G21-29 right lower molar; TSR-F20-14, left lower fragment of tooth; TSR-G21-21, right lower tooth; TSR-C15-11a, atlas; TSR-C15-11b, axis; TSR-C15-11c, third vertebra; TSR-D13-22, distal epiphysis of a left humerus; TSR-E20-8, right ulna; TSR-G16-16, left proximal epiphysis of ulna; TSR-G21-71 right ulna (articulated with TSR-G21-70, radius); TSR-G21-70, proximal epiphysis of right radius; TSR-36, right proximal epiphysis of McIII.

Description

The specimen TSR- G17-6 is a maxilla with very worn out right and left P2-M3; further, the left one lacks the M1. Diagnostic features can not be observed at this stage of wear, that compared with the extant *Diceros bicornis* (Louguet, 2002), corresponds to an individual with an estimated age between 25-40 years.

The specimen TSR-F20-24 is a left maxilla with P3-M3 poorly preserved. A few characters can be detected: including the partially vestibular cingulum and the base of a strong paracone fold at P4; a double crochet at M1; a multiple (3) crochet, (or a double crochet and a single crista) without any vestibular cingulum in M2; and single crochet, no crista and anticrochet with horizontal vestibular cingulum in M3.

The specimen TSR-D18-24 are two mandibular rami with the left p2-p4 and right p4 preserved (Fig. 15, A). Their poor preservation limits the description and comparison because either the talonid or the trigonid of each tooth is damaged. The right p4 is an exception, preserving the U-shaped lingual valleys whose bottoms have great height difference. Additionally, it has deep and wide vestibular groove. Besides, the left side teeth preserve deep and wide vestibular grooves and the p3 has a U- shaped posterior lingual valley.

The specimen TSR-G21-47 is a right upper D4 (Fig. 15, B), well preserved. It has trapezoidal outline, single strong crochet, no crista, no antecrochet, closed mediofossette and weak protocone constriction. There is a mesial continuous horizontal prominent cingulum and a strong paracone fold and mesostyle developed. The specimen TSR-F14-19 in a right P4 (Fig. 15, C), with single crochet and crista, quite worn out with closed lingual valley and remains of a mesial cingulum.

The specimen TSR-E19-9 is a poorly preserved left M2, with single crochet and single crista. The specimen TSR-D19-8 is a partially preserved left M3 with double crochet, single antecrochet, no distal cingulum, and a quite strong paracone fold. The specimen TSR-165 is a poorly preserved right upper M3 with double crochet (the second

is not preserved but its “root” is present), no crista. The partially preserved paracone fold looks strong and there is a distal oblique, continuous poorly preserved cingulum. The specimen TSR-E19-10 is a right M3 with the distal part preserved (Fig. 15, D). It presents double crochet, absent antecrochet, open mediofossette; the right angle between the metacone and the crochet is not preserved. The paracone fold is broad and prominent with a partially distal, oblique strong cingulum preserved.

The specimen TSR-F14-4 is a quite damaged lower tooth right orientated. It shows an open and shallow vestibular groove, a distal cingulum that looks oblique but not fully preserved. Likewise, the specimen TSR-G21-29 is a right lower molar very damaged with an acute angle of vestibular groove (Fig. 15, E). In addition, there is a small vestibular cingulum at the talonid and partially preserved trigonid. The specimen TSR-F20-14 is a fragment of a left lower tooth, based on the size probably molar. The specimen TSR-G21-21 is right orientated fragment of tooth, with shallow vestibular grove.

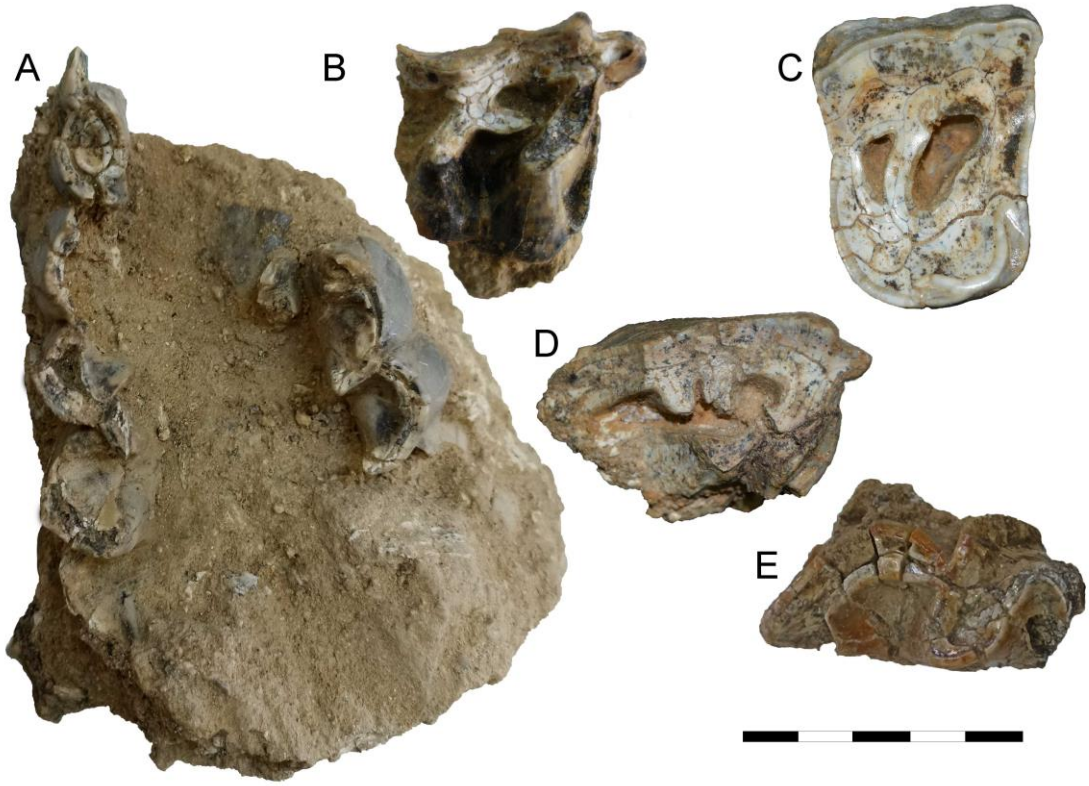

Figure 15 Stephanorhinus sp. *from Tsiotra Vryssi in occlusal view. TSR-D18-24, madibular rami with left p2-p4 and right p4 (A), TSR-G21-47, right D4 (B), TSR-F14-19, right P4 (C), TSR-E19-10, right M3 (D) and TSR-G21-29, right molar (E). Scale bar: 50mm.*

The atlas TSR-C15-11a (Fig. 16 A-C) is a quite well-preserved specimen with the transverse process damaged and slightly deformed. In dorsal view, the dorsal tubercle is robust; the alar (suboccipital) foramina are both present, however, the left one is quite

damaged. In ventral view, the ventral tubercle is visible, protruding posteriorly, and deformed. In anterior view, there are the two articular surfaces for the occipital condyles, but the inferior notch and part of the left articular surface are damaged. The superior notch is shallow U-shaped. In posterior view, the caudal articular surfaces for the axis are much elongated transversally.

The axis of TSR-C15-11b (Fig. 16, B-D) is similarly deformed but quite well-preserved. The dorsal arch is more robust to the ventral side. The anterior articular surfaces are elongated transversally. The centrum is partially preserved, the vertebral canal is filled with sediment, as well as the transverse foramen. The odontoid process is not preserved. The posterior articular process is partially preserved at the right part.

The specimen TSR-C15-11c, a third vertebra (C3) which is very damaged and in poor state only preserving remains of the left transverse foramen and part of its transversal arc.

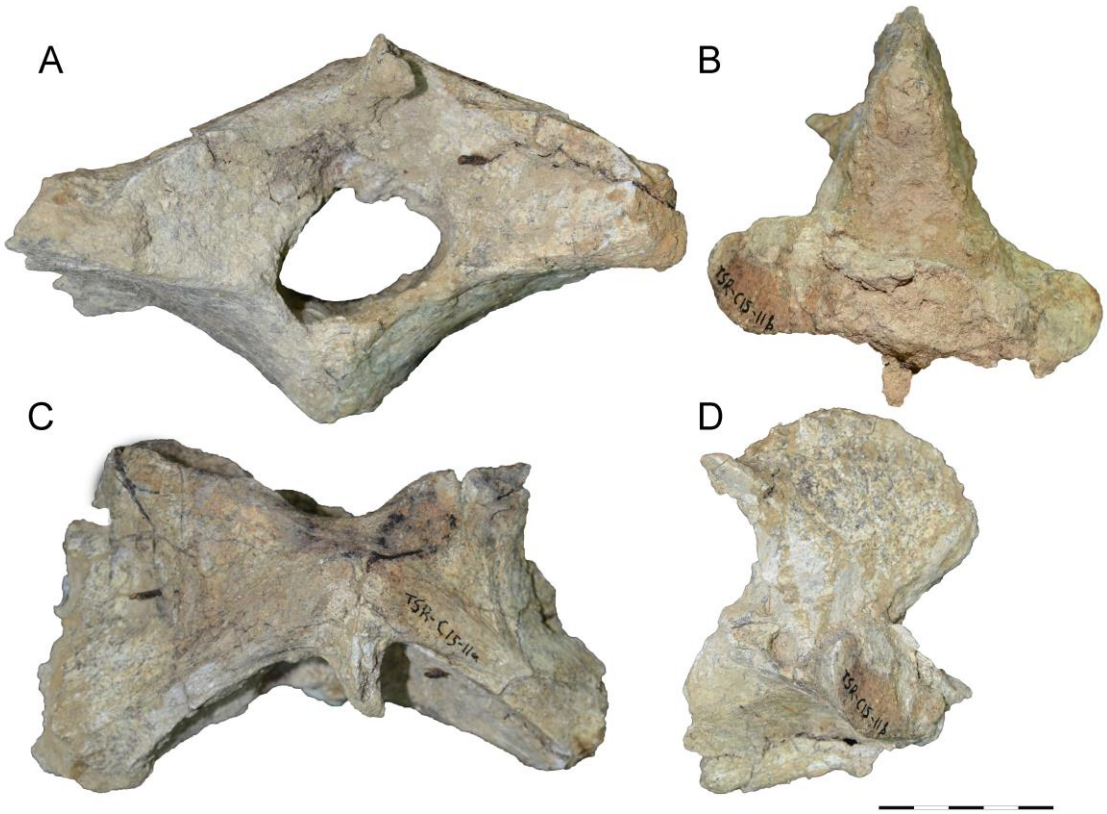

Figure 16 The specimens of Stephanorhinus *sp. TSR-C15-11a (A, C) and TSR-C15-11b (B, D), in A-B proximal, C anterior and D lateral view. Scale 50mm.*

The specimen TSR-D13-22 is a left humerus, badly preserved that looks transversally elongated. The medial lip of the trochlea is curved and slightly concave.

The axis of the trochlea is oblique, and the groove is deep and wide. In posterior view, the olecranon fossa has greater width than height.

The specimen TSR-G16-16 is a left ulna well preserved with the proximal epiphysis and part of the diaphysis but without the olecranon preserved. The trochlear notch is asymmetrical, the difference in height of the distal edge of the medial and lateral articular surface is small. In anterior view, the lateral border of the trochlear notch is concave, while the medial one is rather straight. The lateral border is not parallel with the corpus of the bone. The angle between the two articular surface forms a greek Λ shape. The lateral articular surface is more concave than the medial one plus they are almost perpendicular. The lateral articular surface for the radius, which is very developed, extends towards the lateral articular surface of the trochlear notch. The medial one is much more reduced, extended laterally. In lateral view, the anconeal process projects forward. In lateral view, there is a groove laterally to the lateral articular surface of the trochlear notch. The preserved diaphysis has triangular cross section with flat walls which in medial and lateral views are slightly concave.

The specimen TSR-E20-8 is a right ulna with the proximal epiphysis and part of the diaphysis preserved, without the olecranon. It is very similar with TSR-G21-71, even though the heigh of the lateral articular surface of the trochlea notch in lateral view is smaller. The trochlear notch is asymmetrical, the lateral articular surface is wide in comparison with the more reduced medial one. They form a 90^{o} angle, with the lateral articular surface parallel to the corpus of the bone.

The specimen TSR-G21-71 is a right ulna, articulated with the TSR-G-21-70 (radius), quite well preserved the proximal epiphysis and part of the diaphysis while the olecranon is not preserved. The trochlear notch is highly asymmetrical, the lateral articular surface is more robust and wider, with great heigh difference between the distal part of the medial and lateral articular surface. Both are not as slender as TSR-G16-16, forming a 90^{o} angle, with the lateral articular surface being parallel to the corpus of the bone. In lateral view, the anconeal process is projecting forward, the lateral articular surface is very high and there is a blunt groove laterally. In medial view the medial articular surface is more reduced. The medial and lateral walls of the shaft are slightly concave. In anterior view, the lateral border of the trochlear notch is quite damaged, and the medial is slightly concave. The depression distally the trochlear notch is wide and rather deep. The lateral articular surface for the radius is wide, high, and triangular, while the medial one is elongated transversally.

The specimen TSR-G21-70 is a right proximal epiphysis with part of the diaphysis of a well-preserved radius (Fig. 20, C-F), articulated with the specimen TSR-G21-71 (ulna). In proximal view, the medial articular surface is damaged at the medial and anterior part, the lateral articular surface is concave and square with rounded edges. Its posterior border is straight and obliged, forming a 45^{o} angle. The posterior border of the entire articulation forms an obtuse angle, ~ 120^{o}. In anterior view, both radial and

lateral tuberosities are evident. In anterior view, the proximo-lateral border is concave whilst the lateral is almost straight.

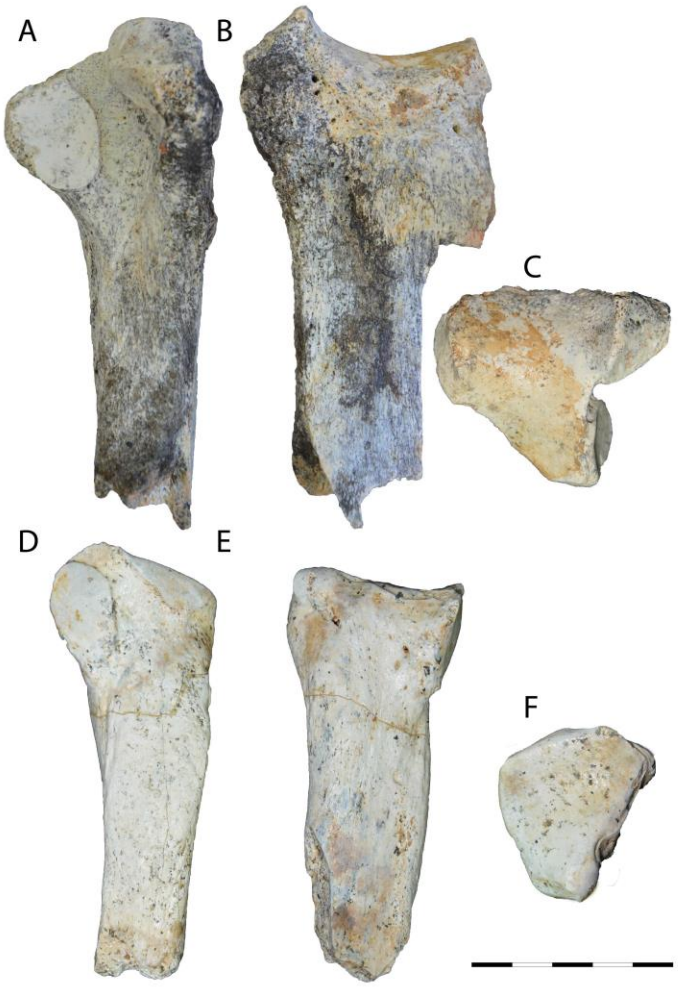

Figure 17 Stephanorhinus *sp. McIII TSR-36 (A-C) and* S. *cf.* hundsheimensis *McIV TSR-F18-67 (D-F), in lateral (A), anterior (B, E), proximal (C, F) and medial (D) view. Scale 50 mm.*

The specimen TSR-36 is a proximal epiphysis with part of the diaphysis of a quite well preserved right McIII (Fig. 17, A-D). In proximal view, the anterior border is slightly convex. The proximal articular surface is trapezoidal, convex anteroposteriorly, and concave proximolaterally. In anterior view, the crest separating the proximal articular surface with the lateral anterior articular surface for the uncinate is acute and the most anterior point of the bone greatly differentiate in heigh from the medial crest. There are two tuberosities in anterior view, one at the lateral part and one in the middle of the diaphysis, distally to the distal border of the proximal articular surface. In lateral view, there are two articular surfaces, the anterior is quite damaged at the distal part, with the most proximal being triangular and the distal elliptic. The overall shape of both articular

surfaces is oval shaped. The anterior articular surface, in the lateral view, is located higher than the posterior articular surface. The flat, large oval shaped posterior articular surface is protruding posteriorly. The two articular surfaces of the lateral view are separated by a strong, wide groove. In medial view, the articular surface for the McII has semi-circular shape and it is flat. There is a much smaller articular surface distally, triangular shaped.

Comparison

The preserved dental material from Tsiotra Vryssi is mostly fragmented and at the case of the maxilla, very worn out, limiting the morphological characters. However, the M3 TSR-E19-10 preserves double crochet, which is rarely observed in *S. etruscus* (Guérin, 1980; Lacombat, 2006). The deep and sharp vestibular grooves at the mandibular TSR-D18-24 are characters common in *S. hundsheimensis* (Lacombat, 2006). On the contrary, there are isolated lower teeth with great difference in size, being much larger, in comparison with *S. etruscus* and the dimensions of TSR-D18-24.

The dimensions, proportions, and morphological characters of TSR-G21-48 (DP4) alone are insufficient to distinguish *S. hemitoechus*, *S. etruscus* and *S. hundsheimensis* (Lacombat, 2006). It is referred that the mediofossette is normally open in *S. hundsheimensis*, although the rest of the morphological characters described are present in all the species. Yet, the proportions are much smaller than in *S. kirchbergensis* (Lacombat, 2006).

The humerus TSR-D13-22 is more robust proportionally than the TSR-133 and the olecranon fossa appears wider than TSR-133 (see below). However, this may be an artefact due to the absence of the lateral epicondyle.

The specimen TSR-36, McIII, distinguish from *S. hundsheimensis* in the greater difference between the crest separating the proximal articular surface from the lateral articular surface and the medial crest, plus the less marked medial tuberosity. However, the preserved proximal articular surface look very similar with *S. hundsheimensis* except from the more acute angle between the contact with the lateral articular surface for the uncinate and that of the McIV (Kahlke, 2001). Similarly, it differs from *S. kirchbergensis* in the greater posterior border than the anterior one, plus the concave anterior border in proximal view (Kahlke, 1975), the much higher medial part in anterior view, and the more distally located medial tuberosity in anterior view (Lobachev et al., 2021). It differs from *S. hemitoechus,* in which the proximal articular surface is delimited by a marked groove in anterior view, while in TSR-36 this groove is limited to the proximal articular surface instead of the lateral articular surface. Additionally, the lateral articular surface in *S. hemitoechus* is more vertical and less pointy, resulting to the less concave proximal border of the articular surface in anterior view. The anterior articular surfaces are more horizontally orientated in lateral view in *S. hemitoechus* (Pandolfi and Tagliacozzo, 2015). The TSR-specimen differs from *S. jeanvireti*, in the narrower antero-posteriorly medial part in proximal view and the more elongated transversally proximal articular

surface; the flatter proximal border in anterior view; and the more reduced anterior and posterior articular surfaces in lateral view (Guérin and Tsoukala, 2013).

The specimen TSR-36 shares similar characters with two specimens of *S. etruscus* from Pirro Nord and one from Poggio Rosso, such as the concave proximal articular surface in anterior view, and the shape of the anterior articular surface in lateral view. The shape of the proximal articular surface is the same with TSR-36 in one of the two specimens of Pirro Nord, while the other is more triangular with reduced antero-posterior length and straight medial border. Moreover, the anterior border in proximal view is similar with TSR-36 in one specimen from Pirro Nord, whereas the other has two indentations close to the medial and the lateral borders. One Pirro Nord specimen has more acute proximal border of the posterior articular surface in lateral view. Both Pirro Nord specimens differ though at the much stronger anterior and medial tuberosities seen in TSR-36 and Poggio Rosso.

The dimensions of the specimen TSR-36 (McIII) are close to both *S. hemitoechus* from Lunel-Viel, Torre del Pagliacetto and Grotte Lina and *S. hundsheimensis* from Untermaßfeld (Fig. 18). Most of the specimens of *S. etruscus* are close to the smaller values, however there is one specimen from Senèze (Se1756) which is significant larger and close to the size of *S. jeanvireti* from Millia. This specimen (Se1756) is larger (greater transversal diameter) than *S. hemitoechus* and almost as large as *S. hundsheimensis* (excluding a specimen). There is no comparative material for *S. kirchbergensis.*

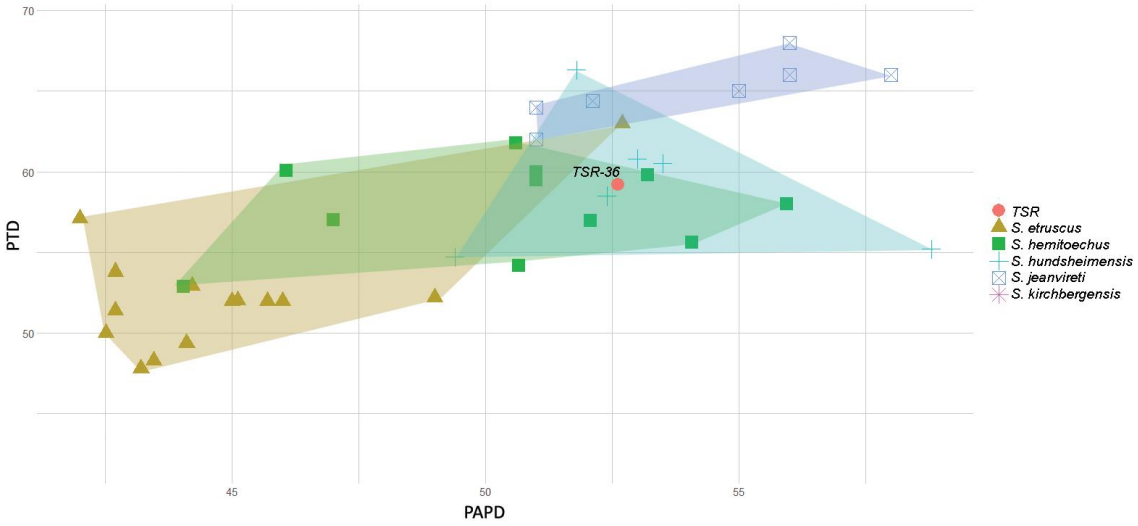

Figure 18 The scatter plot of PTD and PAPD of McIII TSR-36 (in mm). Comparative material retrieved from: Guérin (1972), (1973); Mazza (1988); Cerdeño (1990); Fortelius et al. (1993); Kahlke (2001); Lacombat (2005); Lacombat and Moulle (2005); Tsoukala (2018).

3.5.2 Stephanorhinus etruscus

Material:

TSR-133, distal epiphysis of a left humerus; TSR-G21-73, proximal epiphysis of left ulna; TSR-G21-72, TSR-C17-7 proximal epiphysis of left radii; TSR-50, distal epiphysis of right tibia; TSR-F18-64b, navicular, cuboide, 1st cuneiform, 2nd cuneiform, 3rd cuneiform; TSR-F18-64a, MtII, MtIII, MtIV articulated with TSR-F18-64b.

Description

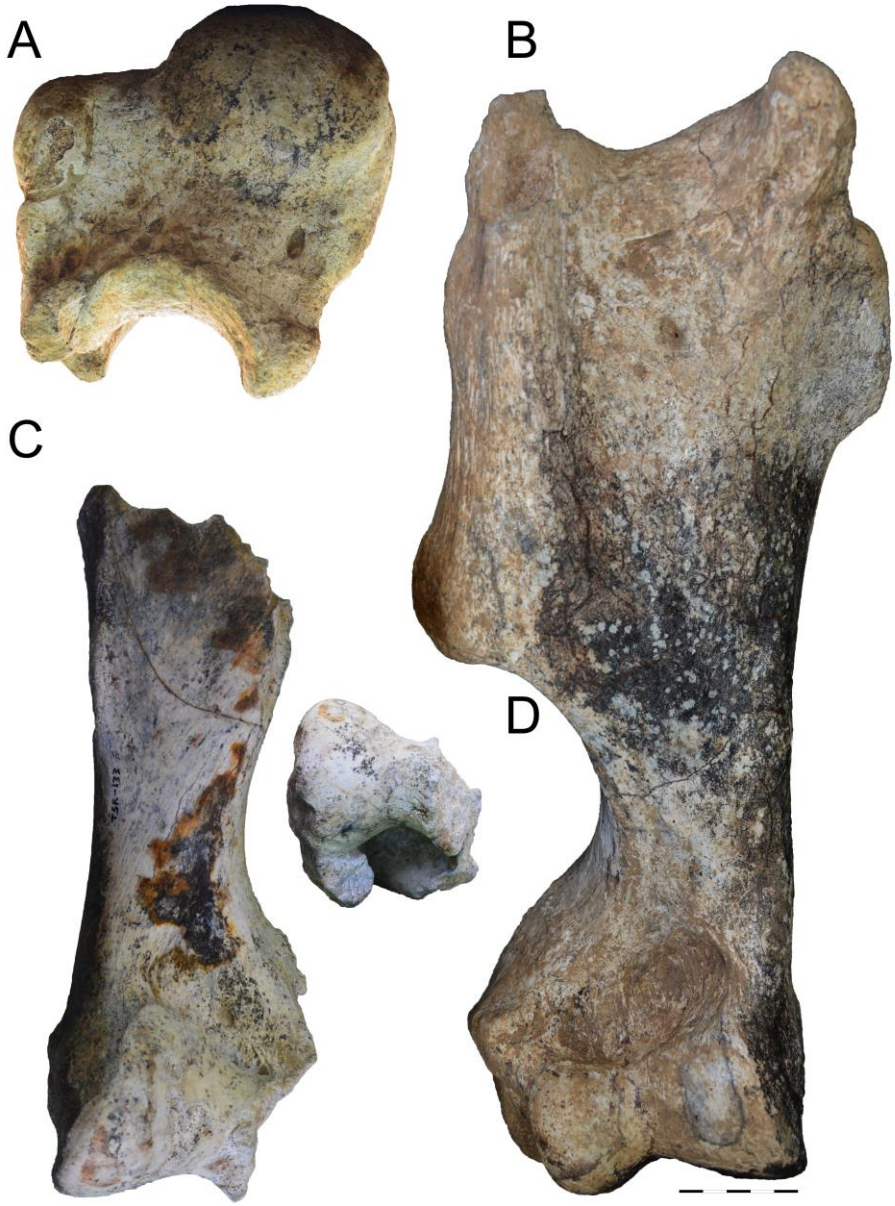

Figure 19 Humeri of S. etruscus *TSR-133 (C) and* S. *cf.* hundsheimensis *TSR-G19-13 (A, B, D) in A. proximal, B-C anterior and D. distal view. Scale bar 50mm.*

The specimen TSR-133 (Fig. 19. C) is a left humerus with taphonomic features such as a pit in the olecranon fossa; a score in the articular trochlea, a furrowing resulting the absence of the lateral tuberosity and part of the lateral lip of the trochlea and punctures at the proximal part of the diaphysis (Konidaris et al., 2015). There is part of the diaphysis preserved with the medial epicondyle. In anterior view, the medial lip of the trochlea has its proximal border straight and then descending towards the trochlea groove. The medial border of the lip is convex, and the trochlea is moderately oblique. In posterior view, the olecranon fossa is deep and high having a triangular shape.

Figure 20 Radii from TSR, in proximal view (A-C) and anterior view (D-E). Stephanorhinus etruscus*: TSR-C17-7 (A, D), TSR-G21-72 (B, E) and* Stephanorhinus *sp. TSR-G21-70 (C, F). Scale bar 50mm.*

The specimen TSR-G21-73 is a quite well-preserved left ulna without the olecranon, articulated with the TSR-G21-72. The trochlear notch is asymmetrical with small difference in heigh of the distal edge of the medial and lateral articular surfaces. In anterior view, the lateral border of the trochlear notch is concave while the medial border of the medial articular surface is damaged. The lateral articular surface is less slender and parallel with the corpus of the bone. Both are perpendicular. The lateral articular surface for the radius is reduced and more distinct from the trochlear notch, the medial one is like a stripe. In lateral view, there is a moderately marked groove laterally the trochlear notch, and an anconeal process that strongly projects forwards.

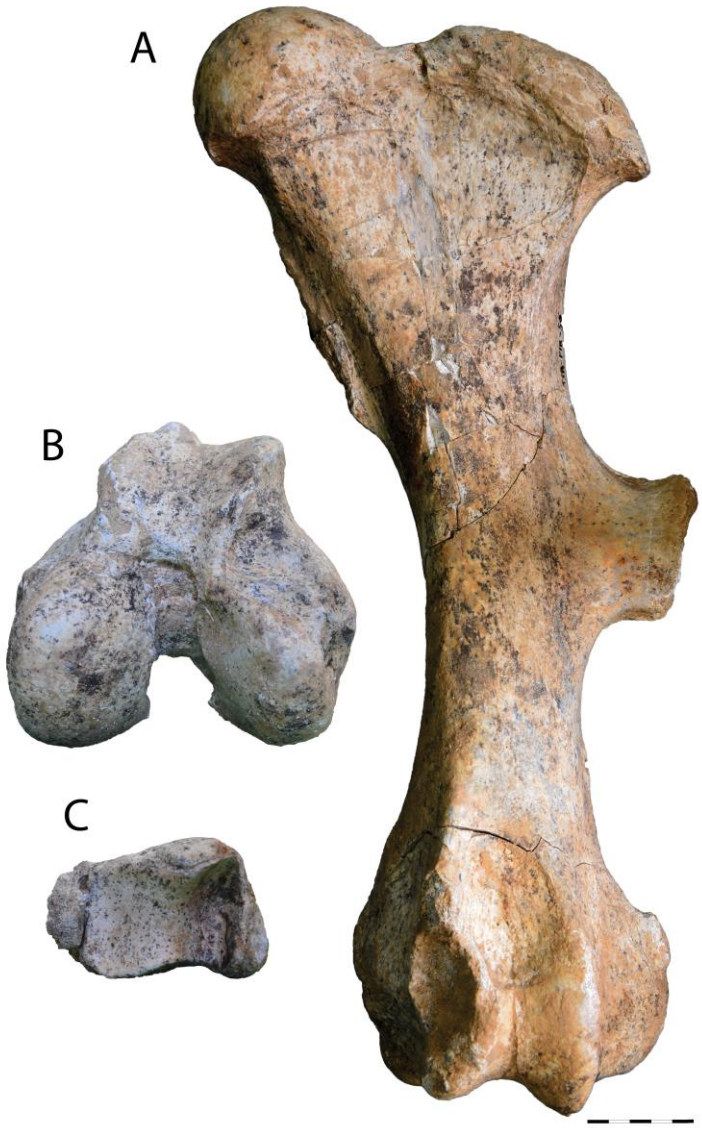

Figure 21 Femori specimens of S. *cf.* hundsheimensis *TSR-F18-56 (A, B) and* S. etruscus *TSR-50 (C), in anterior (A) and distal (B, C) views. Scale bar 50mm.*

The specimen TSR-G21-72 is a left proximal epiphysis of a radius with part of the diaphysis well preserved (Fig. 20, B-E). In proximal view, the medial articular surface is square shaped with a curved medial border whose anterior corner is slightly protruding anteriorly. The lateral articular surface is concave and triangularly shaped with convex anterior border. Its posterior border is straight and oblique forming a 45º with the posterior border. The posterior border of the articulation creates an obtuse angle ~120º. The anterior border is concave at the level of the coronoid process, despite the damage medially the coronoid process. In anterior view, the coronoid process is prominent, the brachii biceps is represented by a rounded relief; the lateral tuberosity is marked. The proximal border of the lateral articular surface is concave and smaller than that of the medial articular surface. They form a slightly obtuse angle. In posterior view, the shape of the medial articular surface is as a reduced elongated stripe. The lateral articular surface is very high and triangular shaped.

The specimen TSR-C17-7 is a proximal epiphysis with part of the diaphysis of a well-preserved radius (Fig. 20, A-D). In proximal view, the medial articular surface is sub-square, and the lateral articular surface is triangular with convex anterior border. Its posterior border is straight and oblique (~45º). The anterior border has a marked concavity at the level of the coronoid process. The posterior border of the entire articulation creates an obtuse angle (~120º). In anterior view, the coronoid process is slightly prominent. The brachii biceps are hardly distinguishable. The proximal border of the medial articular surface is slightly smaller than the lateral one. In posterior view, the medial articular surface is quite polished and long like a stripe. The lateral articular surface is triangular shaped and moderately high.

The specimen TSR-50 is a distal epiphysis, of a right tibia quite well-preserved (Fig. 21, C). In distal view, the medial articular surface has the shape of a narrow and deep groove with prominent and rounded medial malleolus. The lateral articular surface is less concave, elongated transversally with a trapezoidal shape. The caudal apophysis is quite prominent. In lateral view, part of the fibula is attached to the specimens not allowing the description of the distal articular surface for the fibula.

The specimens labeled as TSR-F-18-64 are right tarsals (b) and metatarsals (a) of the same individual. The navicular of TSR-F18-64b (Fig. 22, A-B) is quite well preserved, even though the articular surfaces for the cuboid in the lateral face and part of the posterior view are not preserved. In proximal view, the posterior-medial tuberosity is developed. The proximal articular surface for the astragalus occupies the whole proximal view; is almost square with the anterior-medial corner being very rounded and the posterior-medial corner protruding posteriorly. However, the complete shape cannot be described since the lateral border is damaged. There is not great difference in the heigh between the anterior and the posterior view. In lateral view, the proximal border is concave, and the distal border is damaged. In medial view, the posterior tuberosity has moderate development.

The cuboid of TSR-F18-64b (Fig. 22. C) is very polished and rather damaged. The general size is preserved, but in many cases the sponge tissues are exposed. The distal articular surface for the MtIV is quite well preserved though. In anterior view, its shape is almost parallelogram, with the lateral border higher than the medial one. In proximal view, the proximal articular surface for the astragalus and calcaneus has almost trapezoidal shape with vertical and straight borders except from the posterior-lateral corner which is damaged. In medial view, the anterior border is concave, although there are no articular surfaces preserved. In distal view, the articular surface for the MtIV has sub-circular shape, however the borders are rather polished.

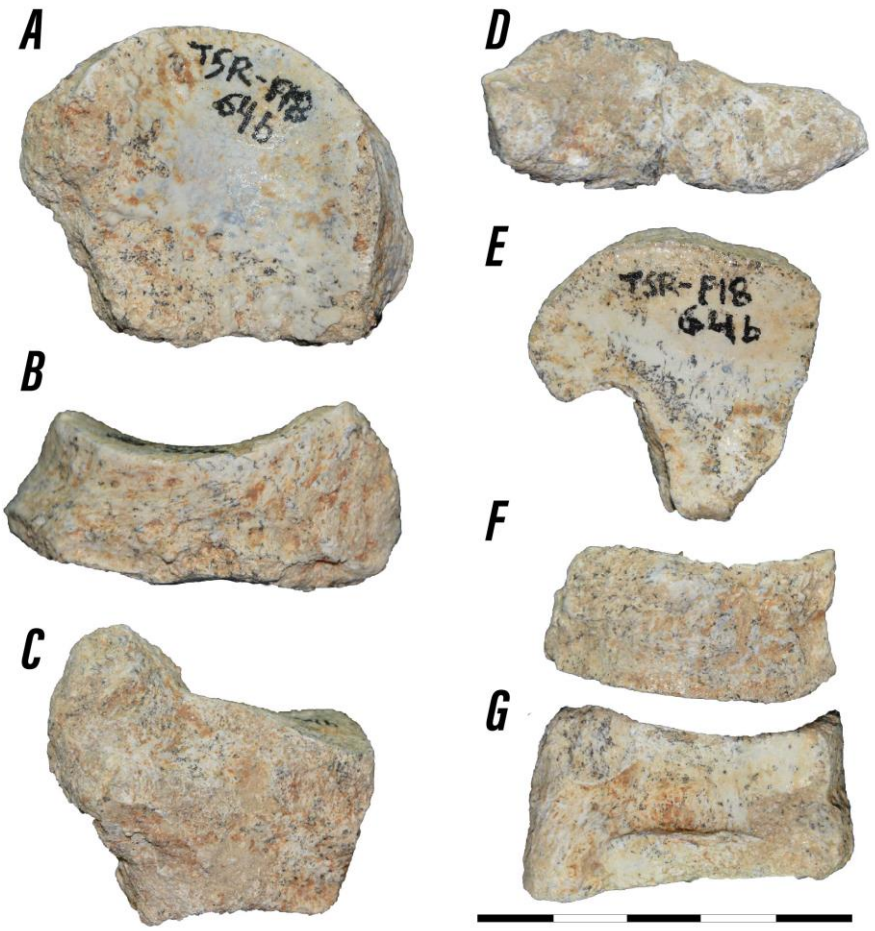

Figure 22 S. etruscus *TSR-F18-64b, the navicular (A, B), the cuboide (C), the 1st cuneiform (D), the 3rd cuneiform (E, F, G). In proximal (A, C, E,), anterior (B, F), lateral (D, G) views. Scale bar 50mm.*

The first cuneiform of TSR-G18-64b (Fig. 22, D) is not well preserved, as it is in two pieces glued and the surface is polished. In lateral view, the specimen is elongated with small difference in width between the most proximal and the most distal part of the bone. In lateral view, at the proximal part, the articular surface is flat, rather sub (semi)

circular and slightly elongated proximo-distally. In proximal view, the proximal articular surface for the navicular is triangular, flat, and occupies all the proximal face. In medial view, there is a tuberosity. In distal view, the articular surface for the MtII is kidney-shaped being wider at the anterior part. At the antero-proximal part of the lateral face, there is a quite damaged articular surface for the 2nd cuneiform, reduced and circular.

In proximal view, the proximal articular surface for the navicular of the second cuneiform TSR-F18-64b is triangular, flat, and occupies all the proximal face. In medial view, there is a tuberosity and the articular surface for the first cuneiform is not preserved. In distal view, the articular surface for the MtII is kidney-shaped being wider at the anterior part and extending towards the lateral. In lateral view, the articular surface for the 3rd cuneiform is a quite damaged, reduced, and circular.

The specimen TSR-F18-64b is a well-preserved right third cuneiform (Fig. 22, E-G) articulated with the other tarsals. In anterior view, the anterior border is convex although the medial border is straight. In proximal view, the articular surface for the navicular, which occupies this face is flat with a concavity running transversally. The posterior border is higher than the anterior one. In lateral view, there are three articular surfaces for the cuboid, the proximal one is elongated transversally. The anterior distal articular surface for the cuboid is larger than the posterior one, semicircular and elongated proximally, occupying the half of the height of the bone. The posterior articular surface is circular, flat, and located more distally. The posterior border in lateral view, is larger than the anterior one, and there is a tuberosity at its proximal part. There is another marked but reduced tuberosity at the anterior proximal part of the lateral face. In anterior view, the outline is almost parallelogram, with the proximal border concave, the distal slightly convex, the lateral border having a concavity at its middle and the medial border straight (vertical). In medial view, there is a strong concavity creating a vertical corner, whereas in the anterior part there is an articular surface that has reduced circular shape and being vertical to the distal articular surface.

The MtII of TSR-F18-64a (Fig. 23, A-B) preserves the proximal epiphysis with part of the diaphysis. In proximal view, the proximal articular surface for the second cuneiform is moderately developed transversally and a triangular shape delimited by a groove, except from the contact with the medial tuberosity and the articular surface for the MtIII at the posterior border. The epiphysis has a triangular outline. The lateral border of the epiphysis is slightly concave. In medial view, there is a relatively strong tuberosity close to the posterior border. In posterior view, the articular surface corresponding to the 1st cuneiform is flat, delimited, by a groove, distinguished from the proximal articular surface, and having parallelogram shape.

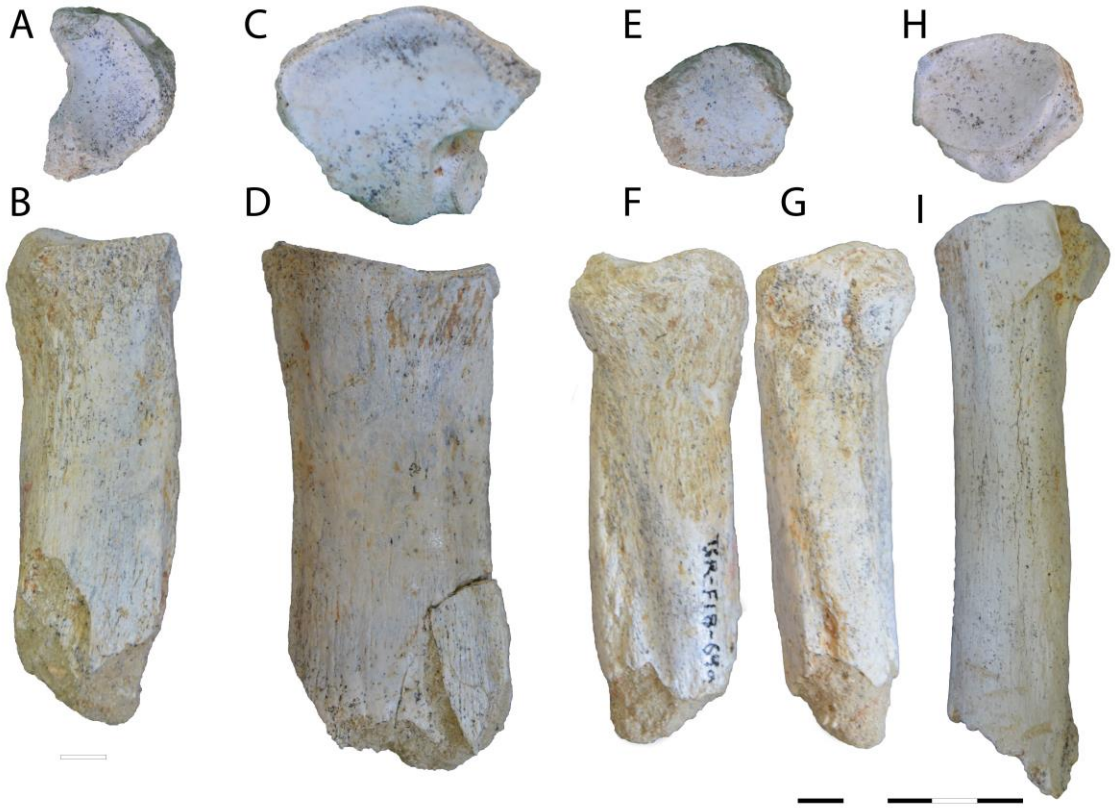

Figure 23 S. etruscus *metatarsals TSR-F18-64a (MtII (A, B), MtIII (C, D) and MtIV (E-G)) and S.* cf. *hundsheimensis MtIV TSR-G16-41 (H, I). Proximal view (A, C, E, H), anterior view (B, D, F) and medial view (G, I). Scale bar in 50mm.*

In lateral view, there are two articular surfaces that are articulated with the MtIII and the 3rd cuneiform. The anterior one is located higher than the posterior one and they are separated with a very wide shallow groove. The anterior articular surface is clearly not in contact with the proximal articular surface for the 2nd cuneiform, slightly protruding and quite damaged at the proximal part. They are separated by a smooth barely visible, slightly concave line. The posterior articular surface is damaged but located lower than the anterior and is in contact with the proximal articular surface for the 2nd cuneiform. The preserved diaphysis is rounded in cross section and quite slender and curved.

The specimen of TSR-F18-64a is a MtIII (Fig. 23, C-D), with the proximal epiphysis and part of the diaphysis well preserved. In proximal view, the epiphysis is occupied from the triangularly shaped proximal articular surface for the 3rd cuneiform. The anterior-lateral corner protruding laterally with a slight concavity at the medial border. It is almost flat, with a slight concavity antero-posteriorly. The anterior border is strongly convex with a slight medial concavity. In anterior view, the proximal border is almost straight and inclined, with great difference in height between the medial and the

lateral corners. There is a tuberosity close to the medial border. In lateral view, there are two articular surfaces articulated with the MtIV, both reduced and almost of the same size, with the anterior slightly larger and located higher. The anterior one is in contact with the proximal articular surface, is trapezoidal shaped, flat and has parallel orientation with the sagittal plane. The posterior articular surface is clearly distinguished from the proximal articular surface for the 2nd cuneiform with a relatively wide groove; it has almost rounded shape, it is flat and strongly angled (~ 30º) compared with the proximo-distal axis. The two articular surfaces for thee MtIV in lateral view, are separated by a strong deep and wide groove with harsh surface. In medial view, there are two articular surfaces for the MtII, much smaller than those of the lateral. The anterior one is located higher than the posterior one, and they are clearly separated and both in contact with the proximal articular surface. The anterior one is flat and triangularly shaped. The posterior one is flat, and trapezoidal shaped. The section of the diaphysis is elliptical shaped with convex anterior and posterior borders.

The MtIV of TSR-F18-64a (Fig. 23, E-G), is a well-preserved proximal epiphysis with part of the diaphysis. The proximal articular surface for the cuboid is sub-square shaped, flat with a slight concavity antero-posteriorly. In lateral view, there is a tuberosity. In medial view, there are two articular surfaces for the MtIII, the anterior one is slightly higher than the posterior. The anterior one is also elongated oval shaped. The posterior articular surface is sub-circular shaped, flat and protrudes from the corpus of the bone. In anterior view, the proximal border is straight with a minor concavity and the lateral border is quite damaged. The section of the preserved diaphysis is trapezoidal-like with rounded corners.

Comparison

The preserved TSR-133 have quite limited diagnostic characters, since it is quite damaged at its lateral part, however, the slender diaphysis is diagnostic of *S. etruscus.* The preserved specimen shares common characters with APL-408 humerus, such as the oblique trochlea and the straight-oblique medial border of the medial lip, in anterior view. However, the TSR-133 has a slender diaphysis.

Regarding the radius specimens from Tsiotra Vryssi, both TSR-C17-7 and TSR-G21-72 are different from *S. jeanvireti* from Angelochori because, the lateral border is larger and more convex in anterior view. Additionally, the posterior angle is not as obtuse as in *S. jeanvireti* (Guérin, 1980; Tsoukala, 2018). The specimens from TSR- have sub-square medial and sub-triangular lateral articular surfaces, which are different from the sub-circular and sub square shape, respectively of *S. hemitoechus* (Pandolfi and Tagliacozzo, 2015). Both specimens share common characters with *S. etruscus*, such as the posterior angle of the entire articulation in proximal view and the concave posterior-lateral border. They differ from the radius of *S. hundsheimensis* in the straighter anterior border and the very obtuse posterior angle of the entire articulation in proximal view, as well as the straighter proximo-medial border and the less concave and wide lateral border in anterior view (Kahlke, 2001). In anterior view, the proximal border

of TSR-C17-1 is undulated forming a more obtuse angle, with less protruding coronoid process than the TSR-G21-72.

The tibia TSR-50 differs from that of *S. hundsheimensis,* as the latter taxon has wider medial articular surface and more prominent medial malleolus in distal view (Kahlke, 2001). Furthermore, it differs from *S. kiechbergensis*, by means of a more elongated transversally epiphysis, wider medial groove, and more rounded lateral articular surface with limited anteroposterior development (Lobachev et al., 2021). TSR-50 shares common characters with *S. etruscus* from Poggio Rosso though, as it is more developed anteroposteriorly, with rounded medial malleolus, and has similar shape of the medial and lateral distal articular surfaces.

The specimen TSR-F18-64b (navicular) shares common characters with *S. etruscus* from Valdarno, Olivola and Poggio Rosso, such as the medial border which is straight and towards the anterior border in proximal view and the moderate development of the posterior tuberosity in medial view. It differs from *S. hundsheimensis*, as in TSR-F18-64b the proximal articular surface is less developed antero-posteriorly in comparison with the proximal face (Kahlke, 2001) and the medial extension of the anterior border is reduced (Pandolfi and Tagliacozzo, 2015). It differs from *S. hemitoechus*, as in TSR-F18-64b the posterior tuberosity is strongly developed and more elongated in shape in medial view (Pandolfi and Tagliacozzo, 2015). It differs from *S. kirchbergensis,* as in TSR-F18-64b the medial border is strongly concave in proximal view and the proximal border looks convex in medial view (Lobachev et al., 2021).

The specimen TSR-F18-64b is a very polished cuboid with limited preserved morphological characters to compare, however mainly in anterior view, the shape of the articular surface look distinctive. In *S. etruscus* from Poggio Rosso and *S. hemitoechus*, both medial and proximal borders are straight and perpendicular to each other, while the proximo-lateral corner is convex (Pandolfi and Tagliacozzo, 2015). In *S. jeanvireti* the medial border has a marked concavity, and the proximo-lateral corner creates a more acute angle (Guérin and Tsoukala, 2013). *S. hundsheimensis* cuboid, is similar to that of *S. jeanvireti*, however the medial border is straight without any concavity (Kahlke, 2001).

The morphological comparison of the second cuneiform is very limited, between *S. etruscus* from Poggio Rosso and *S. hundsheimensis* (Kahlke, 2001). The proximal and distal articular surfaces of *S. etruscus* from Poggio Rosso and TSR-18-64b are more like right triangle in comparison with *S. hundsheimensis* which are equilateral.

The TSR third cuneiform differs from that of *S. hemitoechus,* because in TSR taxon the proximal border is straight in anterior view (Pandolfi and Tagliacozzo, 2015). As for *S. hundseimensis*, it is referred that the proximal border is slightly more concave than in *S. hemitoechus* and the lateral border is slightly higher than the medial one in anterior view (Pandolfi and Tagliacozzo, 2015). However, the different specimens from Poggio Rosso, Olivola and Valdarno show a vast variability at the level of the concavity of the anterior border and differences in height. The specimen TSR-F18-56b shares

common characters with *S. etruscus*, such as the concave proximal border in anterior view, the triangular shape in proximal view and the shaped of the articular surfaces in lateral view.

The MtII (TSR-F18-64a) shares common characters with *S. etruscus* from Olivola, Valdarno, Poggio Rosso and Pirro Nord, such as the elongated transversally proximal articular surface for the second cuneiform with moderate antero-posterior development, the moderate difference in height of the articular surfaces in lateral view, and the concave proximal border in anterior view. It differs from *S. hundsheimensis* in the less antero-posterior development of the proximal articular surface (Pandolfi and Tagliacozzo, 2015). It differs from *S. hemitoechus* in the straighter proximal border in anterior view and the wider groove separating the two articular surfaces in lateral view (Pandolfi and Tagliacozzo, 2015). It differs from *S. jeanvireti* in the much higher location of the anterior articular surface in comparison with the posterior one in lateral view and in the stronger anterior tuberosity (Pandolfi et al., 2019). In addition, it differs from *S. kirchbergensis,* in the much wider articular surface in proximal view, with a marked anteroposterior concavity (Pandolfi and Tagliacozzo, 2015; Lobachev et al., 2021).

The straight and inclined proximal border in anterior view of the MtIII specimen TSR-F18-64a along with the convex anterior border with a slight concavity at the medial part in proximal view are common with *S. etruscus* from Valdarno, Poggio Rosso and Olivola. However, in *S. etruscus* specimens the proximal border may be more concave. TSR-F18-64a differs from *S. hundsheimensis* in the almost horizontal proximal border in anterior view and the less transversally developed proximal articular surface in proximal view (Kahlke, 2001). It differs from *S. hemitoechus,* as TSR-F18-64a preserves strongly concave anterior border with more transversally developed anterior part in proximal view, less inclined proximal border in anterior view, and great difference in height between the two articular surfaces in lateral view (Pandolfi and Tagliacozzo, 2015). It differs from *S. kirchbergensis,* in the much greater difference in height between the two articular surfaces and the sub-elliptical posterior articular surface in lateral view (Kahlke, 1975). It differs from *S. jeanvireti*, in the less inclined proximal border in anterior view and the greater difference in height of the articular surfaces in lateral view (Guérin and Tsoukala, 2013; Pandolfi et al., 2019).

The MtIV from TSR-F18-64a differs from *S. kirchbergensis*, in the triangular shaped proximal articular surface in proximal view and more elongated oval shaped articular surfaces in posterior view (Pandolfi and Tagliacozzo, 2015; Lobachev et al., 2021). No difference between *S. jeanvireti, S. etruscus* and *S. hemitoechus* have been observed*. S. hundsheimensis,* may have a squarer articular surface but the comparison is based only on drawings (Kahlke, 2001; Guérin and Tsoukala, 2013; Pandolfi and Tagliacozzo, 2015; Pandolfi et al., 2019).

The specimen TSR-F18-64a MtIV, differs from TSR-G16-41, since the latter has more transversally elongated proximal articular surface in proximal view and is

proportionally larger. Additionally, in medial view, the articular surfaces have different shape, plus the posterior articular surface is in contact with the lateral tuberosity, resulting a posterior extension.

The dimensions of the diaphysis of TSR-133 are close to the larger sized *S. etruscus* and into the variability of *S. hundsheimensis* (Fig. 24).

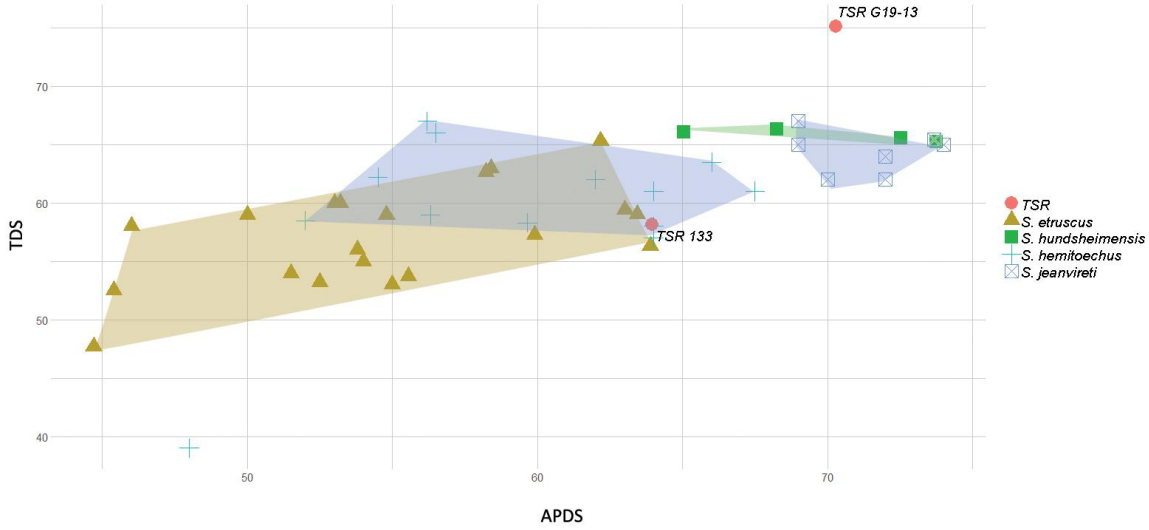

Figure 24 The scatter plot of TDS and APDS of the humeri specimens from TSR-(in mm). Data from: Guérin and Heintz (1971); Guérin (1972), (2004); Mazza (1988); Fortelius et al. (1993); Mazza et al. (1993); Kahlke (2001); Lacombat and Moulle (2005); Pandolfi (2011); Pandolfi and Tagliacozzo (2015); Pandolfi et al. (2017).

The biometrical comparison of the proximal epiphysis of the radius of the specimens from Tsiotra Vryssi, shows that they are dimensionally into the variability of *S. etruscus* and close to the smaller values of *S. hundsheimensis* (Fig. 25), with the transversal development alone being into the variability of *S. hundsheimensis*. The comparative specimens closer to the dimensions of TSR specimens are from Saint Vailler (Drome) (*S. etruscus)* and Mosbach (*S. hundsheimensis)*.

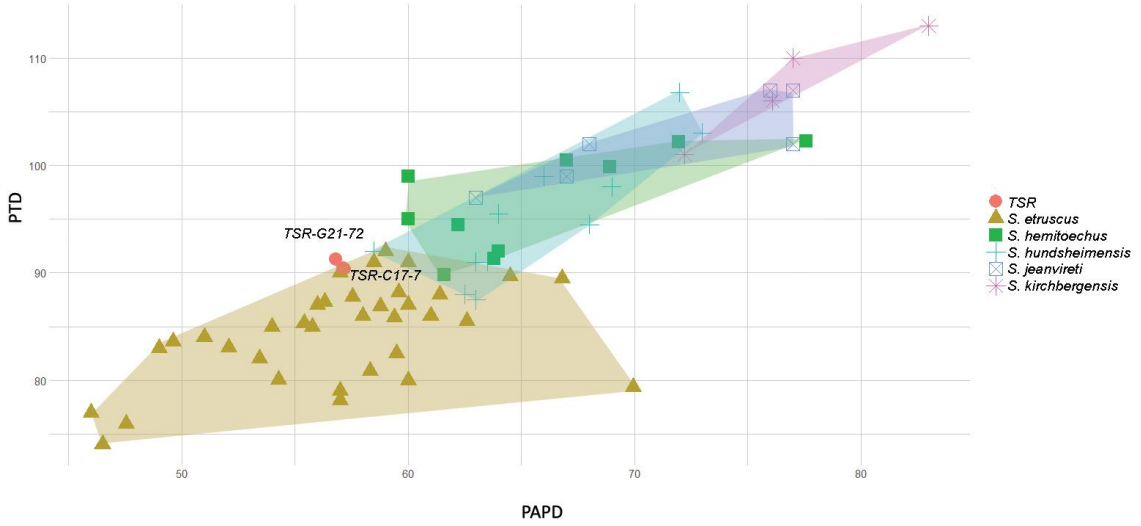

Figure 25 The scatter plot of the PTD and PAPD of the radius from TSR (in mm). Comparative material retrieved from: Guérin and Heintz (1971); Guérin (1972), (2004); Guérin and Santafe-Llopis (1978); Santafe-Llopis and Casanovas-Cladellas (1987); Mazza (1988); Fortelius et al. (1993); Mazo (1997); Kahlke (2001); Guérin and Tsoukala (2013); Pandolfi and Tagliacozzo (2015); Tsoukala and Guérin (2016); Pandolfi et al. (2017).

The size of the distal epiphysis of TSR-50 (tibia) falls into the variability of *S. etruscus,* clearly distinguished from the rest of the studied species (Fig. 26).

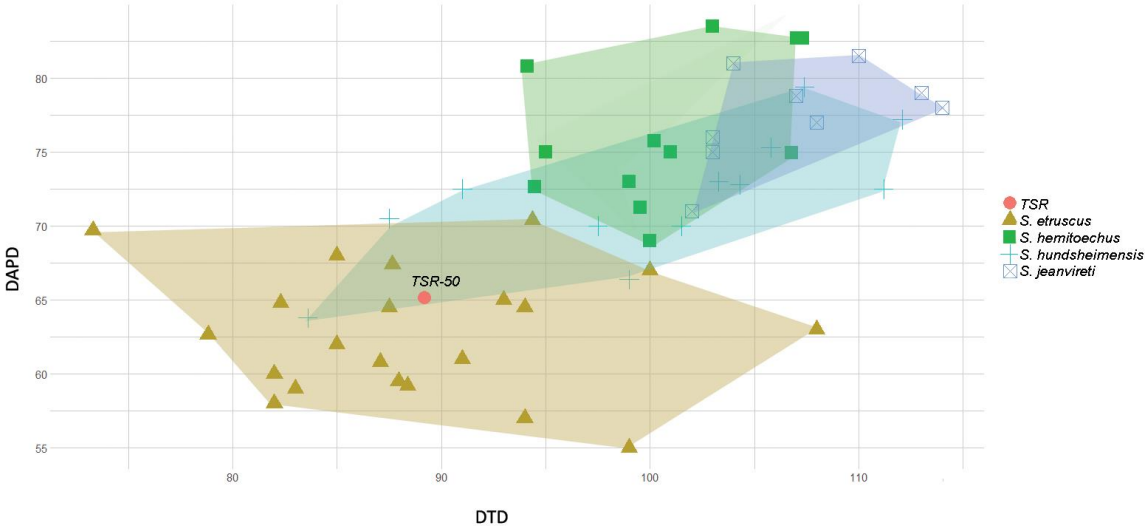

Figure 26 The scatterplot of DAPD and DTD of tibia TSR-50, in mm. Comparative material from: Guérin (1972), (2004); Mazza (1988); Fortelius et al. (1993); Kahlke (2001); Lacombat and Moulle (2005); Guérin and Tsoukala (2013); Pandolfi and Tagliacozzo (2015); Pandolfi et al. (2017).

The preservation of most of the tarsals is poor, however the cuboid TSR-F18-64a falls into the variability of the smaller sized specimens of *S. etruscus* (Fig. 27). Nevertheless, *S. etruscus* shows great variability, especially at the Lmax and overlaps with all the specimens of *S. hundsheimensis* and with some specimens of smaller heigh of *S. jeanvireti*.

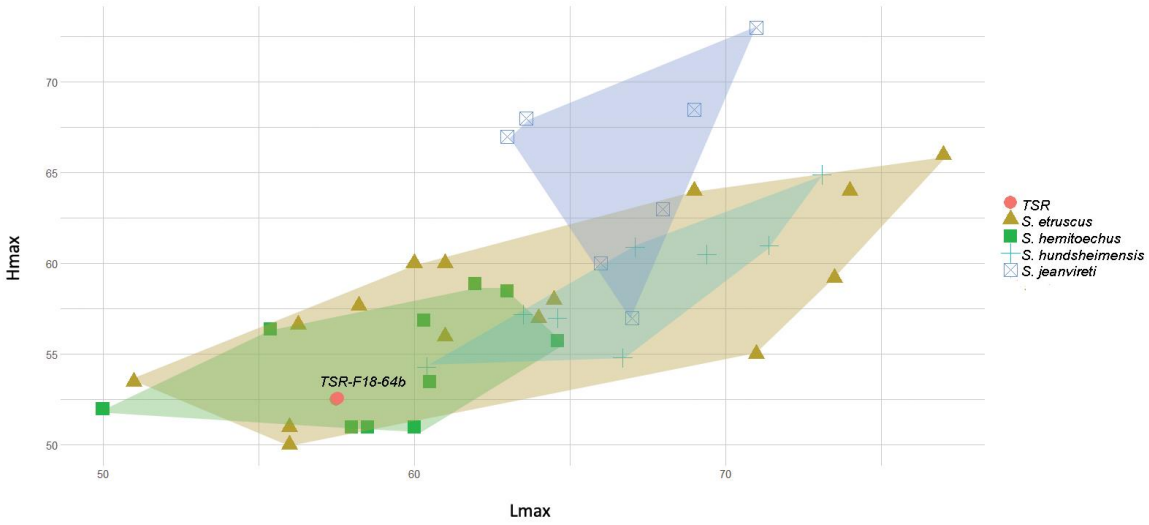

Figure 27 The scatter plot of the Hmax and Lmax of the cuboid, TSR-F18-64a in mm. Comparative material from: Guérin and Heintz (1971); Guérin (1972); Fortelius et al. (1993); Kahlke (2001); Guérin and Tsoukala (2013); Pandolfi and Tagliacozzo (2015); Pandolfi et al. (2017).

The scatter plot of the dimensions of the proximal epiphysis of the MtIII shows a great overlapping between *S. etruscus*, *S. hemitoechus* and *S. hundsheimensis*, with the TSR-F18-64a specimen being close to the larger specimens of *S. etruscus* and into the range of the larger specimens of *S. hemitoechus* and *S. hundsheimensis* (Fig. 28).

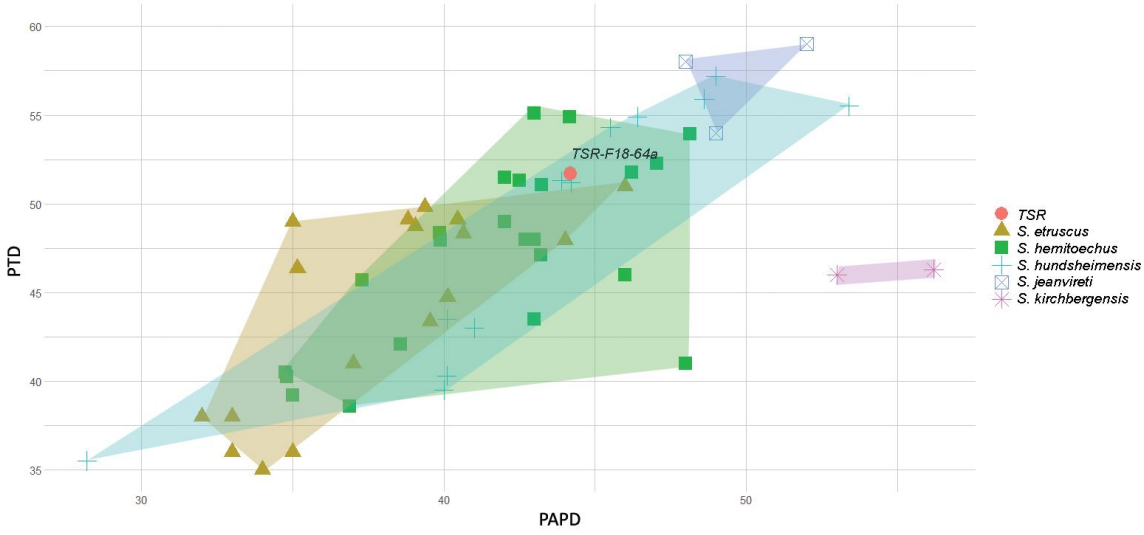

Figure 28 The scatter plot of PTD and PAPD of the MtIII TSR-F18-64b in mm. Comparative material from: Guérin (1972); Mazza (1988); Fortelius et al. (1993); Kahlke (2001); Guérin and Tsoukala (2013); Pandolfi et al. (2017).

The proximal epiphysis of MtIV TSR-F18-64a (Fig. 29) is within the variability of *S. etruscus* and close to a specimen of S. hundsheimensis from Untermaßfeld.

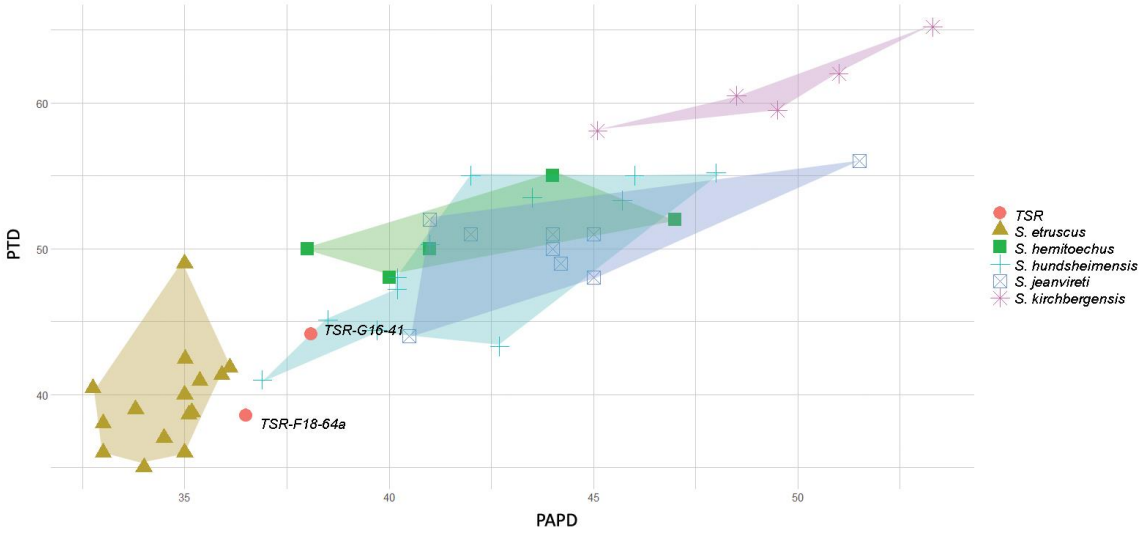

Figure 29 The scatter plot of the two MtIV from TSR in mm. Comparative material from: Guérin (1972); Mazza (1988); Fortelius et al. (1993); Kahlke (2001); Lacombat (2005); Guérin and Tsoukala (2013); Pandolfi et al. (2017).

3.5.3 *Stephanorhinus* cf. *hundsheimensis*

Material:

TSR-G19-13, complete right humerus; TSR-F18-64, left proximal epiphysis of McIV; TSR-F18-56, left complete femur; TSR-G20-50, TSR-D16-27, TSR-F22-3, diaphysis of femori; TSR-G16-41, proximal epiphysis of MtIV

Description

The specimen TSR-G19-13 (Fig. 19, A-B-D) is a complete well-preserved right humerus. In proximal view, the articular head looks rounded shaped extending posteriorly. The greater tubercle is quite damaged. Nevertheless, the greater tubercle convexity is developed but the lesser tubercle convexity is weakly developed. The bicipital groove is wide, concave, and in proximal view, the anterior border has roughly half trapezoidal shape. There is a marked groove at the convexity of the greater tubercle that is getting narrower at its anterior part, and another marked and wide groove between the lesser tubercle and the convexity of the lesser tubercle. The olecranon fossa is large with an elliptic outline and greater height than the width. The coronoid fossa has a weak rugosity at the level of the trough. The lateral epicondyle is distally and laterally protruding, while the medial epicondyle is not protruding. In lateral view, the epicondylar crest is not present. The distal epiphysis and the trochlea are obliqued.

The specimen TSR-F18-67 (Fig. 17, D-E-F) is a left McIV with the proximal epiphysis and part of the diaphysis well preserved. In proximal view, the proximal articular surface has the shape of an equilateral triangle with rounded corners. The anterior border in proximal view is slightly wavy, however in anterior view is strongly concave. In proximal view, the medial border is convex, and the latero-posterior one is straight with a concavity posteriorly to the articular surface for the McV. The articular surface for the McV is reduced, in contact with the proximal articular surface and almost circular. In medial view, there are two articular surfaces for the McIII and the magnum, clearly distinct from each other. The anterior one is elongated triangular shaped in contact with the proximal articular surface. The posterior one is elongated vertically and elliptic shaped. The section of the preserved diaphysis is triangular close to the proximal epiphysis.

The specimen TSR-F18-56 (Fig. 21, A-B) is a left complete femur well preserved. In proximal view, the shape of the femoral head is rounded, and slightly transversally elongated. It has a clear ligament fossa located at the posterior and medial part. The neck is narrow, the great trochanter has its top slightly damaged, however it has limited extension with marked great trochanter convexity. The third trochanter is slightly enlarged outward, broken at the lateral part, located at the middle of the diaphysis. The blunt lesser trochanter is extended until the height of the third trochanter. The distal epiphysis is strongly asymmetrical in distal view. The medial trochlear ridge is damaged, and the difference in height with the lateral one is not traceable, they form an angle of about 90º. There is a triangular shaped, lateral-distal depression between the lateral lip

of the trochlea and the tuberosity (referred to as sulcus popliteus in Tsoukala (2018). The medial epicondyle is as developed as the lateral one, the medial condyle though is more robust, rounded and twice as wide as the lateral one. The intercondyle fossa is moderately developed.

The specimen TSR-G16-41 (Fig. 22, H, I) is a right proximal epiphysis with part of the diaphysis of a well-preserved left MtIV. In proximal view, the articular surface for the cuboid is elliptical with irregular anterior border. The medial border is straight close to the anterior part, forming an obtuse angle. The posterior border of the proximal articular surface is convex. At the posterior part there is a marked distinct deep and narrow groove that separates the articular surface from the strong lateral tuberosity. In posterior view, this strong protruding lateral tuberosity creates a bridge that is in contact with the lateral articular surface for the MtIII, resulting its protrusion. In medial view, there are two articular surfaces for the MtIII, the posterior one is eye-shaped and flat, protruding posteriorly and being in contact with the lateral tuberosity, clearly distinct from the proximal articular surface. The anterior articular surface is trapezoidal shaped, flat, in contact and perpendicular to the proximal articular surface; it is located higher than the posterior one. They are separated from each other by a rather deep and wide groove. The cross section of the preserved diaphysis is circular.

Comparison

The specimen TSR-G19-13, share common characters with *S. etruscus*, such as the deep trochlea groove, and the concave proximal border of the trochlea in anterior view. In comparison with specimens of *S. etruscus* from Olivola and Pirro Nord, the TSR-G19-13 has a similarly high olecranon fossa with elliptic shape but differs from *S. etruscus* from Poggio Rosso as in the latter the olecranon fossa is much reduced in height and wider. Those characters discriminate the humeri from *S. hundsheimensis* (Kahlke, 2001). The TSR humeri differ from those of *S. hemitoechus,* as in the latter the medial border of the medial lip of the trochlea sinuous and the proximal border of the trochlea are slightly curved (Pandolfi and Tagliacozzo, 2015). There are not adequate data for morphological comparison with the humeri of *S. jeanvireti* and *S. kirchbergensis*. However, biometrically these two species are much larger. TSR-G19-13 differs from TSR-133, since the latter preserves a much slender diaphysis and a flat medial part of the proximal border of the medial lip of the trochlea.

The radius TSR-C17-70 shows some differences from the specimen TSR-G21-72, the latter one showing a much smoother brachii biceps and more concave lateral articular surface in anterior view, plus more protruding anteriorly, medial border in proximal view. However, it is damaged and most of the morphological characters are not preserved

The specimen TSR-F18-56 is the best preserved and most complete femur. It shares common characters with *S. etruscus* from Poggio Rosso and Pirro Nord, such as the rounded and less projecting femoral head; the moderate development of the medial condyle, and the asymmetry of the trochlea and the intercondyle fossa. It differs from *S.*

hundsheimensis from Ceci, in the projecting medially femoral head, the shorter neck of the femoral head and the development of the lateral lip. However, the most important characters as the development of the trochlea (width, asymmetry, angle between the lips) and the development of the medial lip, are not preserved in TSR-F18-56. TSR femur differs from *S. jeanvireti*, in the shape of the condyles in distal view (Guérin, 1972). The rest of the Tsiotra Vryssi material are only parts of the diaphysis which are different from those of *S. jeanvireti* as they tend to be wider (Cirilli et al., 2020).

The dimensions of the diaphysis of the humerus TSR-G19-13 (Fig. 23) are much larger than the TSR-133, and closer to the dimensions of the much larger species *S. jeanvireti*. Metrically the two humeri specimens (TSR-133 and TSR-G19-13) differ significantly in their dimensions; TSR-133 is much smaller and its dimensions are between those of *S. etruscus* and *S. hundsheimensis* (Fig.24).

The dimensions of the proximal epiphyses of the McIV (Fig. 30) of Pleistocene Rhinoceroses shows that *S. etruscus* has the smaller dimensions, followed by *S. hemitoechus* and *S. hundsheimensis* and progressively *S. jeanvireti.* The first two have similar ranges of anteroposterior diameter, however *S. hemitoechus* have greater transversal diameter. It seems like *S. jeanvireti* have greater PTD values with transversal diameter similar to the one specimen from *S. kirchbergensis.* The specimen from TSR-F18-6 is larger than *S. etruscus*, however it is in the middle of the range of *S. hemitoechus* and *S. hundsheimensis* and close to the smaller values of *S. jeanvireti*.

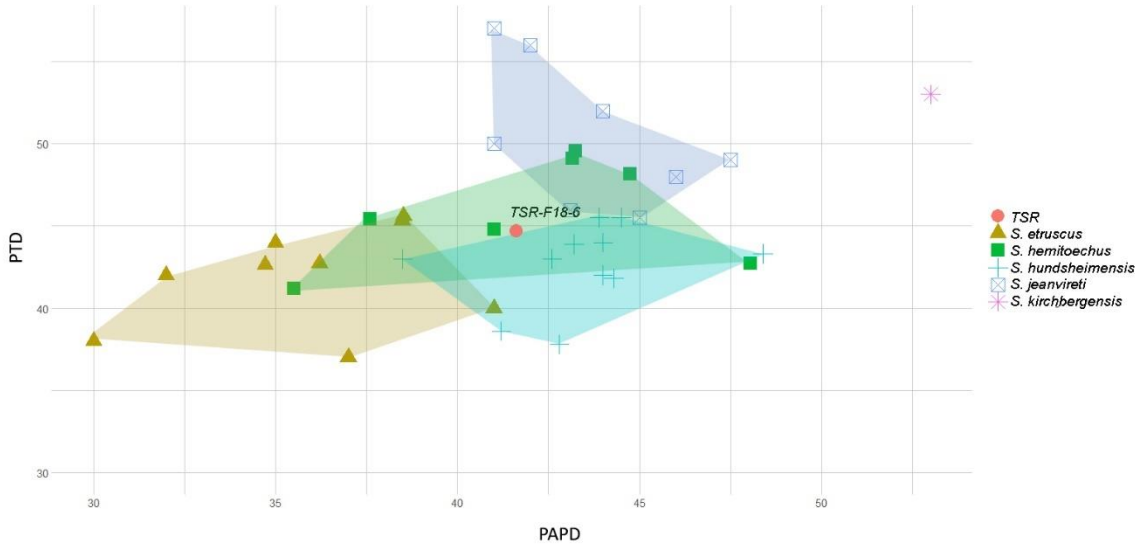

Figure 30 The scatter plot of the dimensions of the proximal epiphysis (PTD and PAPD) of the McIV (in mm). Comparative material from: Guérin (1972); Cerdeño (1990); Fortelius et al. (1993); Kahlke (2001); Lacombat (2005); Pandolfi and Tagliacozzo (2015); Pandolfi et al. (2017).

Most of the femora of TSR have only the diaphysis preserved, where most biometric data are obtained (Fig. 31). The dimensions of the diaphysis distally to the

third trochanter are all closer to the range of the greater anteroposterior values of *S. hundsheimensis* and *S. etruscus*, although their transversal diameter is greater, placed between the values recorded for *S. hemitoechus* and *S. hundsheimensis*.

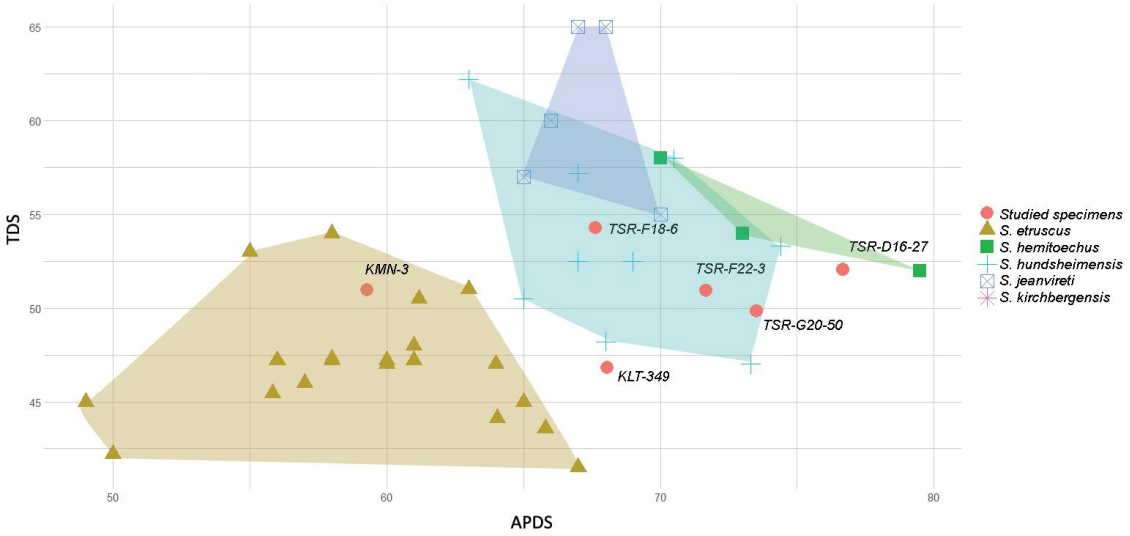

Figure 31 Scatter plot of the APDS and TDS of the diaphysis of the femur distally to the third trochanter (in mm). Comparative material from: Guérin (1972); Mazza (1988); Fortelius et al. (1993); Mazza et al. (1993); Kahlke (2001); Tsoukala and Guérin (2016); Pandolfi et al. (2017).

However, considering the dimensions of the femoral head, the TSR-F18-56 falls into the range off *S. hundsheimensis* (Fig. 32) close to the maximum recorder values of *S. etruscus*.

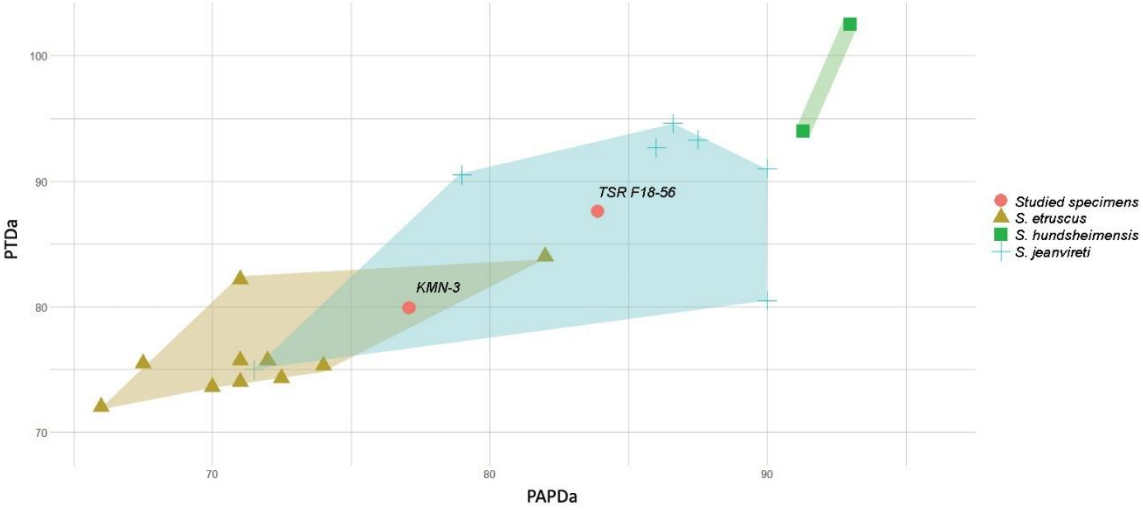

Figure 32 The scatter plot of PTDa and APDa of the femoral head (in mm). Comparative material from: Guérin (1972); Mazza (1988); Fortelius et al. (1993); Mazza et al. (1993); Kahlke (2001); Tsoukala and Guérin (2016); Pandolfi et al. (2017).

The dimensions of the proximal epiphysis of TSR-G16-41 (Fig. 28) are much larger than TSR-F18-64a, and into the variability of *S. hundsheimensis*.

Site Krimni (KRI, KRM)

3.6.1 *Stephanorhinus* sp.

Material:

KRI-16/1978, left maxilla with P3, damaged DP4, M1 and M2; KRI-17/1978, right P3; KRI-18/1975, right P4; KRI-23/1978, astragalus; KMN-63, fragment of a juvenile tooth; KMN-3, a femur of a subadult; KMN-98, a diaphysis of femur; KMN-100, astragalus.

Description

The specimen KRI-16/1978 (Fig. 33, A) is a left maxilla with P3, damaged DP4, M1 and M2. The P3 shows a strong paracone fold with a parastyle preserved and a distally horizontal continuous cingulum. Even though it is partially damaged, at the lingual side, the lingual valley looks closed. Regarding the internal folds, there is a strong crochet, but it is quite filled with sediment, creating uncertainties about the presence of the antecrochet and crista. The DP4 is completely damaged, with only a part of the ectoloph preserved. The M1 is more worn out, without the ectoloph preserved; it is high crowned with a strong single crochet, a single crista, clearly open lingual valley, closed postfossette, weak protocone constriction, and a distally continuous and strongly oblique cingulum. The M2 has a trapezoidal outline, slightly damaged and missing the ectoloph. However, it preserves a high crown, a strong single crochet, an antecrochet a clearly open lingual valley with weak protocone constriction limited at the base of the tooth and not extending to the occlusal part, a postfossette filled with sediment and a distal oblique strong continuous cingulum.

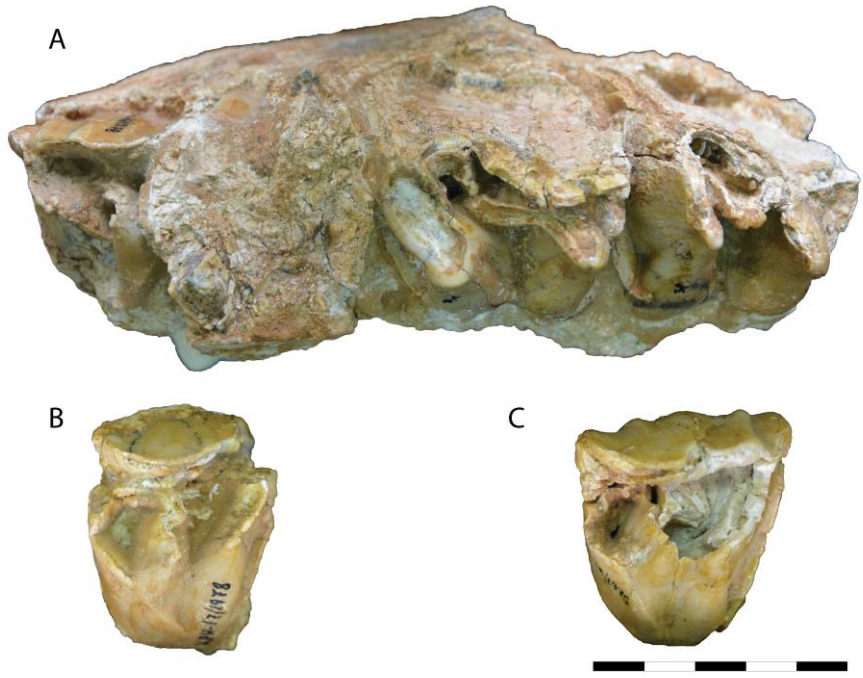

Figure 33 Stephanorhinus *sp. KRI-16/1978 (A), KRI-17/1978 (B) and KRI-18/1975 (C), in occlusal view. Scale bar 50mm.*

The specimen KRI-17/1978 (Fig. 33, B), is a right high crowned P3 with very high ectoloph but damaged at the mesial part. It has mesial strong horizontal continuous cingulum and in the lingual side, an obliged continuous cingulum. The crochet is damaged, but the remains seem to be double. There are some remains that could indicate a crista and a closed postfossette.

The specimen KRI-18/1975 (Fig. 33. C) is a right P4 with a strong paracone fold, a rather moderate parastyle and metastyle and closed postfossette. Regarding the internal folds there is a double crochet, a single crista and no antecrochet. Mesially, it has a horizontal undulated continuous cingulum and closed lingual valley.

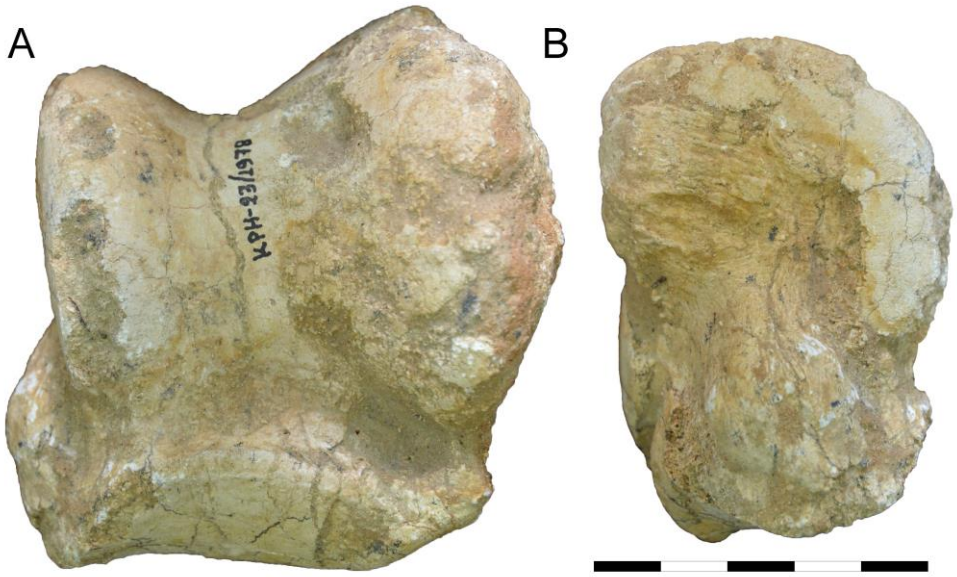

Figure 34 The astragalus Stephanorhinus *sp. KRI-23/1978 in anterior (A) and medial (B) views. Scale bar 50mm.*

The specimen KRI-23/1978 (Fig. 34) is a left small astragalus quite well preserved. In anterior view, the trochlea has the weak inclination. There is a small difference in height between the medial and lateral lip, although the lateral border of the lateral lip is damaged. The groove separating them is deep and quite wide. There is sediment at the lateral-distal of the trochlea, so it is not possible to detect a concavity. Additionally, the proximal part of the distal articular surface expands to the anterior side, and it is very close to the lateral lip. The two lips of the trochlea are parallel. The depression distally the trochlea is very reduced. The distal articular surface extends significantly anteriorly (like a quarter of the whole bone). In medial view, the medial tuberosity is rounded, well-marked, located disto-posterior part and extends medially. The lateral side is not so well preserved. In posterior view, the lateral anterior articular surface is rounded shaped but with damaged borders, concave and highly located. It has a reduced and damaged disto-lateral prolongation. It is separated from the anterior-medial articular surface by a narrow groove that is filled with sediment. The lateral distal

part of this view is quite damaged. The medial articular surface is elongated proximo-distally but with a marked medial extension, flat with part of the lateral border quite damaged. Its distal part is in contact with the posterior extension of the distal articular surface with which there is a protruding barrier created. At this barrier the groove separating the medial-proximal and medial-distal articular surfaces, finishes. The distal medial articular surface is damaged at the medial part, so it is not possible to directly recognize the shape, but the preserved part extends significantly to the proximal direction. In distal view, the medial articular surface is almost rhomboidal shaped with the medial border quite damaged, but the preserved antero-medial corner is rounded. The lateral articular surface is damaged at the lateral part. The two articular surfaces of the distal articular surface are separated by a smooth crest that becomes blunter at the anterior part.

The specimen KMN-3 is a right juvenile femur with the unfused distal epiphysis missing. The proximal epiphysis has only the femoral head preserved, which is rounded and slightly projecting. The third trochanter is quite damaged at its lateral part, but the preserved shape is square.

Figure 35 The astragalus Stephanorhinus *sp. KMN-100, in anterior (A), posterior (B) and medial view (C). Scale bar 50mm*.

The specimen KMN-100 (Fig. 35) is a right astragalus, well preserved, with signs of osteopathology in the posterior side. In anterior view, the trochlea is elongated transversally, asymmetrical, its axis is slightly oblique and there is a broad central, deep, and high depression distally the trochlea. The two lips are separated by a wide and deep groove. The medial lip is rounded, while the lateral one is wider transversally. In medial view, the medial tuberosity is large and located close to the distal border and on the axis of the bone. In posterior view, the proximo-lateral articular surface is strongly concave, oval shaped with moderate distal prolongation. The medial articular surface is oval shaped. At the proximo-medial and latero-distal part the spongy bone tissue is revealed, indicating the present of advanced osteoarthritis (Regnault et al., 2013). These articular

surfaces are separated by a very deep, wide groove, which presents distally abnormal bone texture, candle wax or lumpy texture (Stilson et al., 2016). The latero-distal articular surface is elongated oval shaped. In distal view, the medial articular surface is rectangular shaped and the anterior border slightly convex, and the lateral is orthogonal. Both articular surfaces are separated by a crest that is acute anteriorly but smooth towards the posterior side. There is an indentation preserved at the posterior side at the contact of the articular surfaces. The anterior edge of the distal articular surface is weakly undulated.

Comparison

The maxillary fragment KRI-16/1978 shows similarities with *S. hundsheimensis* form Voigsted (IQW 1966/7415), such as the open lingual valleys in M1 and M2 and the closed lingual valley in P3. Considering the similar wear of the teeth, they also share the single crochet, and single antecrochet in M2, plus the presence of a single crochet in M1. On the contrary, the molars of the specimen KRI-16/1978 differ at the undeveloped lingual cingulum (photos provided from Luca Pandolfi) which is always present in the M1-M2 of *S. hundsheimensis* according to Ballatore and Breda (2013).

The specimen KRI-17/1978 (P3) shares common characters with *S. hundsheimensis*, such as the lingual cingulum which can be variable according to Ballatore and Breda (2013), however it is horizontal and continuous in *S. hundsheimensis* from Voigsted. Additionally, the specimen KRI-17/1975 shares with *S. hundsheimensis* the absence of antecrochet (Ballatore and Breda, 2013). It differs from *S. kirchbergensis,* in the presence of the medial and lingual cingula (Lacombat, 2006)**.** It also shares common characters with *S. hemitoechus*, such as the mesial strong continuous and horizontal cingulum, but it differs in the obliged lingual cingulum. The paracone fold which discriminate the species (Lacombat, 2006) is not preserved here**.**

The specimen KRI-18/1975 (P4) differs from *S. hundsheimensis* at the thin paracone fold, and mainly in the obliged lingual cingulum. Ballatore and Breda (2013) claim that the lingual cingulum is always present and horizontal in *S. hundsheimensis* though Lacombat (2006b) mentions that it can be absent. The hypsodonty of KRI-18/1975 (H.I.: 121.1667) and the prominent paracone fold are common with *S. hemitoechus*.

The astragalus specimen KRI-23/1978 shares common characters with the *S. etruscus* specimens from Valdarno, such as the slight obliquity of the axis of the trochlea in anterior view, the slight inclined major axis of the same articular surface in distal view, the straight anterior border of the articular surface for the cuboid, the laterally protruding lateral articular surface and the presence of the concavity in the lateral border. However, it differs from *S. etruscus* from Olivola at the development of the medial tuberosity, and in posterior view the rounded, less elongated medial-distal articular surface for the calcaneus. Additionally, it differs in anterior view, at the development of the medial lip. It differs from *S. hundsheimensis*, in the greater inclination of the axis of the trochlea in anterior view, the great axis of the oval mesio-distal articular surface in posterior view,

and the less transversally elongated distal articulation (Toula, 1902; Kahlke, 2001). *S. jeanvireti* presents shallower groove in anterior view, with more protruding medial tuberosity and a more convex medial border of the distal articulation in distal view (Lacombat and Mörs, 2008), characters that are different from KRI-23/1978. Similarly, KRI-23/1978 differs from the astragalus of *S. hemitoechus* as the latter one presents a trochlea of a less transversal development in comparison with its height, as well as a shallower groove in anterior view and not inclined axis of the trochlea and less protruding medial tuberosity. Additionally, KRI-23/1978 has straight anterior border of the distal articulation in distal view compared to the concave one of *S. hemitoechus* (Pandolfi and Tagliacozzo, 2015). Finally, KRI-23/1978 differs from the astragalus of *S. kirchbergensis* in the stronger proximal protrusion of the medial lip in anterior view, the greater and higher depression distally the trochlea and the narrower lateral lip in anterior view (Kahlke, 1975; Lobachev et al., 2021).

As KMN-3 preserves only the femoral head and the diaphysis with the third trochanter, there are limited diagnostic features, which are usually at the distal epiphysis that this specimen lacks.

The astragalus KMN-100 has a certain pathologies and for this reason, any morphological comparison should be considered with caution. Nevertheless, it shares common characters with *S. etruscus* from Valdarno such as the slightly oblique axis of the trochlea, the transversally elongated lateral lip in anterior view; the elliptical distal-medial articular surface which is perpendicular to the sagittal plane; and in distal view, the slightly concave anterior border of the articular surface for the cuboid. However, it differs from *S. etruscus* from Olivola, at the position of the medial tuberosity in medial view, plus in posterior view the rounded medial-latera articular surface for the calcaneus. In both Olivola specimen and APL-213 this articular surface is oval shaped. Additionally, in anterior view, KMN-100 differs from *S. etruscus* at the sharper and narrower medial lip of the trochlea, characters similar to *S. hundsheimensis.* It differs from *S. hundsheimensis* in the shallower trochlea groove; the inclined axis of the trochlea in anterior view; the more inclined axis of the elliptical distal-medial articular surface and the less transversally elongated distal articulation (Kahlke, 2001; Toula, 1902). It differs from *S. hemitoechus* in the more proximo-distal development, the shallower groove of the trochlea and the lack of inclination of the axis of the trochlea in anterior view; the less protruding medial tuberosity and in the medially concave anterior border of the distal articulation (Pandolfi and Tagliacozzo, 2015). The astragalus KMN-100 differs from *S. jeanvireti* in the shallower groove, the marked and more protruding medial tuberosity in anterior view; the more convex medial border of the distal articular surface plus the convex anterior border of the articular surface for the cuboid (Lacombat and Mörs, 2008). It differs from *S. kirchbergensis* in the more proximally protruding medial lip, the greater and higher depression distally the trochlea, and the less transversally developed lateral lip in anterior view; and finally, the more elongated oval shape of the proximo-lateral articular surface in posterior view (Kahlke, 1975; Lobachev et al., 2021).

The buccal length of the specimen KRI-16/1978 (M2), falls into the range of *S. hundshemensis* and close to the range of *S. jeanvireti.* It is worth mentioning that no specimens from *S. etruscus* are included in the data base (Fig. 36).

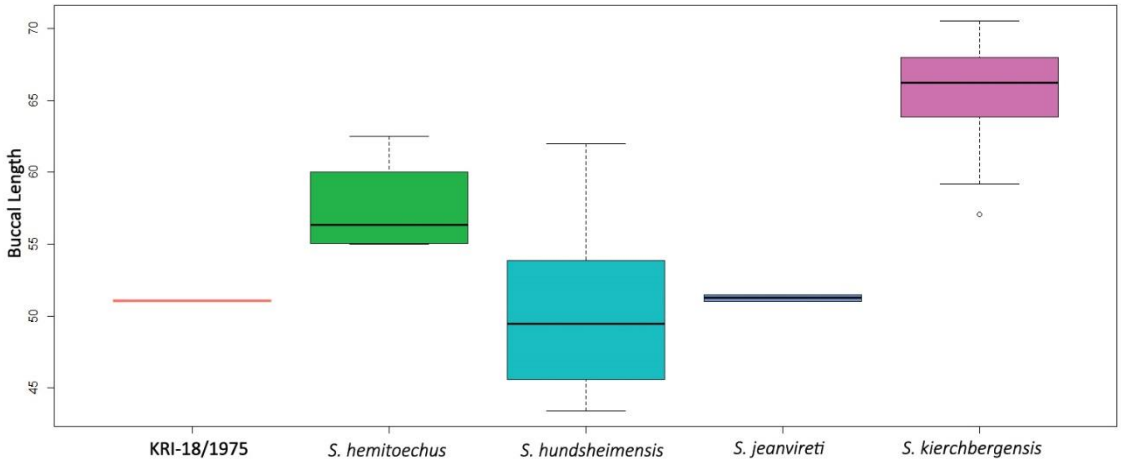

Figure 36 Box plot of the range of Buccal length in M2 (in mm), data from: Lacombat (2006), (2010); Billia (2008); Billia and Petronio (2009); Ballatore and Breda (2013); Guérin and Tsoukala (2013); Pandolfi and Marra (2015).

The dimensions of the femoral head of KMN-3 are falling into the range of the larger sized *S. etruscus* and the smaller sized *S. hundsheimensis*. It is smaller than the TSR specimen.

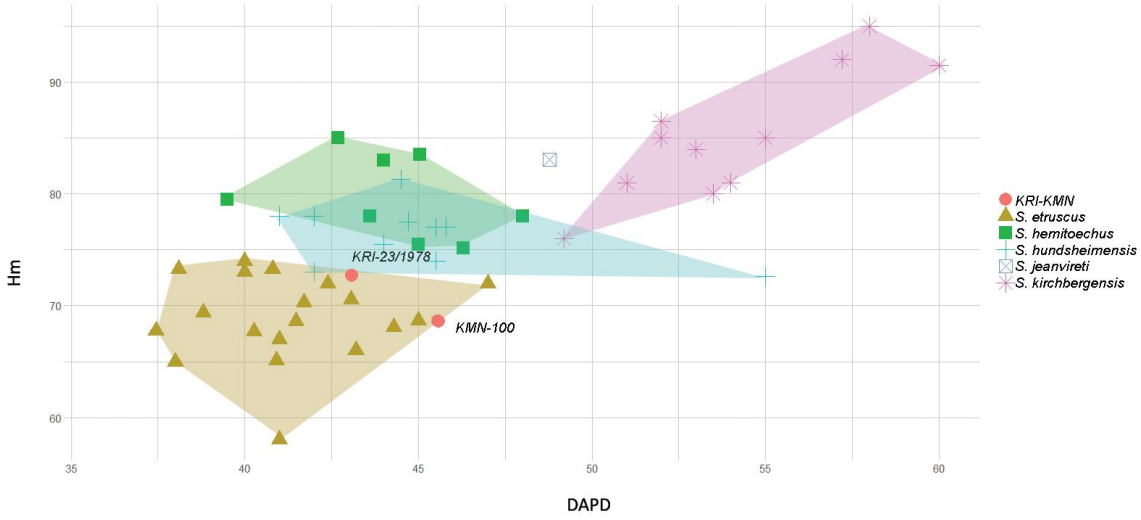

Figure 37 The scatter plot of Hm and DAPD of the astragali of Krimni. Data from: Guérin and Heintz (1971); Guérin (1972), (2004); Ruiz-Bustos (1973); Santafe-Llopis and Casanovas-

Cladellas (1987); Mazza (1988); Cerdeño (1989); Fortelius et al. (1993); Kahlke (2001); Lacombat (2005); Lacombat and Mörs (2008); Guérin and Tsoukala (2013); Pandolfi and Tagliacozzo (2015); Tsoukala and Guérin (2016); Pandolfi et al. (2017).

At the locality of Krimni, there are two astragali specimens, one from each site. The scatterplot from Hm and DAPD puts both specimen close to the variability of *S. etruscus,* however the KRI-23/1978 specimen is closer to the specimen of *S. hundsheimensis* from Mosbach (Fig. 32)

3.6.2 *Stephanorhinus* cf. hundsheimensis

Material:

KMN-1, juvenile skull

Description

The specimen KMN-1 (Fig. 38) is an almost complete cranium moderately preserved with strong damages at the parietal, basicranial and right-side parts and a neurocranial portion twisted to the left side. There are no teeth preserved apart from a non-erupted either DP4 or P4. Regularly the sutures are not visible due to damages, although there are some exceptions that will be noted.

Figure 38 The specimen S. *cf.* hundsheimensis *KMN-1, in anterior (A) and lateral (B) views. Scale 50mm.*

In dorsal view, the nasal bones are wide caudally becoming rather abruptly narrower toward the rostral tip; their length is about 183.4 cm. Close to the nasal tip there is a small elliptical rugosity, probably corresponding to a horn boss. The ventral surface of the nasals is flattened. The fronto-nasal suture is observable in dorsal view; it is placed slightly in front of the anterior level of the orbits. In lateral view, the top profile of the nasals is flat caudally but slight convex to the front and bends downwards in front of the horn boss imprint. Nasal septum is not developed.

Most of the maxillary is damaged. The contact of the lacrimal bone and the nasal is not visible, and the lacrimal tubercle (preorbital process) is quite damaged but moderately developed.

The widest part of the frontal bone is at the supra-orbital part. The dorsal surface of the frontals is flat, subhorizonal and slightly raising toward the parietal. Just behind the fronto-nasal suture there is a small, rounded boss, likely representing the place of a second horn. The braincase is rectangle in dorsal view. The parietal is elongated (Nasal-occiput: 582mm; nasal-occipital condyles: 538mm, width: 124.27 mm), and narrow. The temporal lines are weak but visible and run subparallel to each other. The parietal-interparietal suture is preserved in dorsal view. The shape of the interparietal is as an elongated rectangle.

In occipital view, the sutures of the occipital and the mastoid (of the right preserved side, the left one is damaged and filled with cement) are preserved. The occiput is high. The upper part of the occiput is quite damaged, but its overall outline is trapezoid, with the broadest part at the level of the mastoids. The nuchal crest is severely damaged but rather rounded in posterior view and protruding postero-dorsally.

The postglenoid process and the sphenoid region are not preserved. The external auditory meatus is quite large, rounded. The mastoid process is almost parallel to the occipital posterior profile.

Comparison

The Eurasian Pleistocene juvenile rhino material is very limited. At the literature, there is only one reference for a young cranium of *Stephanorhinus* [*S. kirchbergensis* from China in Tong and Wu (2010)] and very few for *Coelodonta* [*C. nihowanensis* from China and *C. antiquitatis* from Siberia (Tong and Wang, 2014; Protopopov et al., 2015; Iurino et al., 2020)]. There is no record at the literature concerning European juvenile crania, apart from the specimens from Melpignano, with limited distinguished morphological characters, resulting its assignment as Rhinocerotinae (Iurino et al., 2020).

Iurino et al. (2020) suggested that the juvenile crania of *Coelodonta* are characterized by a flatter fronto-parietal profile than that of *S. kirchbergensis*. In the latter one, the fronto-parietal profile creates an angle. In KMN-1, the parietal has a flat profile, but the specimen is seriously damaged near the frontal. The parietal and the jugal

(zugomatic arc) are running in parallel in KMN-1, in difference from *S. kirchbergensis* No. H36 cranium where it forms an acute angle (Iurino et al., 2020). In KMN-1 the lateral profile of the occipital crest is triangular with narrow vertex, like the specimen from Melpignano, and the two juvenile *Coelodonta* specimens, contrary to *S. kirchbergensis* in which the occipital crest is rounded and more dorso-ventrally developed (Iurino et al., 2020). Comparing the external auditory meatus, the KMN-1 is quite bread and circular shaped, in difference from the drop-shaped meatus of *S. kirchbergensis* which is also placed closer to the occipital plane (Iurino et al., 2020). Finally, compared to a juvenile *S. etruscus* from Senèze (photo provided from Pandolfi Luca), the specimen KMN-1 differs at the great length, concave dorsal profile plus the narrow and arched nasals. These characters discriminate it from *S. etruscus*, resulting its attribution, confidently as *S.* cf. *hundsheimensis.*

3.6 Site Platanochori (PLN)

3.7.1 *Stephanorhinus* sp.

Material:

PLN-1: Maxilla with DP3, DP4, M1

Description

The specimen PLN-1 is a maxilla with the left DP3, DP4 and M1 preserved, the alveoli of DP2 is present but the tooth is not preserved (Fig. 39). On the right side there are no teeth preserved, however opposite of M1 and DP4 the teeth were broken with only the outline of the base preserved; additionally, there is an ectoloph of an erupting tooth opposite DP3 (probably P3) plus another one medially (probably P2).

Figure 39 The Stephanorhinus *sp. maxilla of PLN-1 with DP3, DP4 and M1 in occlusal view. Scale bar 50mm*.

The DP3 is slightly damaged, with closed medifossette and postfossete, moderately strong ectoloph. There is a lingual cusp preserved, along with the mesial horizontal cingulum as well as part of a lateral one. The DP4 has moderately strong ectoloph with strong paracone fold, mesial horizontal cingulum, and a lingual cusp.

There is a strong single crochet, a small crista and a moderate protocone constriction, developed parastyle with wide parastyle groove. The M1 has moderate ectoloph, with strong paracone fold, strong single crochet and moderate protocone constriction and mesial horizontal cingulum. The age of death of the individual is estimated at 1.5-3 year old, based on the preserved teeth and the stage of wear (Louguet, 2002).

Comparison

The presence of a mesial cingulum on the molars is considered as a distinguishing character between *S. hundsheimensis* where it is always present and *S. jeanvireti* where it is always absent. In PLN-1 it is present, making common character with *S. hundsheimensis* and different from *S. jeanvireti* (Ballatore and Breda, 2013; Tsoukala, 2018). However, the non-metric characters of *S. hundsheimensis* and *S. etruscus* have minor differences (Fortelius et al., 1993). The specimen PLN-1 differs from *S. kirchbergensis* at the rounded and smooth enamel surface (Fortelius et al., 1993) and from *S. hemitoechus* because of its hypsodonty (Tsoukala and Guérin, 2016).

The length of the M1 from PLN-1 (Maximal length=51.93mm) falls into the range given by Guérin (1980) (50.5-57.5 mm) which is overlapping with that of *S. hundsheimensis* (44.5-63.5mm), however it is closer to the mean of the latter one.

Site Riza (RIZ)

3.8.1 *Stephanorhinus* sp.

Material

RIZ-26 upper premolar.

Description

The specimen RIZ-26 (Fig. 40, D) is a worn-out upper left premolar with a single crochet and a small crista. The ectoloph is almost straight and no cingula present or preserved. It is estimated that the age of this individual is between 10-21 years (Louguet, 2002).

Comparison

The comparison of an isolated premolar, especially at this stage of wear, is very difficult. Nevertheless, based on the size, it differs from *S. kirchbergensis*.

3.8.2 *Stephanorhinus* cf. *hundsheimensis*

Material

RIZ-27, proximal epiphysis of a left ulna; RIZ-27, proximal and distal epiphyses of a left radius.

Description

The specimen RIZ-27 (Fig. 40, A) is an almost complete proximal epiphysis of a left ulna articulated with the radius (RIZ-27). The trochlear notch is robust and asymmetrical. In anterior view, the medial articular surface is parallel to the medial border of the diaphysis, creating a ~45º angle with the lateral articular surface. The articular surfaces for the radius are flat, rectangular shaped, with the lateral one being wider. In lateral view, the preserved part of the olecranon is antero-posteriorly wide and robust. The anconeal process moderately projects forward and is perpendicular to the corpus of the bone. The preserved diaphysis has a triangular cross section.

The specimen RIZ-27 (Fig. 40, B-C) is a left radius in two pieces (the proximal and distal epiphyses) quite well-preserved. In proximal view, the medial articular surface is slightly concave, sub-squared in shape with curved but damaged medial outline. The lateral articular surface is much smaller and more concave than the medial one. The saddle on the articular surface is damaged. The postero-lateral border is oblique and slightly concave with an angle of the entire articulation at ~120 º. The anterior border is slightly concave, although damaged. In anterior view, the proximal border of the lateral articular surface is reduced and concave with small difference in heigh between the medial and the lateral articular surfaces. The brachii biceps is slightly developed. The lateral tuberosity is reduced in size but marked. In posterior view, the lateral articular surface forms a large, half-circle whereas the medial one is not preserved.

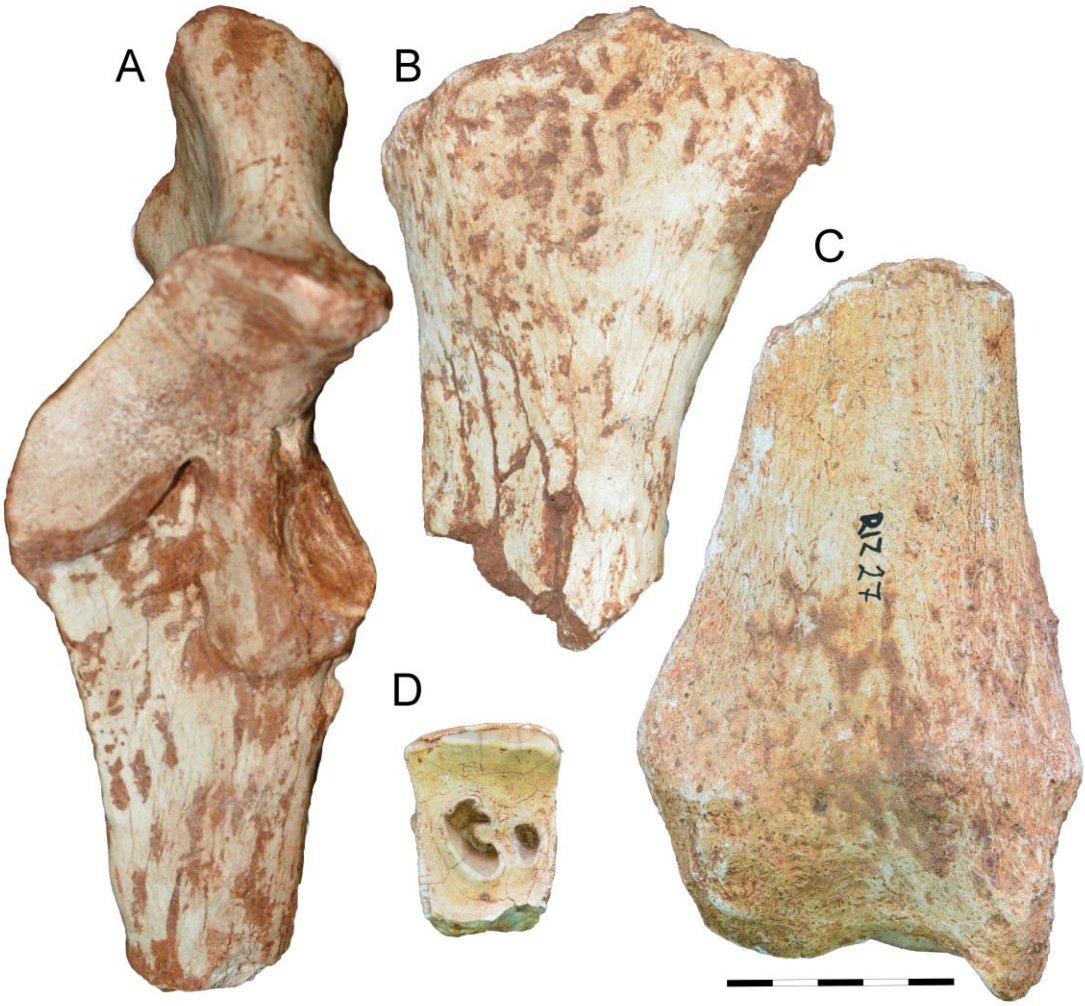

Figure 40 The Stephanorhinus *cf.* hundsheimensis *material from Riza, ulna RIZ-27 (A), radius RIZ-27 in anterior view (proximal (B, A) and distal (C) epiphysises) and the* Stephanorhinus *sp. RIZ-26 in occlusal view (D). Scale bar 50mm.*

In distal view, the articular surface is asymmetrical and robust. The medial part of the articulation is concave at the anterior part, and convex at the posterior part. The lateral part is moderately concave. The posterior convexity of the articular surface for the scaphoid is very reduced. The anterior part protrudes proximally with a convex outline, while the lateral border is slightly concave. Anteriorly of the lateral part of the articulation there is a strong tuberosity. The articulation has a slight inclination. In anterior view, the styloid apophysis is well developed and protruding. There is a great difference in height between this point and the lateral plateau. There are two tuberosities at the medial and lateral sides. The articulation is delimited by a marked groove around all the sides except from the anterior one, distally of which there are partially fused sutures. At the lateral part of the epiphysis there is a very strong tuberosity making the transversal diameter of the epiphysis much greater than that of the articulation.

Comparison

The radius specimen RIZ-27 shares with *S. etruscus* from Valdarno the similar posterior angle of the entire articulation in proximal view and the triangular concave shape of the lateral articular surface. Likewise, they share common characters at the distal epiphysis such as the pronounced styloid apophysis, the marked anterior tuberosity in distal view and the shape of the posterior border. It differs from *S. hundsheimensis*, mainly in the straight anterior border of the articulation in proximal view, and the very wide angle (almost 180º) of the posterior border. However, it shares with this species the protruding styloid apophysis and its great difference in height with the lateral plateau, in anterior view of the distal epiphysis (Kahlke, 2001).

It differs from *S. hemitoechus* from Valle Radice, in the more acute posterior angle of the articulation in proximal view, the stronger posterior process in anterior view, and the difference in heigh between the lateral articular surface (that one for the semilunar) and the styloid apophysis (Pandolfi and Tagliacozzo, 2015). The specimen RIZ-27b differs from *S. jeanvireti* from Milia, as in the later the lateral articular surface of the proximal epiphysis extends outwards in anterior view (Tsoukala, 2018). From direct observations of the distal articulations between *S. jeanvireti* and *S. etruscus*, the medial tuberosity is less marked in *S. etruscus* in anterior view, and the lateral convexity at the articulation of *S. jeanvireti* is very robust in comparison with the weakly marked of *S. etruscus.* It differs from *S. kirchbergensis* from Siberia, in the straight postero-lateral border in proximal view, the straight anterior border of the articulation and the straight proximal borders in anterior view (Lobachev et al., 2021). Compared to the studied specimens, the RIZ-27 differs mostly with APL-278. More specifically, RIZ-27 preserves in proximal view proportionally larger latera articular surface, with a more convex anterior border. Additionally, RIZ-27 preserves in anterior view, a less concave lateral-proximal border, a reduced and more medially placed brachii biceps and a stronger, more distally placed lateral tuberosity. In comparison with the TSR radii, it is very similar to TSR-C17-7, but RIZ-27 differ at the less concave, though slightly damaged, lateral border in anterior view, and the stronger lateral tuberosity. The specimen TSR-G21-72 differs from RIZ-27, since the latter has in proximal view, a less concave lateral articular surface. Moreover, in anterior view, it has less wide lateral-proximal border, reduced brachii biceps and is in general stockier.

The dimensions of the distal epiphysis of RIZ-27 are falling close to the range of *S. hundsheimensis*, andnear the smaller sized specimens, those of the localities of Moshbach and Untermaßfeld. It is also into the variability of *S. jeanvireti*, and close to the smaller specimens from Vialette (Fig. 41).

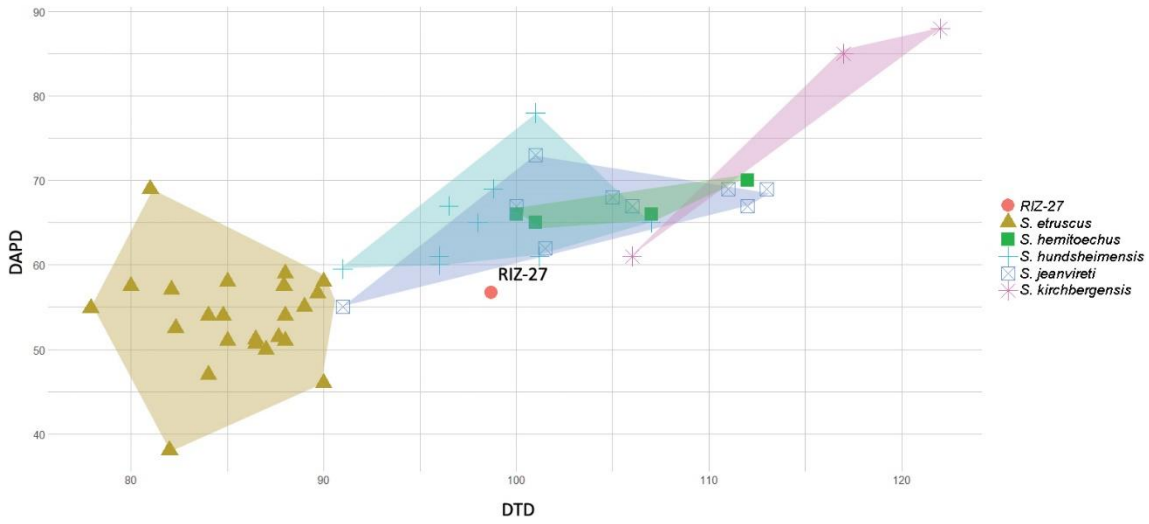

Figure 41 The scatter plot of the dimensions of the distal epiphysis of the radius in mm, data from: Guérin and Heintz (1971); Guérin (1972), (2004); Santafe-Llopis and Casanovas-Cladellas (1987); Mazza (1988); Fortelius et al. (1993); Mazo (1997); Kahlke (2001); Guérin and Tsoukala (2013); Tsoukala and Guérin (2016); Pandolfi et al. (2017).

Site Apollonia (APL)

3.9.1 *Stephanorhinus* sp.

Material

APL-498, left DP4; APL-348, left ulna; APL-665 fragment of calcaneus

Description

The specimen APL-498 is an upper left DP4 with a very strong paracone fold, prominent parastyle and metastyle, single crochet, single crista with a tiny cup. There is a weak protocone constriction, a mesial continuous obliged cingulum, and an opened lingual valley.

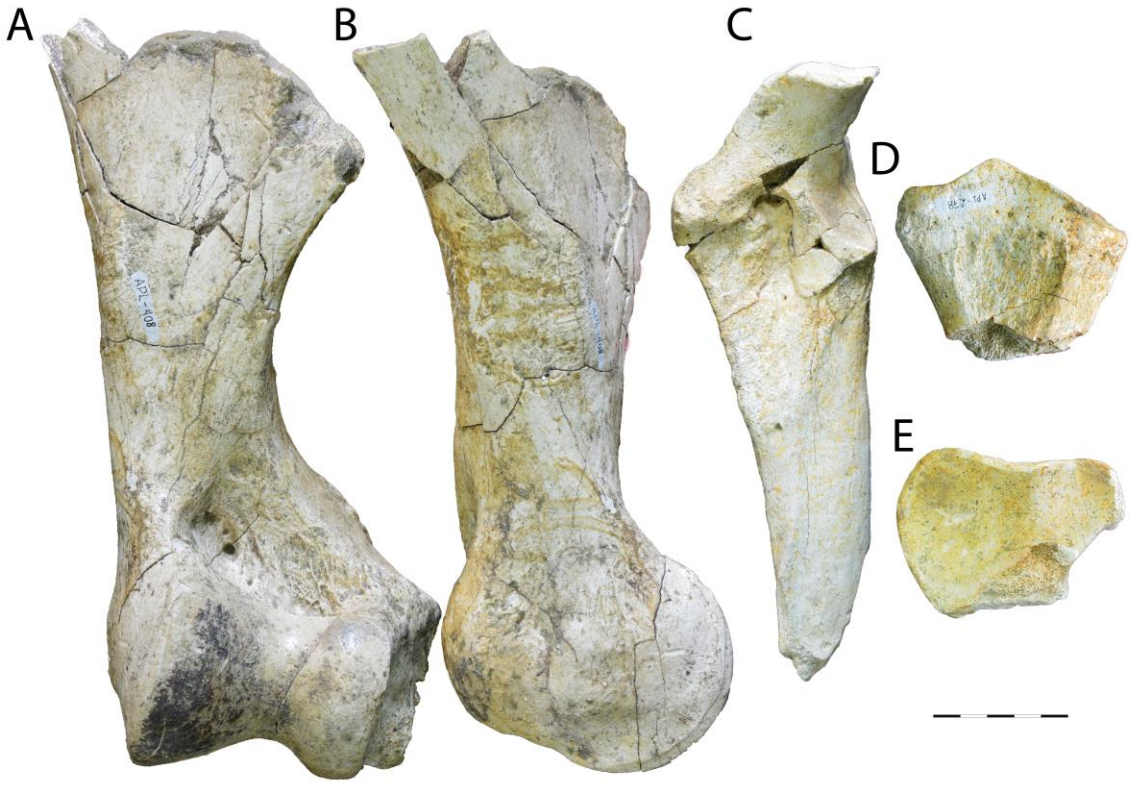

Figure 42 S. etruscus *humerus APL-408 (A, B),* Stephanorhinus *sp. ulna APL-348 (C) and S. etruscus radius APL-278 (D, E) in anterior (A, C, D), proximal (E), and medial (B) views. The scale bar is 50mm.*

The specimen APL-348 is a slender left ulna (Fig. 42. C) with the proximal epiphysis and part of the diaphysis, while the olecranon is missing. The trochlear notch is asymmetrical with small difference in heigh between the distal ends of the medial and lateral articular surface. In anterior view, the medial articular surface is parallel to the corpus of the bone and is almost perpendicular to the lateral one. In lateral view, a shallow and narrow groove delimits the trochlear notch. The lateral articular surface is more concave than the medial one. There is a strong depression distally to the trochlear notch. The medial articular surface for the radius is slightly convex, drop shaped, wide

and protrudes medially towards the medial articular surface. The preserved lateral articular surface for the radius resembles a stripe that is narrower at the lateral part. Its medial part (distally to the contact of the lips) it is damaged. The lateral tuberosity is slightly projecting. In lateral view, the anconeal process is projecting forwards. The surfaces of the preserved diaphysis are flat.

The specimen APL-665 is a fragment of calcaneus.

3.9.2 *Stephanorhinus* etruscus

Material

APL-408, distal epiphysis of a left humerus; APL-278, proximal epiphysis of a right radius; APL-213, left astragalus and a calcaneus

Description

The specimen APL-408 (Fig. 42, A-B) is a left humerus with the distal epiphysis and part of the diaphysis preserved. The diaphysis is robust and the trochlea asymmetric. In anterior view, the axis of the trochlea is oblique, with a wide, deep groove separating the two lips. The proximal border of this groove is concave but not so wide. The medial lip is high and wide with slightly convex medial border. The lateral lip is much more reduced, short, rounded, and parallel to the medial one; the straight lateral border is slightly oblique. In medial view, the medial epicondyle is posteriorly developed, aligned to the medial lip. In lateral view, the lateral epicondyle is damaged at the distal part, the preserved part is robust and protrudes laterally, and partially, to the posterior part. The epicondylar crest is well marked. The coronoid fossa is wide, deep, and relatively high. In posterior view, the olecranon fossa is wide and with triangular outline. There is an average groove separating, posteriorly the epitrochlear to the distal articular surface.

The specimen APL-278 (Fig. 42, D-E) is a well-preserved proximal epiphysis of a radius. In proximal view, the medial articular surface is square shaped, wide antero-posteriorly, slightly concave, and much larger than the lateral one. The latter is damaged at its posterior-lateral part. The lateral articular surface is damaged at the lateral and posterior part, and much smaller than the medial one. In anterior view, the lateral proximal border is concave, slightly oblique and reduced in comparison with the medial straight one; the brachii biceps is like a rough concave surface and the lateral one is evident. In posterior view, the coronoid process is damaged. The lateral articular surface for the ulna has limited height and at its distal part the concavity is smooth. The medial articular surface is reduced and delimited by a groove.

The specimen APL-213 (Fig. 43, A-B-E) is a well-preserved left astragalus. In anterior view, the axis of the trochlea has a subtle inclination. There is slight difference in height between the medial and the lateral lip, which are parallel. The groove between them is wide and deep. The latero-distal part of the trochlea is clearly separated from the body of the bone, creating an acute angle. There is a depression between the trochlea and the distal articular surface, resulting its higher location and clear distinction between the distal articular surface and the trochlea. The anterior extension of the distal articular

surface for the navicular is limited. In medial view, the medial tubercle is marked, rounded, slightly extending medially, and located in the middle of the medial face. In posterior view, the lateral-anterior articular surface is concave, with square shape. The distal-lateral prolongation is triangular shaped. It is separated from the medial(proximal) articular surface with a narrow deep groove. The medial articular surface is elongated proximo-distally, oval shaped, flat, slightly damaged at the lateral part and in contact with the distal articular surface. The medial-distal articular surface is elongated, tear shaped, fused with the distal articular surface, and with a concave distal border. The medial distal articular surface is separated with the proximal-medial articular surface by a shallow and narrow groove that is stopped by the crest formed by the distal articular surface and its contact with the articular surface. In distal view, the articular surface is slightly tilted and large. The medial articular surface is square shaped, almost flat on its surface. The lateral articular surface is irregular, generally like a half oval. The crest separating the two articular surfaces of the distal articulation is smooth and the posterior corner is protruding.

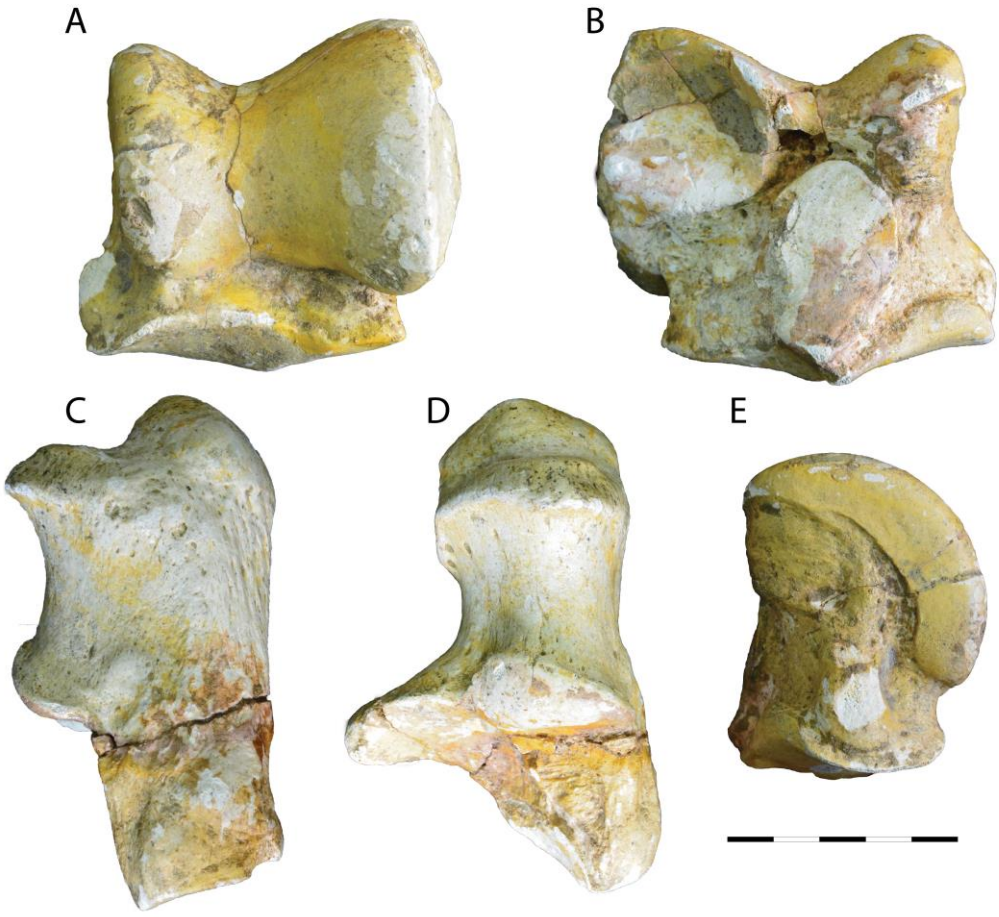

Figure 43 The S. etruscus *astragalus (A, B, E) and calcaneus (C,D) of APL-213. A: anterior view, B: posterior view, C: lateral view, D-E: medial view. Scale bar 50mm.*

The specimen APL-213 (Fig. 43, C-D) is a well-preserved calcaneus. In lateral view, the difference in height between the most proximal part of the well-developed summital tuberosity and the anterior point of the tuber calcanei is great. The beak has slightly greater width than the tuber calcanei in lateral view. The posterior border is straight in lateral view. In medial view, the anterior articular surface has almost square shape, with no extension to the lateral side. It is separated from the most posterior articular surface with a very narrow and shallow groove. The most posterior articular surface is triangular shaped and almost flat. The distal articular surface for the cuboid is elongated and triangular shaped. The sustentaculum talii is short and reduced, located slightly more distally from the middle of the bone. In distal view, the distal articular surface is medio-laterally concave and almost rectangular shaped.

Comparison

The humerus APL-408 shares common characters with *S. etruscus*, such as the wide, profound olecranon fossa with triangular outline; the oblique medial epicondyle, that is aligned with the medial lip; the wide and deep trochlea groove; the profound and high coronoid fossa. It differs from *S. hundsheimensis,* in the shallow trochlear groove and in the slightly undulated and inclined anterior border of the trochlea. On the contrary, the deep trochlea groove and the concave anterior border of the trochlea are morphological characters common with *S. etruscus* from Poggio Rosso and Olivola. There are not known specimens of *S. kirchbergensis* for a morphological comparison. APL-408 differs from *S. hemitoechus*, in the shallower trochlea groove, sinuous medial border of the medial lip of the trochlea and less curved lateral lip of the trochlea (Pandolfi and Tagliacozzo, 2015).

The radius APL-278 shares common characters with *S. etruscus,* such as the weakly concave and oblique posterior lateral border in proximal view; the moderate concavity of the anterior border; the concave, mainly at the anterior part, medial border and the ~120^{o} angle of the articulation. These characters additionally distinguish the APL-278 radius from *S. hundsheimensis.* It differs from *S. hemitoechus,* as the latter has much stronger concavity at the anterior border in proximal view and more concave postero-lateral border (Pandolfi and Tagliacozzo, 2015). It differs from *S. jeanvireti* in the more concave anterior border in proximal view, and the curved medial border (Tsoukala, 2018). It differs from *S. kirchbergensis* in the more inclined proximo-medial border in anterior view. Likewise, it differs from *S. kirchbergensis* from Siberia at the straighter anterior border in proximal view, the straighter medial borders in proximal view and the more elongated transversally articular surface (Lobachev et al., 2021).

The astragalus APL-213 shares common characters with the specimens of *S. etruscus* from Valdarno such as the slightly oblique axis of the trochlea and the elongated transversally lateral lip in anterior view. In posterior view, both APL-213 and *S. etruscus* astragali have oval shaped distal-medial articular surface with the major axis slightly inclined and straight anterior border of the articular surface for the cuboid in distal

view. Additionally, common characters with *S. etruscus* are the lateral articular surface that protrudes laterally and the lateral border, which is concave. APL-213 differs from *S. hundsheimensis* in the shallower trochlea groove, the more inclined axis of the trochlea in anterior view; the oval shaped medial- distal articular surface in posterior view that is also inclined to the sagittal plane; the less transversally elongated distal articulation in distal view (Toula, 1902; Kahlke, 2001). It differs from *S. jeanvireti*, in the shallower anterior groove of the trochlea, the more protruding medial tuberosity in anterior view and the more convex medial border of the distal articulation in distal view (Lacombat and Mörs, 2008). APL-213 differs from *S. hemitoechus,* in the less transversal development of the trochlea in comparison with the proximo-distal one in anterior view, the shallower groove of the trochlea, the perpendicular to the sagittal plane oval shaped medio-distal articular surface and the less protruding medial tubercle; the concave medially anterior border of the distal articulation in distal view (Pandolfi and Tagliacozzo, 2015). It differs from *S. kirchbergensis* at the more proximally protruding medial lip, the greater and higher depression distally the trochlea, and the narrower lateral lip in anterior view (Kahlke, 1975; Lobachev et al., 2021).

The calcaneus APL-213 shares common characters with *S. etruscus* from Valdarno, Poggio Rosso and Olivola, such as the great difference in heigh between the most proximal part of the summital tuberosity and the anterior part of tuber calcanei and the straight posterior border in lateral view. Additionally, resembles in the moderate development of the sustentaculum tali in posterior view, the slightly greater width of the beak in comparison with that of tuber calcanei in lateral view and the rounded end of the sustentaculum tali. It differs from *S. hundsheimensis*, in the difference in heigh of the most proximal part of the summital tuberosity and the anterior part of tuber calcanei in lateral view, the convex proximally posterior border in lateral view. Furthermore, the same width of the beak and the tuber calcanei and the vertical end of the sustentaculum tali (Toula, 1902; Kahlke, 2001). It differs from *S. jeanvireti*, in the shape of the end of the sustentaculum tali which is slightly convex and distally rounded. It differs from *S. hemitoechus* in the straight posterior border in lateral view, with a concavity close to the distal part (Pandolfi and Tagliacozzo, 2015; Tsoukala and Guérin, 2016). Correspondingly, it differs from *S. kirchbergensis* in the small difference in heigh between the most proximal part of the summital tuberosity and the anterior part of tuber calcanei (Kahlke, 1975).

The dimensions of the proximal epiphysis of the radius APL-278, shows that it falls into the range and close to the larger specimens, of *S. etruscus,* but also close to the smaller sized specimens of *S. hundsheimensis* (Fig. 44). The specimens proportionally closer to APL-178 are those from Mosbach (*S. hundsheimensis*), Valdarno and Magra Valley (*S. etruscus*).

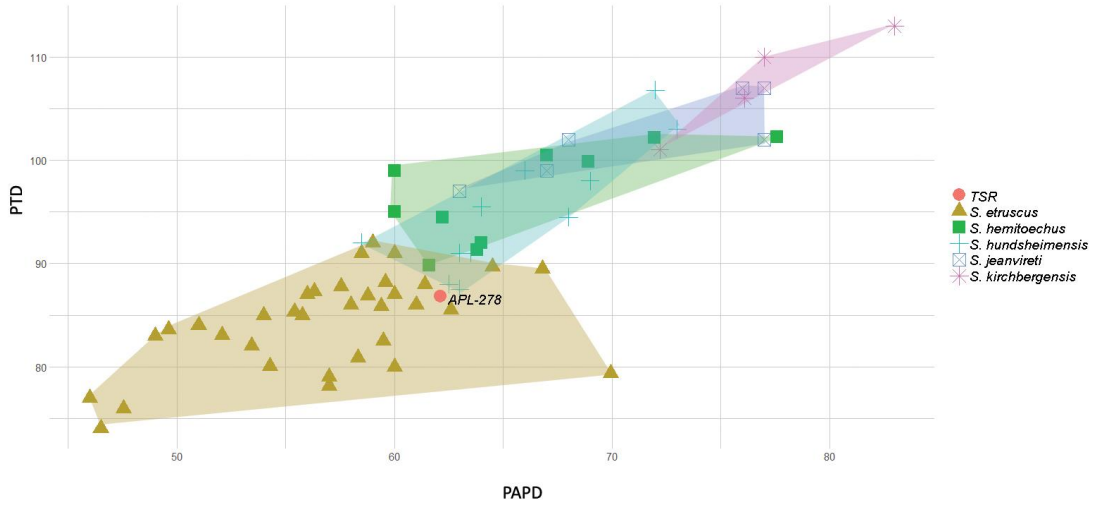

Figure 44 Proximal epiphysis of radius APL-278 in mm. Comparative material from: Guérin and Heintz (1971); Guérin (1972), (2004); Mazza (1988); Santafe-Llopis and Casanovas-Cladellas (1987); Fortelius et al. (1993); Mazo (1997); Kahlke (2001); Guérin and Tsoukala (2013); Pandolfi and Tagliacozzo (2015); Tsoukala and Guérin (2016); Pandolfi et al. (2017).

The scatter plot of the lateral heigh against the transversal diameter of the distal articular surface of the astragalus from Apollonia, shows that it clearly falls into the variability of *S. etruscus* (Fig. 45).

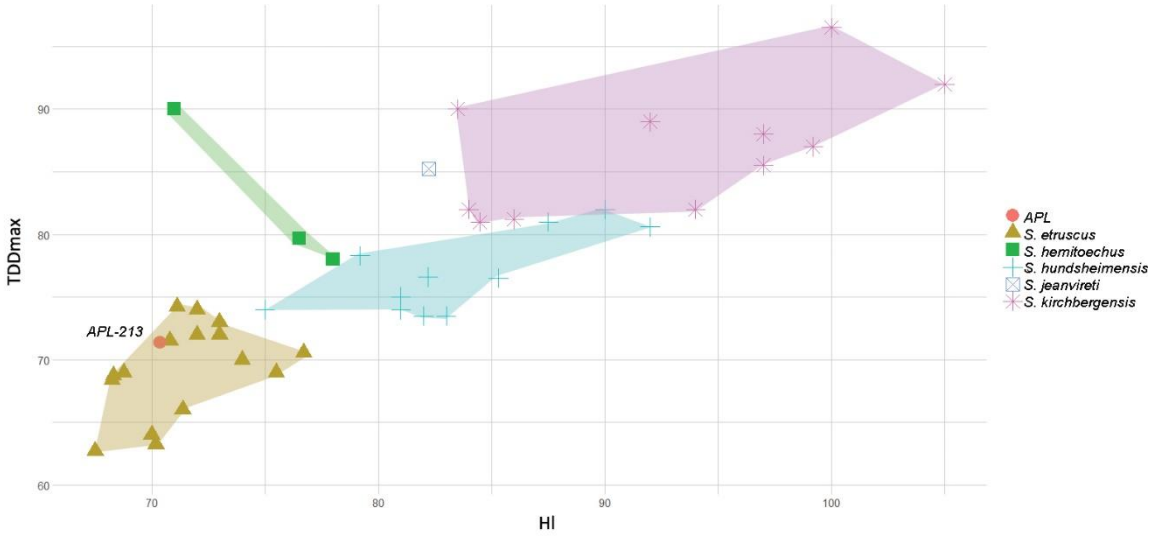

Figure 45 The scatterplot of TDDmax and HI of the astragalus APL-213, in mm. Comparative material from: Guérin and Heintz (1971); Guérin (1972), (2004); Ruiz-Bustos (1973); Santafe-Llopis and Casanovas-Cladellas (1987); Mazza (1988); Cerdeño (1989); Fortelius et al. (1993); Kahlke (2001); Lacombat (2005); Lacombat and Mörs (2008); Guérin and Tsoukala (2013); Pandolfi et al/ (2017).

The dimensions of the calcaneus indicate that APL-213 is slightly smaller than the known range of *S. etruscus* (Fig. 14), however with greater height than that of LIB-180.

Site Kalamotó (KLT, KAL)

10.1 *Stephanorhinus* sp.

Material

KAL-44 m1; KLT-149, left P2; KLT-532, diaphysis and humeral head of a humerus; KLT-279, humeral head of a right humerus; KLT-970, KLT-293, left ulnae; KLT-117, right ulna; KLT-349, diaphysis of a left femur; KLT-408 distal epiphysis of a left tibia.

Description

The specimen KAL-44 is a lower molar, previously diagnosed as m1 (Tsoukala and Chatzopoulou, 2005). The vestibular groove is open and shallow, the posterior valley is broad U shaped, the anterior narrow U shaped. Their difference in heigh from the bottom of the valley is great. Although the tooth is damaged at its proximal and distal parts, its age of death is estimated at 6-7 years (Louguet, 2002)

The specimen KLT-149 (Fig. 48, A) is a left P2**,** quite worn out, whose age is estimated at 10-12 years (Louguet, 2002). The ectoloph profile is flattened with a marked mesostyle. The valley is closed, the postfossete is small, posteriorly opened and with mesial cingulum present.

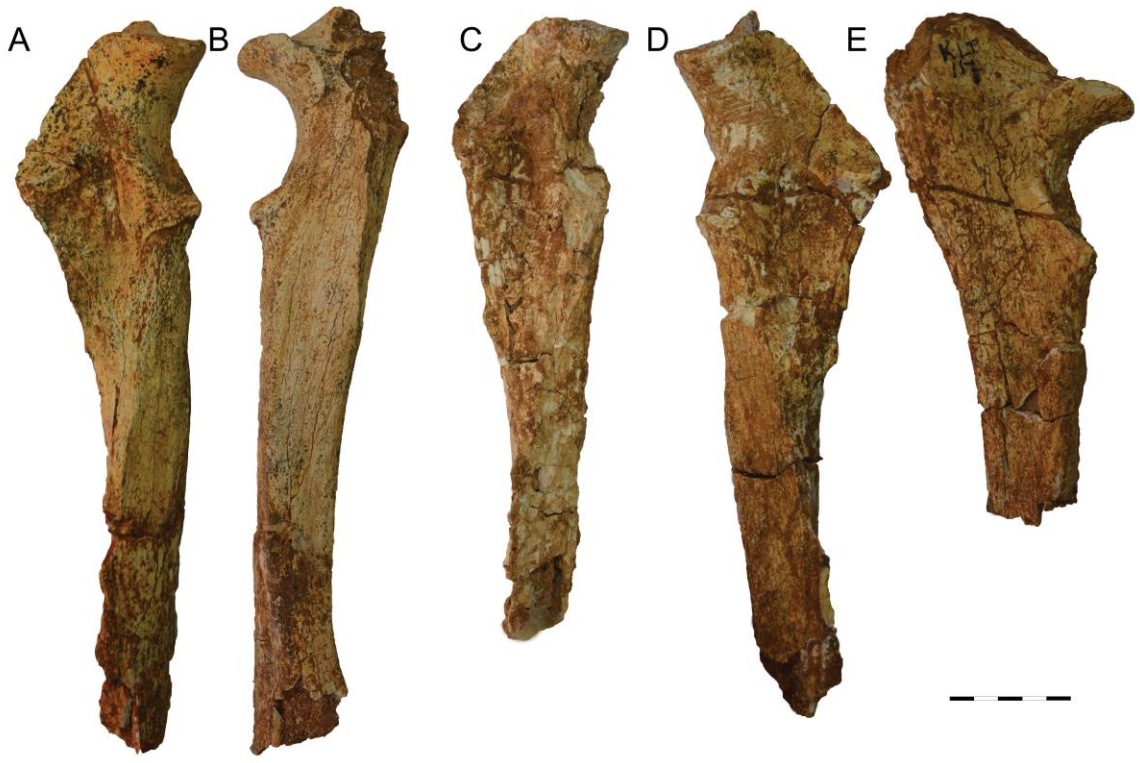

Figure 46 The Stephanorhinus *sp. specimens KLT-970 (A, B), KLT-293 (C) and KLT-117 (D,E). In anterior (A, C, D) and lateral (B, E) views. Scale 50mm.*

The specimen KLT-532 (Fig. 47, A) is a right humerus, with part of the articular head and the diaphysis preserved with limited diagnostic elements. The proximal part of the olecranon fossa is partially preserved and seems relatively wide. The overall specimen is small. The articular head is slightly projecting and have trapezoidal shape, slightly curved.

The specimen KLT-279 (Fig. 47, E) is a fragment of a right humerus with humeral head only preserved.

The specimen KLT-970 (Fig. 46, A-B) is a well-preserved left ulna lacking the olecranon and the distal epiphysis. The trochlear notch is asymmetrical, with great difference in height between the distal borders of the medial and lateral articular surface. In anterior view, the lateral border of the trochlear notch is concave, while the medial one is straight, both perpendicular to each other. There is a strong depression distally the trochlear notch. The lateral articular surface is slightly inclined compared to the body of the bone. The trochlear notch is moderately wide with the medial articular surface narrower and shorter than the concave lateral one. The lateral articular surface for the radius is very developed and triangular shaped. The medial articular surface for the radius, is very reduced like a stripe with limited height. In lateral view, the anconeal process slightly projects more forward than the distal edge of the trochlear notch. The preserved diaphysis has triangular cross section with flat walls, slightly concave in medial and lateral view.

Figure 4746 The humeri from Kalamotó: Stephanorhinus *sp. KLT-532 (A),* S. etruscus *KLT-533 (B, C),* S. etruscus *KLT-312 (D),* Stephanorhinus *sp. KLT-279 (E) in anterior (B, E) and posterior (A, C, D) views. Scale bar 50mm.*

The specimen KLT-293 (Fig. 46, C) is a poorly preserved left ulna lacking the olecranon and the distal epiphysis. The trochlear notch is asymmetrical, with the medial articular surface being more reduced than the lateral one, but damaged. The concave lateral one looks perpendicular to the body of the bone; its lateral border is damaged. The angle between the two articular surface looks less than 90º. There is a great depression distally the trochlear notch. The anconeal process looks quite projecting, although the distal end of the trochlear notch and the articular surfaces for the radius are not preserved.

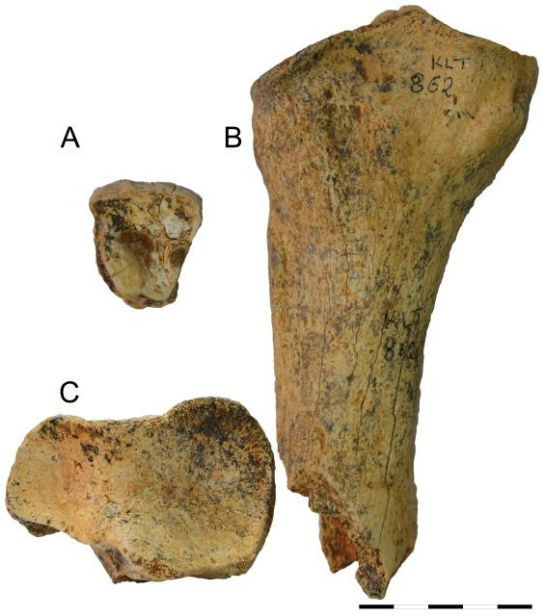

Figure 48 The specimens Stephanorhinus *sp. left P2 KLT-149 (occlusal view, A) and* S. etruscus *radius KLT-862 in anterior (B) and proximal (C) views. Scale bar 50mm.*

The specimen KLT-117 (Fig. 46, D-E) is a right ulna, preserving the proximal articulation, and part of the olecranon. The anconeal process is strong and projecting. The trochlear notch is slightly asymmetric with limited difference in height between the distal edge of the medial and lateral articular surface, which are perpendicular to each other. The trochlear notch is very large and high. In anterior view, the lateral border of the trochlear notch is concave, while the medial one is straight. The lateral articular surface for the radius is triangular shaped, while the medial one is reduced and like a stripe. In lateral view, the anconeal process is strongly projecting.

The specimen KLT-349 (Fig. 49, A) is a left diaphysis of a femur with part of the distal epiphysis preserved, but without the trochlea. In anterior view, the third trochanter is slightly curved and broken at the lateral part. In distal view, the medial condyle is slightly wider and more squarish than the lateral one which is less wide and rounded. The medial epicondyle is more developed than the lateral one, however the general development is moderate.

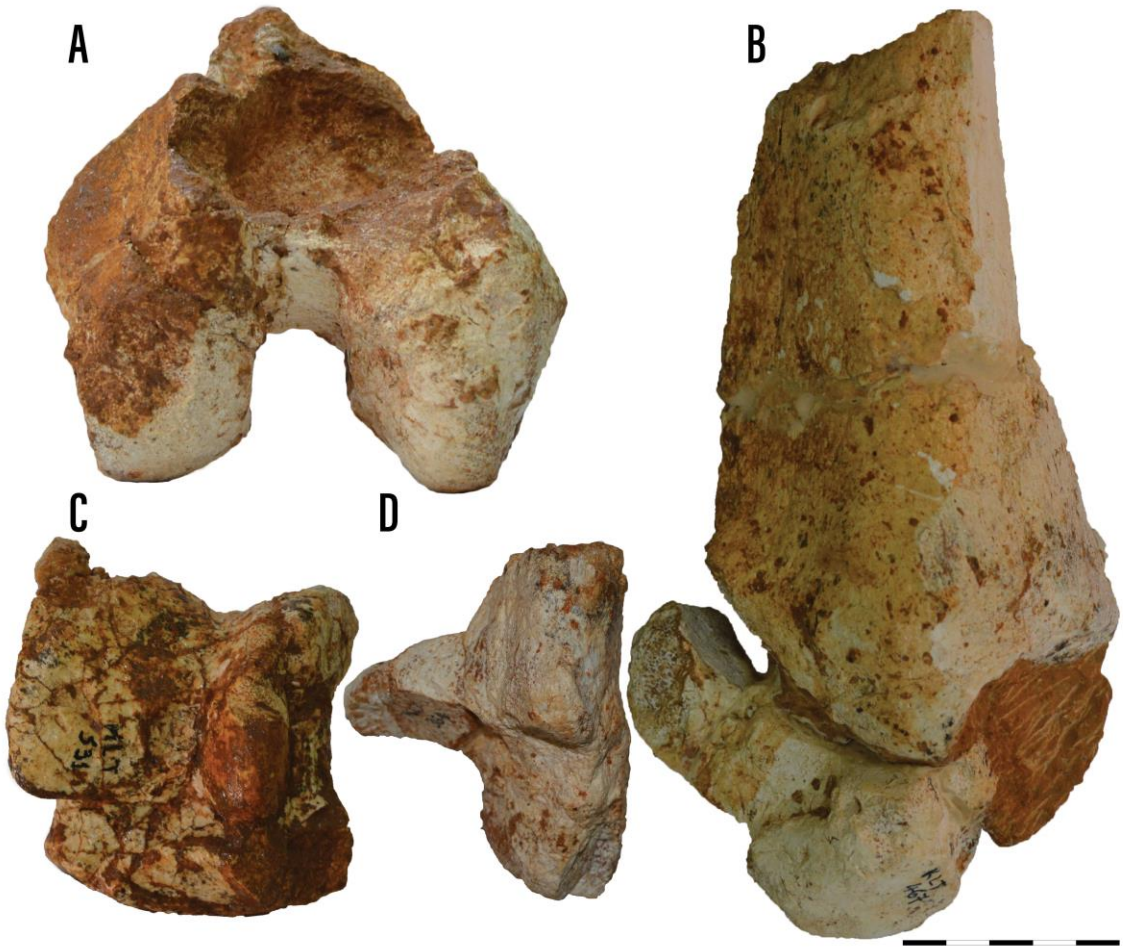

Figure 49 Stephanorhinus *sp. femur KLT-349 (A), tibia KLT-408 (B), and* S. etruscus *astragalus KLT-531 (C) and calcaneus KLT-364 (D), in anterior (B, C) distal (A) and medial (D) views. Scale bar 50mm.*

The specimen KLT-408 (Fig. 49, B) is a distal part of a left tibia, which is in touch with a semilunar. The distal epiphysis is not accessible, making the morphological description impossible. Only the dimensions of the distal epiphysis were taken.

Comparison

The open and shallow vestibular groove and the absence of vestibular cingulum of the m1 specimen KAL-44 are common characters with *S. etruscus*, on the contrary to the deep and sharp groove and strong cingulum in *S. hundsheimensis* (Pandolfi and Erten, 2017; Lacombat, 2006). However, the distinction of these two species from isolated teeth, should be considered with caution (Fortelius et al., 1993).

The level of the wear of P2 the specimen KLT-149, do not allow any morphological comparison. However, the more triangular shape of the specimen is similar to *S. etruscus*, as the teeth appears squarer shaped in *S. hundsheimensis* (Lacombat, 2006; Ballatore and Breda, 2013).

3.10.2 *Stephanorhinus etruscus*

Material

KLT-533, distal epiphysis and diaphysis of a left humerus; KLT-312, distal epiphysis of right humerus; KLT-862, proximal epiphysis and part of the diaphysis of a left radius; KLT-531, left astragalus; KLT-364, left calcaneus

Description

The specimen KLT-533 (Fig. 47, C-B) is a quite well-preserved left humerus with part of the diaphysis and the distal epiphysis preserved. In anterior view, the trochlea is strongly asymmetrical with parallel lips. The lateral lip is smaller than the medial one, with curved proximal and distal borders. The proximal border of the trochlea is oblique and almost straight. The coronoid fossa is deep, as wide as the lips and relatively high. In medial view, the trochlea is projecting distally whereas the medial epicondyle posteriorly. The lateral epicondyle is unfortunately damaged. In posterior view, the olecranon fossa is wide, moderately high, and rather deep. In posterior view, there is a marked groove separating the epitrochlear from the lateral epicondyle.

The specimen KLT-312 (Fig. 47, D) is a distal epiphysis of a humerus. In anterior view, the proximal border of the trochlea is smooth and concave; the medial one is convex, with less asymmetry and difference in size between the lips than in KLT-533. The coronoid fossa is deep with a groove separating it from the proximal border of the trochlea. In lateral view, the condyle is damaged although it is more protruding laterally than the lateral lip, and rather wide. The medial epicondyle is aligned with the medial lip, and slightly developed. In medial view, the trochlea protrudes distally, and the medial epicondyle posteriorly. In posterior view, the olecranon is triangular shaped, high, and wide but rather damaged at its lateral side. The groove separating the epitrochlear posteriorly to the distal articular surface is well-marked.

The specimen KLT-862 (Fig. 48, B-C) is a left radius with the proximal epiphysis and part of the diaphysis. In anterior view, the medial proximal border is straight and tilted while the lateral one has much more reduced length and shows a concave profile. The lateral tuberosity is strong whereas the radial one is moderately developed. In proximal view, the medial articular surface has trapezoid shape with the antero-medial border projecting anteriorly. The lateral articular surface is much more reduced, triangular with convex anterior border. The posterior border is wide, forming an angle of 120^{o}; the anterior border -slightly damaged at the middle- is undulated. In posterior view, the medial articular surface is elongated transversally, but wide and with a concave medial proximal border. The lateral border is undulated and the lateral articular surface triangular shaped. The lateral tuberosity is strongly marked, besides the presence of a groove between the lateral tuberosity and the articular surface.

The specimen KLT-531 (Fig. 49, C) is a quite damaged left astragalus, preserving limited features. In anterior view, the lips of the trochlea are parallel and oblique. The medial lip is narrow and convex but damaged, probably bitten. The lateral lip is damaged at its proximal part; it is wide but less concave and less extending distally

than the medial lip. The trochlea is quite deep; its axis is slightly oblique. there is a great and high depression distally of the trochlea; there is an indentation between the corpus of the bone and the distal part of the lateral lip. In lateral view, the astragalus is strongly damaged. In medial view, the tubercle is medially located, however partially damaged. Distal and posterior views are poorly preserved. Nevertheless, the groove separating the proximal medial and lateral articular surfaces is deep and narrow, the lateral articular surface is strongly damaged, whereas the medial one is very elongated with triangular distal border.

The specimen KLT-364 (Fig. 49, D) is a left calcaneus poorly preserved, with the summital tuberosity and the tuber calcanei damaged. In anterior view, the sustentaculum tali is moderately developed, projecting, oblique to the distal with thick and rounded end. The articular surface of the sustentaculum tali is oval shaped, the other two articular surfaces are poorly preserved.

Comparison

The humeri from KLT (KLT-533, KLT-312 and KLT-279) share common characters with *S. etruscus,* such as the deep trochlea groove in anterior view, and the concave proximal border. The olecranon fossa of KLT-533 is similarly wide and high to that of Poggio Rosso. However, the higher and more oval shaped olecranon fossa of KLT-312 is similar to those of humeri from Olivola and Pirro Nord. They differ from *S. hemitoechus* in the sinuous medial lip of the trochlea in anterior view, and the slightly curved proximal lip of the trochlea (Pandolfi and Tagliacozzo, 2015). They differ from humeri of *S. hundsheimensis,* in the lack of concavity of the proximal border of the trochlea and its narrower groove (Kahlke, 2001). There are no well-preserved humeri of *S. kirchbergensis* and *S. jeanvireti* yet both species are known for the largest postcranial bones, discriminating them from the slender, small-sized specimens from Kalamotó.

The radius KLT-862 differs from *S. jeanvireti* in the wider and more convex proximo-latera border in anterior view and the less obtuse posterior angle of the entire articulation in proximal view (Tsoukala, 2018). It differs from *S. hemitoechus*, in the sub circular medial articular surface and sub-square lateral articular surface in proximal view (Pandolfi and Tagliacozzo, 2015). In addition, the specimen KLT-862 differs from *S. hundsheimensis*, the straighter anterior border and the very obtuse posterior angle of the entire articulation in proximal view. Moreover, the straighter proximo-medial border and the lateral border of the articulation in proximal view are less concave and wide in *S. hundsheimensis* (Kahlke, 2001). KLT-862 shares some common characters with *S. etruscus*, such as the posterior angle of the entire articulation in proximal view, and the concave postero-lateral border.

The astragalus KLT-531 has some crucial parts damaged and the preservation allows limited observations, however it shares common characters with *S. etruscus* from Valdarno, such as the slightly oblique axis of the trochlea and the straight anterior border of the articular surface for the navicular in distal view. It differs from *S. hundsheimensis* in the more inclined axis of the trochlea in anterior view and the less transversally

elongated distal articulation in distal view (Toula, 1902; Kahlke, 2001). It differs from *S. jeanvireti* on the more protruding medial tuberosity in anterior view (Lacombat and Mörs, 2008). It differs from *S. hemitoechus*, in the less transversal development of the trochlea in anterior view, and the less inclined axis of the trochlea (Pandolfi and Tagliacozzo, 2015). Likewise, it differs from *S. kirchbergensis* in the more proximally protruding medial lip (Kahlke, 1975; Lobachev et al., 2021).

The calcaneus KLT-364 preserves limited diagnostic characters, however the rounded end of the sustentaculum tali and its moderate length in posterior view are common with *S. etruscus* from Valdarno, Poggio Rosso and Olivola as well as with *S. hemitoechus* (Pandolfi and Tagliacozzo, 2015). It differs from *S. hundsheimensis* in the strong and vertical end of the sustentaculum tali (Toula, 1902; Kahlke, 2001). From *S. jeanvireti*, it differs in the distally rounded sustentaculum talii (Tsoukala and Guérin, 2016; Pandolfi et al., 2019).

The dimensions of the proximal epiphysis of the radius KLT-862 fall into the variability of the smaller specimens of *S. etruscus* (Fig. 50).

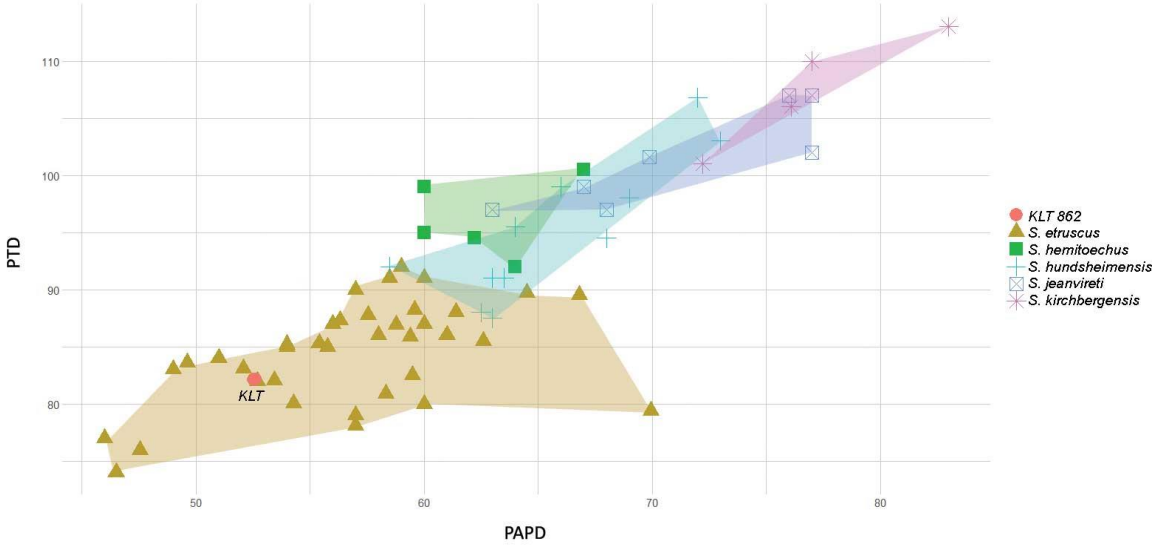

Figure 50 The scatter plot of PTD and PAPD of radius KLT-862, in mm. Comparative material from: Guérin and Heintz (1971); Guérin (1972), (2004); Santafe-Llopis and Casanovas-Cladellas (1987); Mazza (1988); Fortelius et al. (1993); Mazo (1997); Kahlke (2001); Guérin and Tsoukala (2013); Tsoukala and Guérin (2016); Pandolfi et al. (2017).

The dimensions (transversal diameter and anteroposterior diameter) of the diaphysis of the femur from Kalamotó are close but slightly larger than that of *S. etruscus* and closer to *S. hundsheimensis* (Fig. 31).

The dimensions of the calcaneus from KLT-364 fall it into the range of *S. etruscus*, near the smaller values and close to calcaneum specimens from the type locality of *S. etruscus,* Valdarno (Fig. 51)

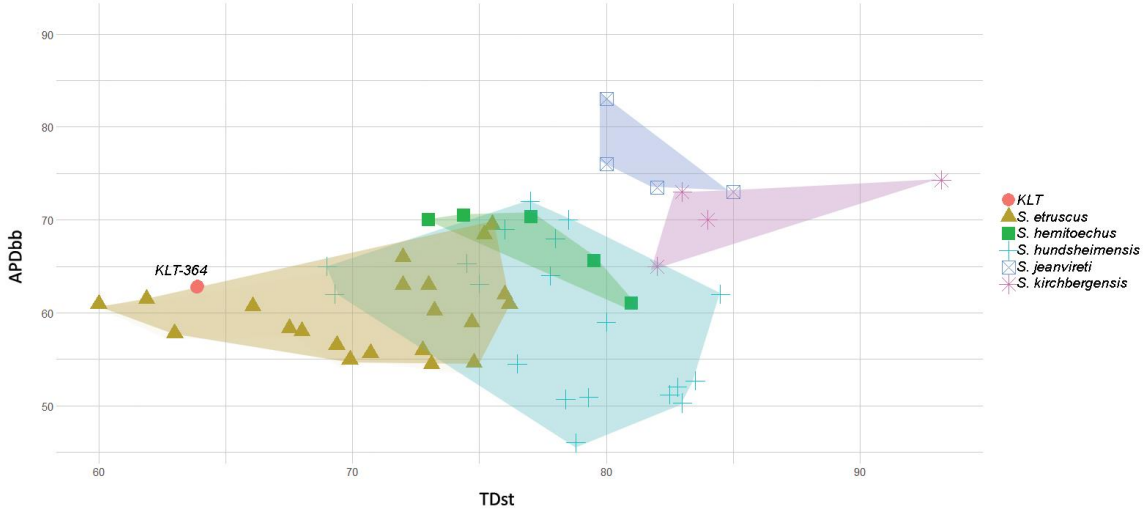

Figure 51 The scatter plot of APDb and TDst the calcaneus KLT-364, in mm. Comparative material from: Guérin (1972), (2004); Santafe-Llopis and Casanovas-Cladellas (1987); Mazza (1988); Fortelius et al. (1993); Kahlke (2001); Lacombat (2005); Guérin and Tsoukala (2013); Pandolfi and Tagliacozzo (2015); Tsoukala and Guérin (2016); Pandolfi et al. (2017).

4. DISCUSSION

Based on the most recent report of Greek rhinocerotids (Giaourtsakis 2022), the Greek Plio-Pleistocene fossil rhino record (Fig. 52) is very scarce, resulting to most specimens being classified simply as" Rhinocerotidae indet". Efforts are made here to reexamine the material in an attempt to shed light to the situation.

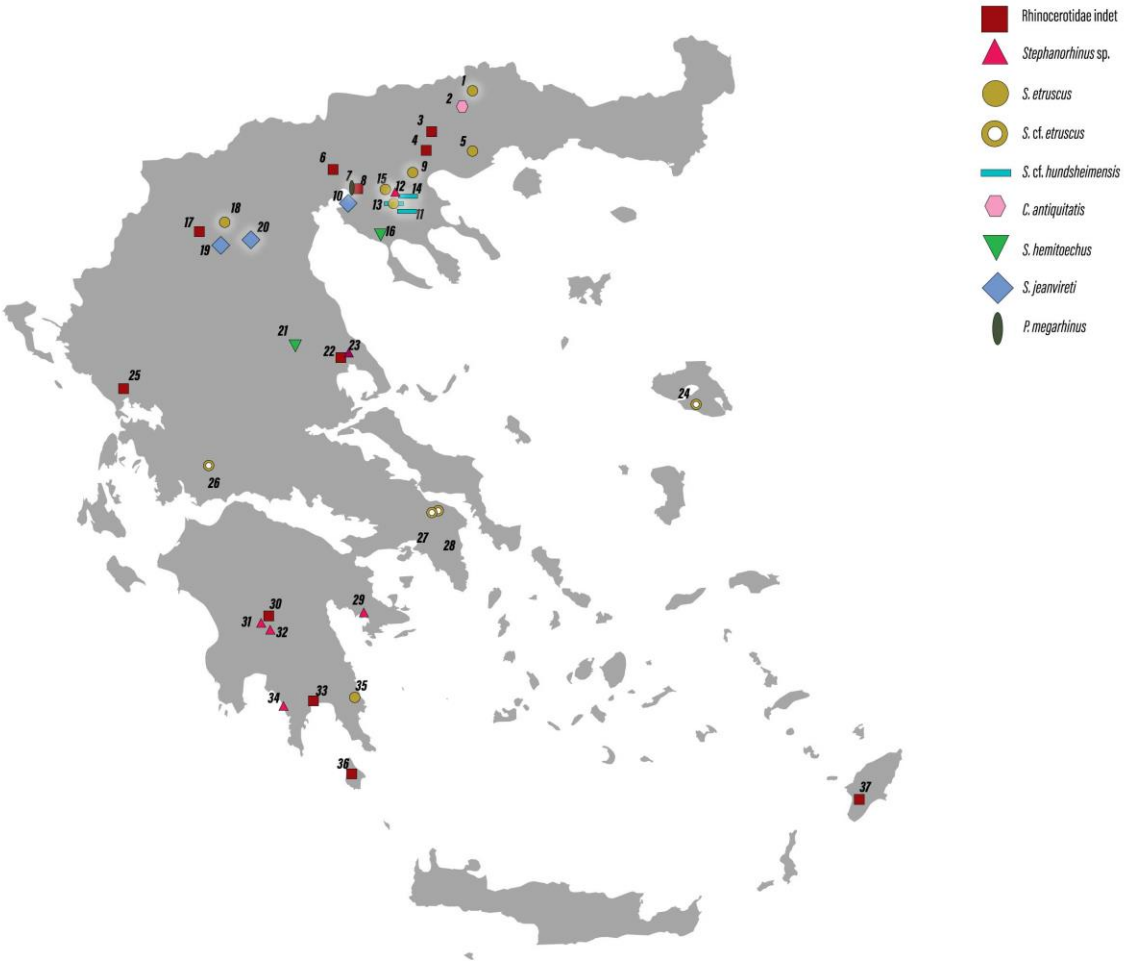

Figure 52 Plio-Pleistocene localities of Greece with rhinocerotids based on Giaourtsakis (2022), including the revised material of this thesis (in white outer glow). 1,Volax; 2, Aggitis; 3, Serres basin; 4, Nigrita; 5, Aivaliki; 6, Gephyra; 7, Allatini; 8, Agia Triada; 9, Apollonia; 10, Angelochori; 11, Riza; 12, Platanochori; 13, Tsiotra Vryssi; 14, Krimni; 15, Kalamotó1-2; 16, Petralona; 17, Neapolis; 18, Libakos; 19, Milia; 20, Dafnero; 21, Penios riverbank; 22, Alikes; 23, localities of Sesklo; 24, Vatera; 25, Asprochaliko; 26, Molikrio; 27, Tourkovounia 3-5; 28, Psychiko; 29, Karnezeika; 30, Marathousa; 31, localities of Megalopolis; 32, Kyparissia; 33, Lakonis-1; 34, Kalamakia; 35, Richea; 36, Kythera; 37, Apolakkia. Source: Vemaps.com, modified.

The rhino taxa recovered from the fossiliferous localities included in this thesis are summarized in the following table (Table 1). *Stephanorhinus* sp., is only mentioned in the Platanochori site. Due to the scarcity of the material several species assignation in the remaining sites is given with some reservation.

Table 1 Age and taxonomy of the studied localities.

Locality	Literature	Age	Attribution
Allatini	Syrides (1990)	Rouscinian	*P. megarhinus*
Dafnero	Benammi et al. (2020)	MN17/2.3 Ma	*S.* cf. *jeanvireti*
Volakas	Koufos and Vlachou (1997)	MN17	*S. etruscus*
Livakos	Koufos 2001	MN 17	*S. etruscus*
Tsiotra Vryssi	Konidaris et al. (2021)	1.78 to ~1.5 Ma	*S. etruscus* *S.* cf. *hundsheimensis*
Krimni	Kostopoulos et al. in press	Between 1.78- 1.0 Ma	*S. cf. hundsheimensis*
Platanochori	Konidaris et al. (2015)	1.0-1.2 Ma	*Stephanorhinus* sp.
Riza	Koufos (2001)	1.0-1.2 Ma	*S. cf. hundsheimensis*
Apollonia	Koufos et al., 1992	1.3-1.2 Ma	*S. etruscus*
Kalamoto	Tsoukala and Chatzopoulou (2005)	Early Pleistocene / Latest Villafranchian (MNQ 20)	*S. etruscus*

The presence of *P. megarhinus* in the locality of Allatini, represents the first occurrence of this taxon in Greece, however the poor stratigraphy and chronology of the site restrict any conclusion. The rhino of the locality of Allatini is usually mentioned in the literature as “Rhinocerotidae indet.” (Symeonidis et al., 2006; Tsoukala and Guérin, 2016; Giaourtsakis, 2022), without any description or photographs. The age of the fossiliferous clays is Lower Pliocene (Rouscinian), belonging to the Trilophos Formation (Syrides, 1990). No further systematic excavations were performed in this locality, which apart from the rhino radius yielded only some remains of *Eucyon odessanus* (Koufos, 2022).

This species has its earliest occurrence in Hungary during the Late Miocene, in Italy at the end of Miocene (MN13) and later, during the Early and Late Pliocene (MN14 and MN15) it appears in Western Europe. Additionally, in Turkey it is present during the second half of the Pliocene (Guérin, 1980; Guérin and Sen, 1998; Pandolfi, 2013; Pandolfi et al., 2015).

Based on the younger occurrence of *P. megarhinus* in Russia, Fukuchi et al. (2009) suggested that the taxon dispersed directly from Europe to Asia, however this hypothesis is contradicted by Pandolfi et al. (2015) who advocates that the species may have persisted longer in Asia, and therefore *P. megarhinus* could have spread from Asia to Eastern Europe during the Late Miocene. The localities with *P. megarhinus* are more or less the same age as Allatini are Baccinello V3 (Tuscany), central Italy dated to Latest

Miocene (Pandolfi, 2013) and Montpellier, France dated to the Early Pliocene (MN14) (Guérin, 1980).

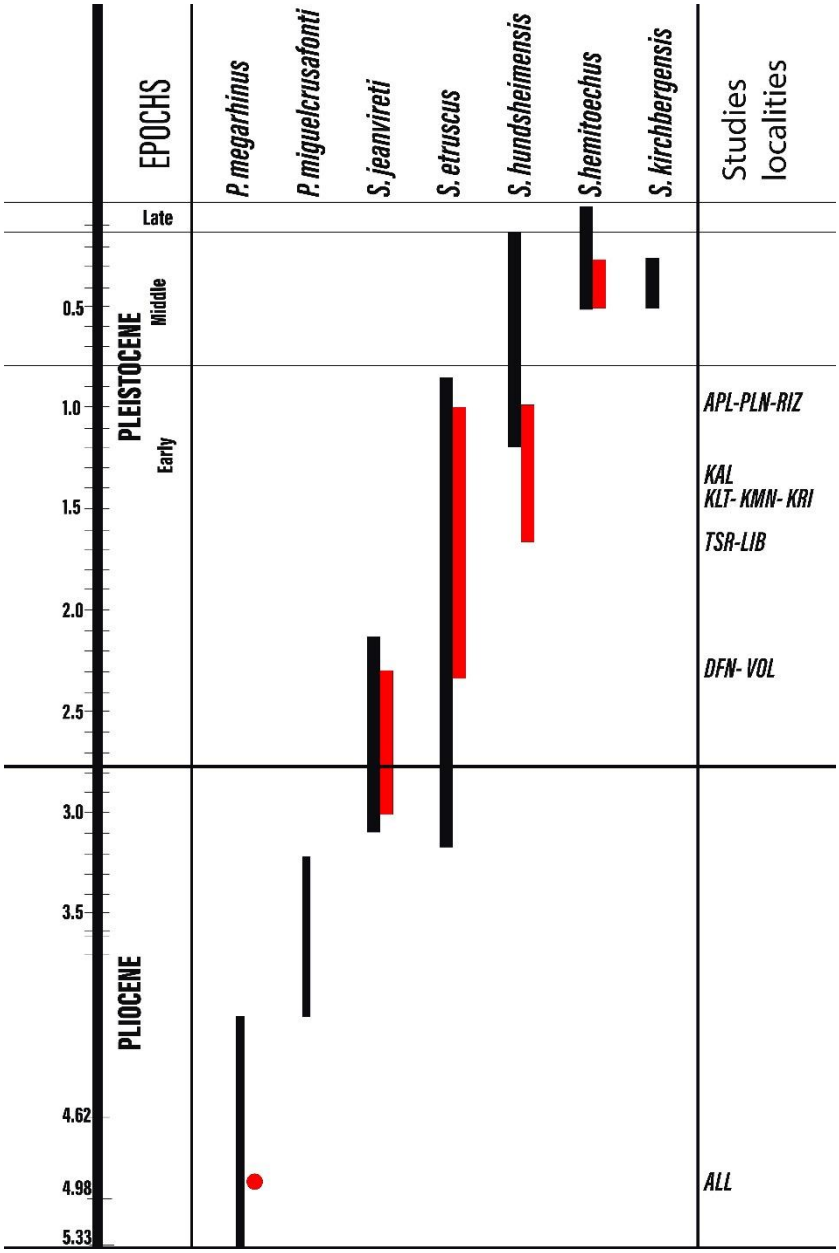

Figure 5347 Chronological range of Plio-Pleistocene Rhinoceratidae in Europe and Greece Data from: Agustí et al. (2009); Deng et al. (2011); Masini and Sala (2017); Pandolfi et al. (2018); Puzachenko et al. (2021).

The species *S. jeanvireti* is a relatively rare rhinoceros, usually recorder during the Late Pliocene, and characteristic of the early Villafranchian (MNQ16). It persists in Europe until the Early Pleistocene in Coltesti, Romania (MNQ17-MNQ18) (Pandolfi et al., 2019). In the Greek record the species is docimented at the localities Milia,

Angelochori and Saint George Priporos, all dated to the Late Pliocene, biozone MN16 (Guérin and Tsoukala, 2013; Tsoukala, 2018; Giaourtsakis, 2022). The presence of *S.*cf. *jeanvireti* in Dafnero site marks its last known occurrence in Greece, in agreement with the Coltesti record (Pandolfi et al., 2019).

The species *S. etruscus* is the best documented and most common and widespread *Stephanorhinus* species in Europe and Greece. It first occured in Europe in the latest Pliocene in several Spanish, Italian, French and Romanian localities (Pandolfi et al. (2017 and references therein)). Its last occurrences are debatable, and likely diachronic in different Eurasian areas. In Greece *S. etruscus* is reported from various localities (Aivaliki, Richea, Psychiko and Molikrio, Tourkovounia 3-5, Vatera, Krimni, Kalamotó, Libakos) (Symeonidis et al., 2006; Kampouridis et al., 2018; Giaourtsakis, 2022) spanning from the middle Villafranchian (MN17) to the Epivillafranchian (MNQ19).

S. cf. *etruscus* is already recorded in the Early Pleistocene from Vatera DS, Aivaliki and Tourkovounia (3-5). The presence of *S. etruscus* in Volax likely marks its first confirmed Greek occurrence and roughly coincides chronologically with that of Vatera, Lesvos Island. Late Villafranchian *S. etruscus* was already known in Greece from the locality of Libakos, and it is further supported here by the Tsiotra Vryssi's and Kalamoto-2 records. The last Greek occurrence of *S. etruscus* is in Apollonia, dated at 1.2-1.0 Ma. In conclusion, the widespread *S. etruscus* is present in Greece from ca. 2.4-2.3 Ma to ca. 1.2-1.0 Ma. Although the taxon seems to disappear from Central Europe somewhen earlier (Pandolfi et al., 2017) it persists till 1.2-1.0 Ma in Italy, Iberian Peninsula and according to our data in Greece.

Taking into account the Dafnero record, that is roughly isochronous with those from Vatera in Lesvos and Volax in Drama, it seems that *S. etruscus* co-occurred for a short time period with *S. jeanvireti* during the early Pleistocene in Greece (Fig. 53).

The species *S. hundsheimensis* is reported from Europe and Turkey since the late Early Pleistocene (ca. 1.2 Ma) (Pandolfi and Erten, 2017). Then after it is present in several localities in central Europe (France, Germany), in the Italian and Iberian Peninsulas, as well as in Romania (Pandolfi and Erten (2017 and references therein). The lineage *Stephanorhinus* ex gr. *etruscus/hundsheimensis* has been recorded in Dmanisi (Georgia) establishing its first occurrence. Recently, its last occurrence was documented in Servia (Bogovina Cave), in ca. 600ka, however the chronology of the site is disputed (Radović et al., 2020).

In Greece, *S. hundsheimensis* was referred in Platanochori (Konidaris et al., 2015), based on a single mandible with deciduous teeth that is here, however, assigned to *Stephanorhinus* sp., in agreement with Giaourtsakis (2022). It was also reported from in Apollonia-1 (Konidaris et al., 2015), nevertheless the revision of APL the material shows that it is morphologically and biometrically closer to *S. etruscus.* On the contrary, material from Krimni-1 previously attributed to *S. etruscus* (Sakellariou et al., 1979) is here recognized as *S*. cf. *hundscheimensis*. The presence of *Stephanorhinus* cf.

hundsheimensis in Riza, Krimni-1 and Krimni 3 and Tsiotra Vryssi, likely represent the first and earliest record of this species in Greece. The age of the locality of Riza (1.0-1.2 Ma) coincides with the first occurrence of the species in both Europe and Turkey (Pandolfi and Erten, 2017), in the localities Vallparadis, Vallonet, Untermasfeld and Denizli (Guérin, 1980; Kahlke, 2001; Lacombat and Moulle, 2005; Madurell-Malapeira et al., 2010; Pandolfi and Erten, 2017). The possible presence of *S. hundscheimensis* in Krimni1, 3 and especially in Tsiotra Vryssi, where it co-occurs with *S. etruscus*, indicates that the taxon may appear earlier in SE Europe at least, altering its occurrence since ~1.78-1.5 Ma. It is worth to mention that *S. etruscus* and *S. hundsheimensis*, are for the first time confirmed to co-exist in the same locality, as they are usually seen as occupying different habitats (Pandolfi et al., 2021a). Their co-existence has been reported in Trlica (Montenegro), however from different stratigraphic units and based on isolated teeth (Vislobokova and Agadjanian, 2015), this led Pandolfi et al. (2017) to question their common presence. The relationships between *S. hundsheimensis* and other *Stephanorhinus* species is still debated. Guérin (1980) suggests the evolution of both *S. hundsheimensis* and *S. hemitoechus* from *S. etruscus,* while others link *S. hundsheimensis* with *S. jeanvireti* (Fortelius et al., 1993; Lacombat, 2007) or to some Asian immigrant (Mazza, 1988).

5. CONCLUSIONS

The limited and usually fragmentary rhinocerotid material in most Plio-Pleistocene localities studied here make their systematic attribution challenging. Nevertheless, based on morphological and biometrical comparison, the presence of *P. megarhinus* in Allatini is evident, which confirms its first incidence in Greece. Meanwhile, *S.* cf. *jeanvireti* in Dafnero site corresponds to the last known occurrence of this species in Greece, also establishing a short time of coexistence with *S. etruscus,* already known from Tourkovounia and Volax. The species *S. etruscus* is similarly confirmed in Libakos, Apollonia and Kalamotó sites, altogether spaning in Greece from 2.3 to ~1.0 Ma. Also, *S.* cf. *hundsheimensis,* is confirmed in Krimni-1,3, Tsiotra Vryssi and Riza, establishing the possible presence of this species in Greece, from ca. 1.78 to ~1.0 Ma. The Tsiotra Vryssi record in particular suggests that *S.* cf. *hundsheimensis*, possibly appears earlier in SE Europe and confirms its co-existence here with *S. etruscus.* The rhino morph from Platanochori is assigned as *Stephanorhinus* sp. The scarce material, limited to postcranial elements, necessitates more extensive excavations.

REFERENCES

Agustí, J., Vekua, A., Oms, O., Lordkipanidze, D., Bukhsianidze, M., Kiladze, G., Rook, L., 2009. The Pliocene-Pleistocene succession of Kvabebi (Georgia) and the background to the early human occupation of Southern Caucasus. Quat. Sci. Rev. 28, 3275–3280.

Apostol, L., Enache, C., 1979. Étude de l'espèce *Dicerorhinus megarhinus* (de Christol) du bassin carbonifère de Motru (Roumanie) [Romanian summ.]. Trav. du Muséum d'Histoire Nat. "Grigore Antipa", Bucuresti.

Arambourg, C., Piveteau, J., 1929. Les vertébrés du Pontien de Salonique. Ann Paléontol 18, 1–82.

Ballatore, M., Breda, M., 2013. *Stephanorhinus hundsheimensis* (Rhinocerontidae, Mammalia) teeth from the early Middle Pleistocene of Isernia La Pineta (Molise, Italy) and comparison with coeval British material. Quat. Int. 302, 169–183.

Benammi, M., Aidona, E., Merceron, G., Koufos, G.D., Kostopoulos, D.S., 2020. Magnetostratigraphy and Chronology of the Lower Pleistocene Primate Bearing Dafnero Fossil Site, N. Greece. Quat. Int. 22.

Billia, E.M.E., 2008. Revision of the fossil material attributed to *Stephanorhinus kirchbergensis* (Jäger 1839) (Mammalia, Rhinocerotidae) preserved in the museum collections of the Russian Federation. Quat. Int. 179, 25–37.

Billia, E.M.E., Petronio, C., 2009. Selected records of *Stephanorhinus kirchbergensis* (Jäger, 1839) (mammalia, rhinocerotidae) in Italy. Boll. della Soc. Paleontol. Ital. 48, 21–32.

Cerdeño, E., 1989. Revisión de la sistemática de los rinocerontes del Neógeno de España. Universidad Complutense de Madrid.

Cerdeño, E., 1990. *Stephanorhinus hemitoechus* (Falc.)(Rhinocerotidae, Mammalia) del Pleistoceno medio y superior de España. Estud. geológicos 479, 465–479.

Cerdeno, E., 1995. Cladistic Analysis of the Family Rhinocerotidae (Perissodactyla). Am. Museum Novit. 3143, 1–25.

Cirilli, O., Pandolfi, L., Bernor, R.L., 2020. The Villafranchian perissodactyls of Italy: knowledge of the fossil record and future research perspectives. Geobios 63, 1–21.

Deng, T., Wang, X., Fortelius, M., Li, Q., Wang, Y., Tseng, Z.J., Takeuchi, G.T., Saylor, J.E., Säilä, L.K., Xie, G., 2011. Out of Tibet: Pliocene woolly rhino suggests high-plateau origin of ice age megaherbivores. Science (80-.). 333, 1285–1288.

Forsyth-Major, C.-I., 1894. Le gisement ossifère de Mytilini et catalogue d'ossemens fossiles recueillis à Mitylini, île de Samos, et déposés au Collège Galliard, à Lausanne. Lausanne.

Fortelius, M., Mazza, P., Sala, B., 1993. *Stephanorhinus* (Mammalia: Rhinocerotidae) of western European Pleistocene, with a revision of *S. etruscus* (Falconer, 1868). Palaeontogr. Ital. 80, 63–155.

Fukuchi, A., Nakaya, H., Takai, M., Ogino, S., 2009. A preliminary report on the Pliocene rhinoceros from Udunga, Transbaikalia, Russia. Asian Paleoprimatology 5, 61–98.

Gaudry, A., 1862. Animaux fossiles et géologie de l'Attique, F. Savy Ed. ed. Paris.

Geraads, D., 1988. Révision des Rhinocerotidae (Mammalia) du Turolien de Pikermi. Comparaison avec les formes voisines. Ann Paléontol 74, 13–41.

Geraads, D., Koufos, G.D., 1990. Upper Miocene Rhinocerotidae (Mammalia) from Pentalophos-1, Macedonia, Greece. Palaeontographica 210, 151–168.

Giaourtsakis, I.X., 2022. The Fossil Record of Rhinocerotids (Mammalia: Perissodactyla: Rhinocerotidae) in Greece, Fossil Vertebrates of Greece Vol. 2.

Guérin, C., 1972. Une nouvelle espèce de rhinocéros (Mammalia, Perissodactyla) à Vialette (Haute-Loire, France) et dans d'autres gisements du Villafranchien inférieur européen : *Dicerorhinus jeanvireti* n. sp. Doc. des Lab. Géologie la Fac. des Sci. Lyon 49, 53–150.

Guérin, C., 1973. Les trois especes de rhinoceros (Mammalia, Perissodactyla) du gisement pleistocene moyen des Abimes de la Fage a Noailles (Correze). Publ. du musée des Confluences 11, 55–84.

Guérin, C., 1980. Les rhinocéros (Mammalia, Perissodactyla) du Miocène terminal au Pléistocène supérieur en Europe occidentale. Comparaison avec les espèces actuelles., Documents. ed.

Guérin, C., 2004. Les rhinocéros (Mammalia, Perissodactyla) du gisement villafranchien moyen de Saint-Vallier (Drôme). Geobios 37, 259–278.

Guérin, C., Heintz, E., 1971. *Dicerorhinus etruscus* (Falconer, 1859), Rhinocerotidae, Mammalia, du Villafranchien de la Puebla de Valverde (Teruel, Espagne). Bull. du museum Natl. d'histoire Nat. 3.

Guérin, C., Santafe-Llopis, J.V., 1978. *Dicerorhinus miguelcrusafonti* nov. sp., une nouvelle espèce de rhinocéros (Mammalia, Perissodactyla) du gisement pliocène supérieur de Layna (Soria, Espagne) et de la formation pliocène de Perpignan (Pyrénées-Orientales, France). Geobios 11, 457–491.

Guérin, C., Sen, S., 1998. Rhinocerotidae. In: Sen, S. (Ed.), Le gisement de vertébrés pliocènes de Calta, Ankara, Turquie. Geoodiversitas 20, 397–407.

Guérin, C., Tsoukala, E., 2013. The Tapiridae , Rhinocerotidae and Suidae (Mammalia) of the Early Villafranchian site of Milia (Grevena , Macedonia , Greece). Geodiversitas 35, 447–489.

Heissing, K., 1999. Family Rhinocerotidae, in: Rössner, G.E., Heissig, K. (Eds.), The Miocene Land Mammals of Europe. Munich, pp. 175–188.

Hullot, M., Antoine, P.O., Ballatore, M., Merceron, G., 2019. Dental microwear textures and dietary preferences of extant rhinoceroses (Perissodactyla, Mammalia). Mammal Res.

Iurino, D.A., Conti, J., Mecozzi, B., Sardella, R., 2020. Braincase With Natural Endocast of a Juvenile Rhinocerotinae From the Late Middle Pleistocene Site of Melpignano (Apulia, Southern Italy). Front. Earth Sci. 8, 1–14.

Kahlke, H.-D., 1975. Die Bhinocerotiden-Restc aus den Travertinen von Weimar-Ehringsdorf, in: Kahlke, H.-D. (Ed.), Das Pleistozän von Weimar-Ehringsdorf. pp. 337–397.

Kahlke, H.-D., 2001. Die Rhinocerotiden-Reste aus dem Unterpleistozän von Untermaßfeld., in: Das Pleistozän von Untermaßfeld Bei Meiningen (Thüringen), Teil 2. pp. 501–555.

Kahlke, R.D., Kaiser, T.M., 2011. Generalism as a subsistence strategy: Advantages and limitations of the highly flexible feeding traits of Pleistocene *Stephanorhinus hundsheimensis* (Rhinocerotidae, Mammalia). Quat. Sci. Rev. 30, 2250–2261.

Kahlke, R.D., Lacombat, F., 2008. The earliest immigration of woolly rhinoceros (*Coelodonta tologoijensis*, Rhinocerotidae, Mammalia) into Europe and its adaptive evolution in Palaearctic cold stage mammal faunas. Quat. Sci. Rev. 27, 1951–1961.

Kampouridis, P., Kargopoulos, N., Svorligkou, G., Giaourtsakis, I., Roussiakis, S., Theodorou, G., 2018. Rhinocerotidae (Mammalia , Perissodactyla) remains from the new Pleistocene locality of Richea (Laconia , Greece) 15784.

Kirillova, I. V., Chernova, O.F., Van Der Made, J., Kukarskih, V. V., Shapiro, B., Van Der Plicht, J., Shidlovskiy, F.K., Heintzman, P.D., Van Kolfschoten, T., Zanina, O.G., 2017. Discovery of the skull of *Stephanorhinus kirchbergensis* (Jäger, 1839) above the Arctic Circle. Quat. Res. (United States) 88, 537–550.

Kockel, F., Mollat, H., Walther, H.W., 1977. Erläuterungen zur geologischen Karte der Chalkidiki und angrenzender Gebiete 1:100.000 (NordGriechenland). Bundesanstalt für Geowissenschaften und Rohstoffe 119.

Konidaris, G.E., Kostopoulos, D.S., Maron, M., Schaller, M., Ehlers, T.A., Aidona, E., Marini, M., Tourloukis, V., Muttoni, G., Koufos, G.D., Harvati, K., 2021. Dating of the Lower Pleistocene Vertebrate Site of Tsiotra Vryssi (Mygdonia Basin, Greece): Biochronology, Magnetostratigraphy, and Cosmogenic Radionuclides. Quaternary 4, 1.

Konidaris, G.E., Tourloukis, V., Kostopoulos, D.S., Thompson, N., Giusti, D., Michailidis, D., Koufos, G.D., Harvati, K., 2015. Two new vertebrate localities from the Early Pleistocene of Mygdonia Basin (Macedonia, Greece): Preliminary results. Comptes Rendus - Palevol 14, 353–362.

Kostopoulos, D.S., 1996. The Plio-Pleistocene Artiodactyls of Macedonia (Greece). PhD dissertation, Aristotle University of Thessaloniki, 612 p. (in Greek with English summary; unpublished).

Kostopoulos, D.S., Guy, F., Kynigopoulou, Z., Koufos, G.D., Valentin, X., Merceron, G., 2018. A 2Ma old baboon-like monkey from Northern Greece and new evidence to support the *Paradolichopithecus* e *Procynocephalus* synonymy (Primates : Cercopithecidae). J. Hum. Evol. 121, 178–192.

Kostopoulos, D.S., Konidaris, G.E., Amanatidou, M., Chitoglou, K., Fragkioudakis, E., Gerakakis, N., Giannakou, V., Gkeme, A., Kalaitzi, C.,Tsakalidis, C.,Tsatsalis, V., 2022. The new fossil site Krimni-3 in Mygdonia Basin and the first evidence of a giant ostrich in the Early Pleistocene of Greece. Palaeontol. Zeitschrift (submitted for publication).

Koufos, G.D., 1992. Early Pleistocene Equids from Mygdonia basin (Macedonia, Greece). Palaeontogr. Ital. 79, 167–199.

Koufos, G.D., 2001. The Villafranchian mammalian faunas and biochronology of Greece. Boll. della Soc. Paleontol. Ital. 40, 217–223.

Koufos, G.D., 2018. New Material and Revision of the Carnivora , Mammalia from the Lower Pleistocene Locality Apollonia 1, Greece. Quaternary 1(1), 6.

Koufos, G.D., 2022. The Fossil Record of Canids (Mammalia: Carnivora: Canidae) in Greece., in: Vlachos, E. (Ed.), Fossil Vertebrates of Greece Vol. 2. Springer.

Koufos, G.D., Syrides, G.E., Kostopoulos, D.S., Koliadimou, K.K., 1995. Preliminary results about the stratigraphy and the palaeoenvironment of Mygdonia Basin, Macedonia, Greece. Geobios 28, 243–249.

Koufos, G.D., Syrides, G.E., Kostopoulos, D.S., Koliadimou, K.K., 1992. Apollonia, a new vertebrate site in the Pleistocene of the Mygdonia Basin (Macedonia, Greece); the first fossil freshwater mollusks in the area. Comptes Rendus - Acad. des Sci. Ser. II 315, 1041–1046.

Koufos, G.D., Vlachou, T.D., 1997. *Equus stenonis* from the middle Villafranchian locality of Volax (Macedonia , Greece). Geodiversitas 19, 641–657.

Lacombat, F., 2003. Étude des rhinocéros du Pléistocène de l'Europe méditerranéenne et du Massif Central: Paléontologie, phylogénie et biostratigraphie. Paris, Muséum national d'histoire naturelle.

Lacombat, F., 2005. Les rhinocéros fossiles des sites préhistoriques de l'Europe méditerranéenne et du Massif Central: Paléontologie et implications biochronologiques. BAR Int. Ser, 1419.

Lacombat, F., 2006. Morphological and biometrical differentiation of the teeth from Pleistocene species of *Stephanorhinus* (Mammalia, Perissodactyla, Rhinocerotidae) in Mediterranean Europe and the Massif Central, France. Palaeontogr. Abteilung A Palaozoologie - Stratigr. 274, 71–111.

Lacombat, F., 2007. Phylogeny of the genus *Stephanorhinus* in the Plio-Pleistocene of Europe Phylogenie der Gattung *Stephanorhinus* im Plio-Pleistozän Europas. Hallesches Jahrb. Geowiss. 63–64.

Lacombat, F., 2010. Estudio paleontológico de *Stephanorhinus hundsheimensis* de Fuente Nueva-3 y Barranco León., in: Toro, I., Martínez-Navarro, B., and Agustí, J. (Eds.), Ocupaciones Humanas En El Pleistoceno Inferior y Medio de La Cuenca de Guadix-Baza. Consejería de Cultura, pp. 237–246.

Lacombat, F., Mörs, T., 2008. The northernmost occurrence of the rare Late Pliocene rhinoceros *Stephanorhinus jeanvireti* (Mammalia, Perissodactyla). Neues Jahrb. fur Geol. und Palaontologie - Abhandlungen 249, 157–165.

Lacombat, F., Moulle, P.-E., 2005. Description paléontologique du *Stephanorhinus hundsheimensis* (Toula, 1902) Pléistocène Inférieur de la Tour de Grimaldi (Liguri, Italie). Bull. du Museéum d'Athropologie préhistorique Monaco 44, 33–38.

Lobachev, Y. V., Shpansky, V., Bondarev, A.A., Lobachev, A.Y., Vasiliev, S.K., Klementev, A.M., Grebnev, I.E., Silaev, V.I., 2021. New findings of *Stephanorhinus kirchbergensis* in Siberia. Palaeontol. Electron. 24.

Loose, H., 1975. Pleistocene Rhinocerotidae of W. Europe with reference to the recent two-horned species of Africa and S.E. Asia. Scr. Geol. 33, 1–59.

Louguet, S., 2002. Determining the Age of Death of Proboscids and Rhinocerotids from Dental Attrition. Recent Adv. Ageing Sexing Anim. Bones 179–188.

Madurell-Malapeira, J., Minwer-Barakat, R., Alba, D.M., Garcés, M., Gómez, M., Aurell-Garrido, J., Ros-Montoya, S., Moyà-Solà, S., Berástegui, X., 2010. The Vallparadís section (Terrassa, Iberian Peninsula) and the latest Villafranchian faunas of Europe. Quat. Sci. Rev. 29, 3972–3982.

Mallet, C., Cornette, R., Billet, G., Houssaye, A., 2019. Interspecific variation in the limb long bones among modern rhinoceroses—extent and drivers. PeerJ 2019.

Masini, F., Sala, B., 2007. Large- and small-mammal distribution patterns and chronostratigraphic boundaries from the Late Pliocene to the Middle Pleistocene of the Italian peninsula. Quat. Int. 160, 43–56.

Mazo, A. V, 1997. El yacimiento Rusciniense de Alcalá del Júcar (Albacete). Taxonomía y bioestratigrafía. Estud. Geológicos.

Mazza, P., 1988. The Tuscan Early Pleistocene rhinoceros *Dicerorhinus etruscus*. Palaeontogr. Ital. 75, 1–87.

Mazza, P., Sala, B., Fortelius, M., 1993. A small latest Villafranchian (late Early Pleistocene) rhinoceros from Pietrafitta (Perugia, Umbria, Central Italy) with notes on the Pirro and Westerhoven rhinoceroses. Palaeontogr. Ital. 80, 25–50.

Milliken, T., Emslie, R.H., Talukdar, B., 2009. African and Asian Rhinoceroses-Status, Conservation and Trade A report from the IUCN Species Survival Commission (IUCN/SSC) African and Asian Rhino Specialist Groups and TRAFFIC to the CITES Secretariat pursuant to Resolution Conf. 9.14 (Rev. CoP14) and D. Environmentportal.in 230, 1–18.

Pandolfi, L., 2011. *Stephanorhinus kirchbergensis* (Jäger, 1839) from the Middle Pleistocene site of Riano (Roma, Central Italy). Ital. J. Quat. Sci. 24, 103–112.

Pandolfi, L., 2013. New and revised occurrences of *Dihoplus megarhinus* (Mammalia, Rhinocerotidae) in the Pliocene of Italy. Swiss J. Palaeontol. 132, 239–255.

Pandolfi, L., Bartolini-Lucenti, S., Cirilli, O., Bukhsianidze, M., Lordkipanidze, D., Rook, L., 2021a. Paleoecology, biochronology, and paleobiogeography of Eurasian Rhinocerotidae during the Early Pleistocene: the contribution of the fossil material from Dmanisi (Georgia, Southern Caucasus). Journal of human evolution, 156, 103013

Pandolfi, L., Cerdeño, E., Codrea, V., Kotsakis, T., 2017. Biogeography and chronology of the Eurasian extinct rhinoceros *Stephanorhinus etruscus* (Mammalia, Rhinocerotidae). Comptes Rendus - Palevol 16, 762–773.

Pandolfi, L., Codrea, V.A., Popescu, A., 2019. *Stephanorhinus jeanvireti* (Mammalia, Rhinocerotidae) from the early Pleistocene of Colțești (southwestern Romania). Comptes Rendus - Palevol 18, 1041–1056.

Pandolfi, L., Erten, H., 2017. *Stephanorhinus hundsheimensis* (Mammalia, Rhinocerotidae) from the late early Pleistocene deposits of the Denizli Basin (Anatolia, Turkey). Geobios 50, 65–73.

Pandolfi, L., Fiore, I., Gaeta, M., Szabó, P., Vennemann, T., Tagliacozzo, A., 2018. Rhinocerotidae (Mammalia, Perissodactyla) from the middle Pleistocene levels of Grotta Romanelli (Lecce, southern Italy). Geobios 51, 453–468.

Pandolfi, L., Gasparik, M., Magyar, I., 2016. Rhinocerotidae from the Upper Miocene deposits of the Western Pannonian Basin (Hungary): Implications for migration routes and biogeography. Geol. Carpathica 67, 69–82.

Pandolfi, L., Gasparik, M., Piras, P., 2015. Earliest occurrence of "*Dihoplus*" *megarhinus* (Mammalia, Rhinocerotidae) in Europe (Late Miocene, Pannonian Basin, Hungary): Palaeobiogeographical and biochronological implications. Ann. Paleontol. 101, 325–339.

Pandolfi, L., Marra, F., 2015. Rhinocerotidae (Mammalia, Perissodactyla) from the chrono-stratigraphically constrained Pleistocene deposits of the urban area of Rome (Central Italy). Geobios 48, 147–167.

Pandolfi, L., Pierre-olivier, A., Bukhsianidze, M., Rook, L., Pandolfi, L., Pierre-olivier, A., Bukhsianidze, M., Lordkipanidze, D., 2021b. Northern Eurasian rhinocerotines (Mammalia , Perissodactyla) by the Pliocene – Pleistocene transition: phylogeny and historical biogeography. J. Syst. Palaeontol. 0, 1–27.

Pandolfi, L., Rook, L., 2017. Rhinocerotidae (Mammalia, Perissodactyla) from the latest Turolian localities (MN 13; Late Miocene) of central and northern Italy. Boll. della Soc. Paleontol. Ital. 56, 45–56.

Pandolfi, L., Tagliacozzo, A., 2015. *Stephanorhinus hemitoechus* (Mammalia, Rhinocerotidae) from the Late Pleistocene of Valle Radice (Sora, Central Italy) and re-evaluation of the morphometric variability of the species in Europe. Geobios 48, 169–191.

Pandolfi, L., Sendra, J., Reolid, M., Rook, L., 2022. New Pliocene Rhinocerotidae findings from the Iberian Peninsula and the revision of the Spanish Pliocene records. PalZ.

Protopopov, A., Potapova, O., Plotnikov, V., Maschenko, E., Boeskorov, G., Klimovskii, A., Banderov, A., Ivanov, S., Kolesov, S., Pavlov, I., 2015. The frozen mummy of the woolly rhinoceros , *Coelodonta antiquitatis* (Blum., 1799) calf : a new data on early ontogenesis of the extinct species, in: Proceedings of the 75th Annual SVP Meeting, Dallas, TX. p. 199.

Psilovikos, A., 1977. Palaeogeographic development of the basin and lake of Mygdonia (Langada-Volvi area), Greece. (Doctoral dissertation, PhD thesis, Univ. Thessaloniki).

Puzachenko, A.Y., Levchenko, V.A., Bertuch, F., Zazovskaya, E.P., Kirillova, I. V., 2021. Late Pleistocene chronology and environment of woolly rhinoceros (*Coelodonta antiquitatis* (Blumenbach, 1799)) in Beringia. Quat. Sci. Rev. 263, 106994.

Radović, P., Radonjić, M., Billia, E.M.E., 2020. Pleistocene rhinoceros from bogovina cave: The first report of *Stephanorhinus hundsheimensis* Toula, 1902 (Mammalia, Rhinocerotidae) from Serbia. Palaeontol. Electron. 23, 1–20.

Regnault, S., Hermes, R., Hildebrandt, T., Hutchinson, J., Weller, R., 2013. Osteopathology in the feet of rhinoceroses: Lesion type and distribution. J. Zoo Wildl. Med. 44, 918–927.

Ruiz-Bustos, A., 1973. Estudio de unos restos de *Dicerorhinus etruscus*, Falconer, encontrados en Granada. Cuad. Ciencias Biol. 2, 2–89.

Sakellariou, E., Koufos, G.D., Psilovikos, A., 1979. Contribution to the study of Villafranchian in N. Chalkidiki-Scientific Annals of the Faculty of Physics and Mathematics, Aristoteleian University of Thessaloniki, 19, 279-296.

Santafe-Llopis, J.V., Casanovas-Cladellas, M.L., 1987. *Dicerorhinus etruscus brachycephalus* (Mammalia, Perissodactyla) de los yacimientos pleistocénicos de la Cuenca Guadix-Baza (Venta Micena y Huéscar) (Granada, Espana). Paleontol. i Evol. Espec. 1, 237–254.

Stilson, K.T., Hopkins, S.S.B., Davis, E.B., 2016. Osteopathology in rhinocerotidae from 50 million years to the present. PLoS One 11, 1–27.

Symeonidis, N.K., Giaourtsakis, I.X., Giannopoulis, V.I., 2006. Aivaliki , a New Locality with Fossil Rhinoceroses near Alistrati (Serres, Greece). Beitträge zur Paläontologie 30, 437–451.

Syrides, G.E., 1990. Lithostratigraphic, biostratigraphic and palaeogeographic study of the Neogene–Quaternary sedimentary deposits of Chalkidiki Peninsula, Macedonia, Greece. Sci. Ann. Sch. Geol. Aristotle Univ. Thessaloniki 11, 243.

Szabó, P., Kocsis, L., Vennemann, T., Pandolfi, L., Kovács, J., Martinetto, E., Demény, A., 2017. Pliocene–Early Pleistocene climatic trends in the Italian Peninsula based on stable oxygen and carbon isotope compositions of rhinoceros and gomphothere tooth enamel. Quat. Sci. Rev. 157, 52–65.

Team, R.C., 2020. R: A language and environment for statistical computing. R Foundation for Statistical Computing, Vienna, Austria.

Tong, H.W., Wang, X.M., 2014. Juvenile skulls and other postcranial bones of *Coelodonta nihowanensis* from Shanshenmiaozui, Nihewan Basin, China. J. Vertebr. Paleontol. 34, 710–724.

Tong, H.W., Wu, X.Z., 2010. *Stephanorhinus kirchbergensis* (Rhinocerotidae, Mammalia) from the rhino cave in Shennongjia, Hubei. Chinese Sci. Bull. 55, 1157–1168.

Toula, F., 1902. Das Nashorn von Hundsheim: *Rhinoceros* (Ceratorhinus osborn) *hundsheimensis* nov. form. Mit Ausführungen über die Verhältnisse von elf Schädeln von Rhinoceros (Ceratorhinus) sumatrenis. Geol. Reichsanstalt 19, 1–3.

Tsoukala, E., 2018. Rhinocerotidae from the late Miocene and late Pliocene of Macedonia, Greece. A revision of the neogene - quaternary rhinocerotidae of Greece. Rev. Paleobiol. 37, 609–630.

Tsoukala, E., Chatzopoulou, K., 2005. A New Early Pleistocene (Latest Villafranchian) Site with Mammals in Kalamotó (Mygdonia Basin, Macedonia, Greece) -Preliminary Report. Mitt. Komm. Quartärforsch. Österr. Akad. Wiss. 14, 213–233.

Tsoukala, E., Guérin, C., 2016. The Rhinocerotidae and Suidae of the Middle Pleistocene from Petralona cave (Macedonia, Greece). Acta Zool. Bulg. 68, 243–264.

van Asperen, E.N., Kahlke, R.D., 2015. Dietary variation and overlap in Central and Northwest European *Stephanorhinus kirchbergensis* and *S. hemitoechus* (Rhinocerotidae, Mammalia) influenced by habitat diversity. Quat. Sci. Rev. 107, 47–61.

van der Made, J., 2010. The rhinos from the Middle Pleistocene of Neumark Nord (Saxony-Anhalt). Veröffentlichungen des Landesamtes für Denkmalpfl. und Archäologie 62, 433–527.

Vasileiadou, K., Koufos, G.D., Syridis, G., 2003. Silata, a new locality with micromammals from the Miocene/Pliocene boundary of the Chalkidiki peninsula, Macedonia, Greece. Deinsea 549–562.

Vislobokova, I.A., Agadjanian, A.K., 2015. New data on large mammals of the Pleistocene Trlica fauna, Montenegro, the Central Balkans. Paleontol. J. 49, 651–667.

Vlachos, E., Kotsakis, T., Delfino, M., 2015. The chelonians from the Latest Miocene-Earliest Pliocene localities of Allatini and Pylea (East Thessaloniki, Macedonia, Greece). Comptes Rendus - Palevol 14, 187–205.

Weber, M., 1904. Über tertiäre Rhinocerotiden von der Insel Samos I. Bull Soc Imp Nat. Moscou 4, 477–501.

APPENDIX

Table 2 Teeth measurements of the upper teeth, based on Mazza (1988), in mm.

Locality	Specimen	Tooth	LL	BL	MW	DW
Tsiotra Vryssi	TSR-D18-23	P2		28.73		
Platanochori	PLN-1	DP3	28.43	ca. 32.31	ca. 40.73	42.12
Apollonia	APL- 498	DP3	38.27	49.58	42.45	47.82
Platanochori	PLN-1	DP4	32.02	38.79	46.22	49.82
Tsiotra Vryssi	TSR-G21-47	DP4	26.64	ca. 35.39	ca. 37.7	42.52
Kalamotó	KLT-149	P2	16.3	30.3	32.55	35.25
Krimni	KPI 17/1978	P3	29.85		43.76	45.27
Krimni	KRI-16/1978	P3	ca. 24.94		42.13	42
Krimni	KRI-18/1975	P4	30.63	41.94	49.38	46.8
Tsiotra Vryssi	TSR-F14-19	P4	31.69	37.1	51.04	55.09
Platanochori	PLN-1	M1	34.12	ca. 41.32	ca. 49.65	47.86
Krimni	KRI-16/1978	M1	35.84	42.22		
Krimni	KRI-16/1978	M2	38.36	51.07		
Tsiotra Vryssi	TSR-E19-19	M2		ca. 59.38		
			TL (absolute length)			
Tsiotra Vryssi	TSR-165	M3	ca. 65.73			

Table 3 Teeth measurements of the lower teeth, based on Guérin (1980) [G] and Mazza (1988) [M], in mm.

Locality	Specimen	Tooth	LL (M)	DW (M)	MW (M)	Lmax (G)	Wmax (G)	VL (M)
Tsiotra Vryssi	TSR-F20-14					ca. 52.42		51.84
Tsiotra Vryssi	TSR-G21-21		ca. 55.68	27.4	30.48	ca. 59.82	ca. 31.18	59.26
Tsiotra Vryssi	TSR-D18-24	p3 right	44.12			46		
Tsiotra Vryssi	TSR-D18-24	p2 left	ca. 25.29	14.64				
Tsiotra Vryssi	TSR-D18-24	p3 left	37.94			ca. 36.48		
Tsiotra Vryssi	TSR-D18-24	p4 Left			21.83	45.3		

Table 4 Measurements of the studied humeri, based on Guérin (1972) [G], Mazza (1988) [M], Fortelius et al. (1993) [F] and Lacombat (2003) [L], in mm.

Locality	Specimen	Lmax (G)	PTD (G)	PAPD (G)	TDS (G)	APDS(G)	DTD (G)	DAPDm (G)	DAPDI [L]	Tddelt (M)
Kalamotó	KLT-532									
Kalamotó	KLT-533				71.23	64.3		102.5		
Kalamotó	KLT-312						127.26	104.62	88.62	
Tsiotra Vrysi	TSR-133				58.17	63.95		101.29		
Tsiotra Vrysi	TSR-D13-22									
Tsiotra Vrysi	TSR-G15-2									
Tsiotra Vrysi	TSR-G19-13	418.47	178.11	167.66	75.13	70.28	129.08	111.21	101.25	142.23
Apollonia	APL-408				70.52	66.36	131.25	112.98	97.15	
Libakos	LIB-497				60.95	61.54	125.37	113.09	89.82	

Specimen	DP1 (M)	DP2 (M)	LI (M)	Hmtr (L)	Hltr (F)	Lml (F)	Lf (M)	TDtr (M)	Tdof (F)	PTDa(F)
KLT-532										
KLT-533				70.14	37.54	46.81		90.26		
KLT-312				78.33	61.9	50.78		92.84		
TSR-133				78.29		47.2				
TSR-D13-22				82.18						
TSR-G15-2										
TSR-G19-13	184.3	165.46	404.04	86.21	57.08	52.84	368.56	93.8	44.15	87.97
APL-408				79.12	61.87	47.4		86.84	45.15	
LIB-497				80.43	55.86	53.06		86.4		

Table 5 Measurements of the studied ulnae based on Guérin (1980) [G], Mazza (1988) [M], Fortelius et al. (1993) [F] and Lacombat (2003) [L], in mm.

Locality	Specimen	PAPDol (G)	APDanp (M)	Hs (F)	PTDa (G)	TDS (G)	APDS (G)	Hpa (L)
Riza	RIZ-27	90.87	110.92	54.05	82.54	41.05	48.39	75.9
Tsiotra Vryssi	TSR-G21-73		103.75	55.79		28.44	28.75	71.64
Tsiotra Vryssi	TSR-G21-71		82.2	43.18	81.91	35.44	33.61	72.65
Tsiotra Vryssi	TSR-G16-16		94.13	59.06	80.37	32.61	45.07	68.99
Tsiotra Vryssi	TSR-E20-8		99.93	54.37		35.87	37.57	66.77
Apollonia	APL-348			46.52	77.4	32.58	34.55	69.4
Kalamotó	KLT-970		80.21	48.03	77.72	36.7	31.21	74.68
Kalamotó	KLT-293			44.6				
Kalamotó	KLT-117		103.82	53.37	76.13	38.5	42.35	75.07

Table 6 Measurements of the studied radii based on Guérin (1980) [G] and Mazza (1988) [M], in mm.

Locality	Specimen	Lmax (G)	PTD (G)	PTDa (M)	PAPD (G)	PAPDa (M)	DTD (G)
Riza	RIZ-27		90.88	90.34	54.92	60.43	98.7
Tsiotra Vryssi	TSR-C17-7		90.39	90.49	57.18	56.37	
Tsiotra Vryssi	TSR-G21-72		91.23	89.46	56.81	61.44	
Allatini	Allatini	398	102.8	102	65.1	67.5	100
Apollonia	APL-278		86.82	86.85	62.13	62.07	

Specimen	DTDa (G)	DAPD (G)	DAPDa (G)	TDS (G)	APDS (G)
RIZ-27	77.17	56.72	47.63		
TSR-C17-7				46.21	38.82
TSR-G21-72				43.86	31.19
Allatini	85.7	63.3	50.6	49.7	37
APL-278					

Table 7 Measurements of the studied McIII based on Guérin (1980), in mm.

Locality	Specimen	Lmax	PTD	PAPD	TDS
Tsiotra Vryssi	TSR-36		59.2	52.62	
Dafnero	DFN-340	218.85	55.67	48.46	50.76

Table 8 Measurements of the studied McIV, based on Guérin (1980), in mm.

Locality	Specimen	PTD	PAPD	APDS
Tsiotra Vryssi	TSR-F18-67	44.71	41.61	21.5

Table 9 Measuremens of the studied femori based on Guérin (1980) [G], Mazza (1988) [M], Fortelius et al. (1993) [F], in mm.

Locality	Specimen	Lmax (G)	Ll (M)	PTD (G)	PAPDar (G)	PTDar (G)	TDov3tr (F)	ApDov3tr (F)	TD3tr(G)
Tsiotra Vrysi	TSR-F18-56	475.05	458.22	185.11	83.9	87.6	101.4	42.1	98.14
Tsiotra Vrysi	TSR-G20-50							37.42	
Tsiotra Vrysi	TSR-D16-27								
Tsiotra Vrysi	TSR-F22-3						101.5	37.7	
Krimni	KMN-3				77.08	79.89	113.51	40.92	
Krimni	KMN-68								
Kalamotó	KLT-349								

Specimen	APD3tr (F)	H3tr (G)	TDS (G)	APDS (G)	DTD (G)	DAPDl (F)	DAPDm (G)	TDtr (F)	TDcp (F)
TSR-F18-56	26.9	65.9	67.64	54.28	133.68	120.07	ca. 129.94	58.14	115.1
TSR-G20-50	20.24	55.8	73.52	49.83					
TSR-D16-27	22.91	69.66?	76.67	52.08					
TSR-F22-3	22.23	62.09	71.66	50.91					
KMN-3	25.38	58.43	59.27	50.95					
KMN-68			67.12	48.69					
KLT-349	23.22	61.6	68.05	46.82					120.34

Table 10 Measurements of the studied tibia based on Guérin (1980), in mm.

Locality	Specimen	TDS	APDS	DTD	DAPD	DTDa	DAPDa
Tsiotra Vryssi	TSR-50			89.19	65.16	76.77	55.35
Volax	VOL-215	56.84	47.53	84	59.92		51.61

Table 11 Measurements of the studied astragali based on Guérin (1980) [G], Mazza (1988) [M] and Fortelius et al. (1993) [F], in mm.

Locality	Specimen	Hl (M)	Hm (M)	Tdmax (G)	TDDmax (G)	DAPD (M)	DTDa (G)
Krimni	KRH-23/1978		72.68	85.87	73.43	43.09	68.29
Apollonia	APL-213	70.27	68.42	86.28	71.26	39.88	72.09
Kalamotó	KLT-531		ca. 76.51	86.6		ca. 46.95	72.95
Krimni	KMN 100	70.62	68.58	84.32	71.44	45.58	66.8

Specimen	Htm (M)	APDm (G)	Htl (F)	TDl (G)	DAPDa (G)	Hmax (G)
KRH-23/1978				54.86	42.96	80.36
APL-213	46.46	57.77	57.85	58.29	48.51	77.01
KLT-531	ca. 56.2	ca. 59.8		51.2	44.9	
KMN 100	47.82	52.78	53.03	52.75	44.09	77.39

Table 12 Measurements of the studied calcanei based on Guérin (1980), in mm.

Locality	Specimen	Hmax	APDS	TDs	APDb	TDst	TDmp
Libakos	LIB-180	108.85	60.75	41.92	57.1		29.05
Apollonia	APL-213	116.23	58.47	45.13	56.94	74.74	37.78
Apollonia	APL-665						26.35
Kalamotó	KLT-364				62.83	63.9	

Table 13 Measurements of the studied navicular based on Guérin (1980), in mm.

Locality	Specimen	Lmax	lmax	Hmax
Tsiotra Vryssi	TSR-F18-64b	58.91	45.15	26.06

Table 14 Measurments of the studied cuboid based on Guérin (1980), in mm.

Locality	Specimen	Lmax	lmax	Hmax	lpa	Lpa	Ha
Tsiotra Vryssi	TSR-F18-64b	57.5	38.18	52.53	31.6	39.23	36.74

Table 15 Measurements of the studied 3rd cuneiform based on Guérin (1980), in mm.

Locality	Specimen	lmax	Lmax	Hmax
Tsiotra Vryssi	TSR-F18-64b	43.65	46.94	23.51

Table 16 Measurements of the studied 1st cuneiform based on Guérin (1980), in mm.

Locality	Specimen	Lmax	Tdmax	APDmax
Tsiotra Vryssi	TSR-F18-64b	59.68	24.22	19.68

Table 17 Measurements of the studied 2nd cuneiform based on Guérin (1980), in mm.

Locality	Specimen	Lmax	lmax	Hmax
Tsiotra Vryssi	TSR-F18-64b	35	21.86	15

Table 18 Measurements of the studied MtII based on Guérin (1980), in mm.

Locality	Specimen	PTD	PAPD	TDS	APDS	DTD	DTDa	DAPD
Tsiotra Vryssi	TSR-F18-64a	23.48	26.9	37.59	31.6	26.02		
Volax	VOL-216					34.27	29.47	32.69

Table 19 Measurements of the studied MtIII based on Guérin (1980) [G] and Fortelius et al. (1993) [F], in mm.

Locality	Specimen	PTD (G)	PAPD (G)	TDS (G)	APDS (G)	PTDa (F)	PAPDa (F)
Tsiotra Vryssi	TSR-F18-64a	51.73	44.18	44.23	25.07	50.26	38.78

Table 20 Measurements of the studied MtIV based on Guérin (1980), in mm.

Locality	Specimen	PTD	PAPD	TDS	APDS
Tsiotra Vryssi	TSR-F18-64a	35.52	37.99	26.07	31.97
Tsiotra Vryssi	TSR-G16-41	44.17	3.64	30.01	22.64